JOURNAL OF THE AERONAUTICAL SCIENCES

VOLUME 21 NOVEMBER, 1954 NUMBER 11

Pseudotransonic Similitude and First-Order Wave Structure*

WALLACE D. HAYES†

U.S. Office of Naval Research, London

ABSTRACT

A wave system extending from a body in a supersonic flow has a structure which is controlled by second-order cumulative effects and which provides for attentuation of the energy in the wave system and increase in the entropy of the fluid. A similitude is obtained which takes into account this first-order wave structure; this theory appears as an extension of von Kármán's transonic similitude for supersonic flow and has no subsonic counterpart. This pseudotransonic similitude was first noted by W. Vincenti for conical flows with normal Mach Number close to one. As with transonic similitude, the mean-surface assumption is required and the theory is essentially a first-order one even though second-order effects are involved. The appropriate forms of the similitude are also given for the flow about slender bodies, two-dimensional flow, and the flow at a distance from finite systems.

INTRODUCTION

LINEARIZED METHODS OF analytically investigating the flow about bodies at supersonic speeds have proved themselves useful for predicting the pressure distributions on many types of bodies. The wave systems predicted by linearized theory, however, have only geometric attenuation and do not provide for attenuation of the wave energy. Although the linearized wave systems may be correctly used as a basis for calculating drag they do not give even an approximately correct picture of the actual wave systems at an appreciable distance from the body, even though the requirements of linearized theory are clearly satisfied for the flow about the body. Second-order terms in the differential equations are needed to describe this first-order wave structure.

The classic theory of von Kármán[1] for transonic similitude involves the same phenomena, but has the distinguishing feature that the wave structure always affects the pressure distribution on the body itself; in supersonic flow the first-order wave structure only affects the body significantly in the case of an edge or discontinuity line with the normal Mach Number close to one. The pseudotransonic similitude here developed may be considered to be an extension of transonic similitude to cover first-order wave structure in supersonic flow.

Although many results were noted earlier, particularly the behavior of asymptotic N-waves, the first general investigation of first-order wave structure may be considered to be that of Friedrichs,[2] who gives references to earlier work. The theory of Friedrichs was extended by Lighthill,[3] who made a careful analysis of the errors of first-order wave theory in the one-dimensional unsteady case; Lighthill's approach was applied to the two-dimensional steady case by Pythian.[4] Results for the case of bodies of revolution were first obtained by DuMond et al.,[5] and a thorough analysis of this case is due to Whitham.[6] The spherical nonsteady case has also been studied by Whitham,[7] and Lighthill[8] has investigated the conical flow case. Various workers in second-order flow theory have, of course, noted certain features of first-order wave structure.

The present investigation stems from that of Vincenti,[9] who noted the similitude of this paper in the case of a conical wing with Mach Number normal to the leading edge approximately equal to one. The approach here is one which utilizes the second-order equation for the velocity potential rather than the more generally used approach which studies the geometry of the characteristics and shocks involved.

Presented at the Aerodynamics Session, Twenty-Second Annual Meeting, IAS, New York, January 25–29, 1954.

* The opinions expressed here are those of the writer and not necessarily those of the U.S. Navy.

† Formerly, Scientific Liaison Officer; now Associate Professor of Aeronautical Engineering, Princeton University.

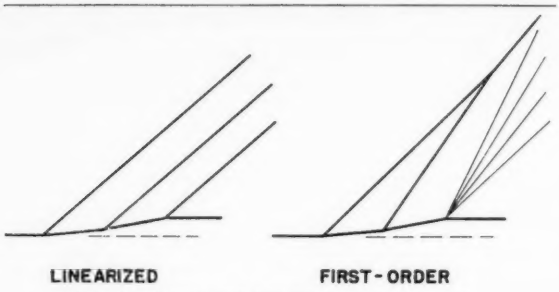

FIG. 1. Linear and first-order wave structure.

It was pointed out to the author by Vincenti after this paper was written that Berndt[10] used the pseudo-transonic similitude parameter for the case of a swept wing in supersonic flow. The results of the section on Cylindrical Flow of this paper are thus not new but confirm those of Berndt.

SYMBOLS

a	= sound velocity in the free stream
b	= wing span
c	= chord
f, g, h	= functions describing body shape
k	= generalized similitude parameter
s	= entropy distribution function
t	= conical coordinate
$\bar{x}, \bar{y}, \bar{z}$	= physical cartesian coordinates
x, y, z	= reduced cartesian coordinates
r, θ, z	= reduced cylindrical coordinates
C_p, C_D, C_L	= pressure, drag, and lift coefficients
D	= drag
K	= similitude parameter
M	= Mach Number in the free stream
N	= cylindrical flow constant
T, S	= absolute temperature and specific entropy
U	= free-stream velocity
AR	= aspect ratio
α	= angle of attack
γ	= ratio of specific heats in an ideal gas
η, ζ	= coordinates for reduced wave equation
κ	= additional second-order term parameter
λ	= constant for conical flow
ρ	= fluid density in the free stream
τ	= thickness ratio
ϕ	= physical perturbation velocity potential
ψ, Ψ, Φ	= reduced potential functions
Γ	= thermodynamic fluid parameter
Π, Δ, Λ	= general functions for pressure, drag, and lift

Subscripts

n	= normal
m	= mean
sl	= slender body

PRELIMINARY CONSIDERATIONS

The disturbance due to a body in a supersonic flow may be considered to be composed of a superposition of three-dimensional wave systems. In general it is possible to identify a reasonably small number of distinct wave systems, and this will be assumed to be so for the purposes of the considerations given here.

Three general principles are now stated which will bear on pseudotransonic similitude. Exceptions to these principles may be found, but their validity may be accepted with minor reservations. These principles are:

(*1*) *Wave Systems Approach Planar Wave Systems.*—By this statement it is meant that relations appropriate to a planar wave system will be approached, not that the overall geometry of a wave system will approach that of a planar system. Focusing wave systems are to some extent exceptions to this principle, but the region of focusing action is of limited extent and the statement is generally true downstream of such a region.

(*2*) *Some Second-Order Effects Have a Cumulative Action That Is Unavoidable.*—By unavoidable it is meant that the action will be of magnitude comparable with the first-order solution. Only such cumulative second-order effects have to be included in a first-order theory.

(*3*) *Relative and Absolute Orientation Must Be Distinguished.*—If the geometry of a structure, in this case that of a wave system or train, is affected by second-order effects, the relative orientation or local geometry of the structure is affected differently from the absolute orientation or location of the structure in the field.

A simple example is that of two consecutive weak shock waves originating a fixed distance apart in a two-dimensional flow (Fig. 1). These shocks will eventually coalesce and form one shock, contrary to the behavior of the linear solution. The coalescence of the shocks is governed by cumulative second-order effects; no matter how weak the shocks are they will always come together. The distance to the meeting point of the shocks is inversely proportional to the sum of the shock strengths. If this pattern is crossed by a wave in the other characteristic direction the relative orientation is not disturbed.

Another example taken from a different aerodynamic subject is appropriate, that of the rolling up of the vortex sheet behind a lifting system (Fig. 2), neglecting instability. The first-order structure of the vortex sheet is governed by its self-induced velocities and the sheet rolls up as a result of the unavoidable cumulative action of second-order effects. The structural pattern (and relative orientation) may be shown to be a function of the reduced downstream distance zC_L/bAR for a given spanwise lift distribution; thus, no matter how small the loading on the wing, there will be a distance z downstream for which a given pattern will appear. Absolute orientation of the vortex system depends on the quantity C_L/AR and would not be the same for wings of different loading.

The linearized potential equation is valid for an arbitrary fluid, while second- or third-order forms of the potential equation are usually expressed for a perfect gas of constant specific heats. This unnecessary restriction will not be made here, and the quantity

$(1/2)(\gamma + 1)$ appearing in usual second-order theories and transonic similitudes is replaced by the equivalent quantity Γ defined for an arbitrary fluid.

The Prandtl-Glauert coordinate transformation, which underlies essentially all similitude theories in compressible aerodynamics, is made at the beginning and the analysis is carried through entirely in the transformed coordinate system. The variable $\bar{z}$ or z is chosen for the axial direction.

The rotation engendered by shock waves is of the third order and is properly excluded in this theory, so that a velocity potential exists. In this theory, as in the ordinary transonic similitude, the entropy rise from shock waves does not affect the basic equations, but is significant in that it represents the eventual energy dissipation and forms the basis of one method of calculating the drag. Shocks are represented by surfaces across which the pressure and the normal component of the velocity are discontinuous, but across which the velocity potential is continuous.

Basic Equations

The equation for the perturbation velocity potential for the irrotational flow of a fluid with the free-stream Mach Number M may be expressed, to second-order terms,

$$\phi_{\bar{x}\bar{x}} + \phi_{\bar{y}\bar{y}} - (M^2 - 1)\phi_{\bar{z}\bar{z}} = \frac{2M^2}{U}\left[\Gamma M^2 \phi_{\bar{x}}\phi_{\bar{x}\bar{x}} + \frac{1}{2}\{\phi_{\bar{x}}^2 + \phi_{\bar{y}}^2 - (M^2 - 1)\phi_{\bar{z}}^2\}_{\bar{z}} + (\Gamma - 1)\phi_{\bar{z}}\{\phi_{\bar{x}\bar{x}} + \phi_{\bar{y}\bar{y}} - (M^2 - 1)\phi_{\bar{z}\bar{z}}\}\right] \quad (1)$$

where

$$\Gamma = (1/a)(\partial \rho a/\partial \rho)_s \quad (2)$$

evaluated under free-stream conditions. The quantity Γ is assumed to be always positive. In the special case of a perfect gas with constant specific heats the quantity Γ may be expressed

$$\Gamma = (1/2)(\gamma + 1) \quad (3)$$

The potential must satisfy the condition

$$\phi = 0 \qquad \text{at infinity} \quad (4a)$$

imposed upstream of the zone of action of the system of interest. The boundary condition

$$\phi_{\bar{y}} = U\tau f\left(\frac{\bar{x}\sqrt{M^2 - 1}}{c}, \frac{z}{c}\right) \quad (4b)$$

where τ is the thickness ratio and c is a reference chord length, is applied for the case of a flat body, with the mean-surface assumption. This particular choice of system is not fundamental to the theory, but the mean-surface assumption is.

The term in $(\Gamma - 1)$ in Eq. (1) is really of the third order and may be dropped. The Prandtl-Glauert coordinate transformation is made, together with a scale reduction by the factor c,

$$x = (\bar{x}\sqrt{M^2 - 1})/c \quad (5a)$$

$$y = (\bar{y}\sqrt{M^2 - 1})/c \quad (5b)$$

$$z = \bar{z}/c \quad (5c)$$

The dependent variable ϕ is transformed at the same time according to the equation

$$\phi = Uc\tau\,(M^2 - 1)^{-1/2}\psi \quad (6)$$

and the quantities K and κ are defined

$$K = \Gamma M^4 \tau\,(M^2 - 1)^{-3/2} \quad (7)$$

$$\kappa = (M^2 - 1)/\Gamma M^2 \quad (8)$$

The resulting equation for ψ is

$$\psi_{xx} + \psi_{yy} - \psi_{zz} = K[\psi_z^2 + \kappa(\psi_x^2 + \psi_y^2 - \psi_z^2)]_z \quad (9)$$

with the boundary condition

$$\psi_y = f(x, z) \qquad \text{on} \qquad y = 0 \quad (10)$$

Pseudotransonic Similitude

No similitude comes immediately out of Eq. (9). The limitation of the theory to those cases for which the term in κ is always much smaller than the other second-order term would be very restrictive. The similitude obtained by requiring both K and κ to be fixed would be of little practical value and could only relate certain systems with different values of Γ.

Only a first-order theory is sought, however, and only such second-order effects which have a cumulative action are to be retained. In any planar wave solution of the linearized equation the quantity $(\psi_x^2 + \psi_y^2 - \psi_z^2)$ is zero, and for any wave system approximating a planar one this quantity may be considered negligibly small. However, it may be of the same order of magnitude as ψ_z^2 in the intersection region of two wave systems or in a markedly nonplanar wave system. The intersection with a planar wave of a planar wave system having the other characteristic direction in two-dimensional flow (Fig. 3) is considered as a representative case. The term in ψ_z^2 due to the wave itself is nonzero and of the same magnitude all along the wave and clearly has a cumulative action. The term in $(\psi_x^2 + \psi_y^2 - \psi_z^2)$ is nonzero only in the intersection and partially cancels itself if the intersecting wave system contains both expansions and compressions; this term is definitely not cumulative. In general, the noncumulative nature of the κ term is connected with the first principle, that of the tendency of wave systems to approach planar ones.

The relative orientation or structure of a wave system is controlled by the cumulative term in ψ_z^2. The absolute orientation, however, is also affected by the κ term and will not follow the similitude to be expressed. In certain exceptional cases, however, the first-order

wave structure may be affected by the absolute orientation; such cases are exceptions to the validity of the similitude.

The κ term in Eq. (9) is now dropped* on the ground that it is noncumulative. The equation becomes

$$\psi_{xx} + \psi_{yy} - \psi_{zz} = 2K\psi_z\psi_{zz} \tag{11}$$

under the boundary condition of Eq. (10). Two solutions are similar with respect to first-order wave structure if, beside following the usual Prandtl-Glauert similitude, they have the same value of K; thus the quantity K is the basic similitude parameter in this theory. In view of the close relation between this theory and that of transonic flow this similitude is termed pseudotransonic.

The pressure perturbation including second-order terms is expressed

$$-\frac{1}{2}C_p = \frac{\tau}{\sqrt{M^2-1}}\left[\psi_z + \frac{1}{2}kK(\psi_x^2 + \psi_y^2 - \psi_z^2)\right] \tag{12}$$

where

$$k = (M^2-1)^2/\Gamma M^4 \tag{13}$$

With the mean-surface assumption included here the second-order term in Eq. (12) is properly dropped in a first-order theory, leaving

$$-(1/2)C_p = \tau(M^2-1)^{-1/2}\psi_z \tag{14}$$

For similarity under the usual Prandtl-Glauert transformation two bodies must have the same values of the incidence-to-thickness ratio α/τ and the reduced aspect ratio $\sqrt{M^2-1}\,AR$. In pseudotransonic similitude the same must be true, leading to the general functional equations

$$C_p = \tau(M^2-1)^{-1/2}\Pi(\sqrt{M^2-1}AR,\ \alpha/\tau,\ K,\ x,\ y,\ z) \tag{15a}$$

$$C_D = \tau^2(M^2-1)^{-1/2}\Delta(\sqrt{M^2-1}AR,\ \alpha/\tau,\ K) \tag{15b}$$

$$C_L = \alpha(M^2-1)^{-1/2}\Lambda(\sqrt{M^2-1}\,AR,\ \alpha/\tau,\ K) \tag{15c}$$

Except in such cases as that of a narrow wing yawed at approximately the wave angle, it is to be expected that the parameter K has little influence upon the values of C_D and C_L.

The theories of transonic and pseudotransonic similitudes have in common the facts that they are connected with the question of first-order wave structure, that they require the mean-surface assumption, that they use the Prandtl-Glauert coordinate transformation, and that they describe the entropy increase in the Trefftz plane. The transonic theory is different from the pseudotransonic theory in that in the transonic case all wave systems are essentially merged, that the pressures on the body are always affected by the second-order terms, and that there is no distinction between relative and absolute orientation.

The quantity Γ may be interpreted from the point of view of unsteady flow as the change in the signal velocity $(u + a)$ divided by the change in u. From this point of view the parameter K may be interpreted as the ratio of the age of the wave at a given corresponding point in the flow field [proportional to $(c/\sqrt{M^2-1}) \times (M/\sqrt{M^2-1})\ (1/a)$] and the time of transit of a signal velocity perturbation across the thickness of a wave system [proportional to $(\sqrt{M^2-1}/\tau UM) \times (1/\Gamma)(c/M)$]. There is an essential connection between first-order wave structure in steady and unsteady problems, and equivalent similitudes may readily be devised for various unsteady flow problems.

In order to generalize the similitude by relaxing the limitation imposed by the mean surface assumption it is necessary to require that $\sqrt{M^2-1}\,\tau$ be fixed as in the generalized Prandtl-Glauert similitude, and thus that the parameter k defined in Eq. (13) be fixed. In this case the only nontrivial similarity obtainable is between flows with different values of Γ. In this case the pressure is given by Eq. (12).

In case M is very large, both κ and k approach Γ^{-1} and K approaches $\Gamma\tau M$. Thus, with M large and with Γ fixed, pseudotransonic similitude goes over into the correct second-order form of hypersonic similitude.

Entropy Distribution

In linearized supersonic flow theory the drag on a finite system may be considered as divided into two parts, the vortex drag represented by the energy in the trailing vortex system arising from the lift distribution, and the wave drag represented by the energy in the outgoing wave system. These drags may correctly be computed in the linearized theory on the basis of the strict linearized vortex and wave patterns. These patterns are calculated at a distance away from the system of interest which is considered to approach infinity, despite the fact that with a small but finite disturbance the nonlinearity effectively destroys them within some finite distance.

The wave system is attenuated by shock waves and the wave drag eventually appears as entropy rise in the Trefftz plane with no contribution from wave energy. The entropy distribution in the Trefftz plane is governed by pseudotransonic similitude and may be used to calculate the drag.

The entropy rise across a weak shock may be expressed

$$T\delta S = (1/6)\ \Gamma M^4 U^2[(1/2)\delta C_p]^3 \tag{16}$$

which from the similitude gives the form

* A feature of the variational approach to linearized supersonic flow is that the volume integral of $(\psi_x^2 + \psi_y^2 - \psi_z^2)$ is minimized. At the New York meeting N. Rott commented that this approach shows the κ term should have little cumulative action and that this might be used as part of the reasoning.

$$T\delta S = \tau^2 U^2 K s(x, y) \tag{17}$$

Although this expression was obtained for a single shock a similar one also holds for the total effect of a number of them, because the entropy increases may be added; thus Eq. (17) will be considered to be the expression for the entropy increase in the Trefftz plane. The drag may be calculated by the integral

$$D = \int\int T\delta S \, d\bar{x} \, d\bar{y} \tag{18}$$

taken over the Trefftz plane. If the surface area on which the drag coefficient is based is equal to c^2AR, the function Δ of Eq. (15b) may be expressed

$$\Delta = (2K/\sqrt{M^2 - 1}\, AR)\int\int s(x, y) \, dx \, dy \tag{19}$$

integrated over the Trefftz plane. In any case Eqs. (18) and (15b) are consistent.

Slender-Body Theory

Slender-body theory applies to a class of bodies of very low aspect ratio and of gradual contour changes, without discontinuities in slope. The fundamental characteristic of any slender body is that in the vicinity of the body the velocity potential is a solution of Laplace's equation in the two lateral variables with the axial variable z as a parameter. The solution depends for any value of z on the body shape alone with no dependence on Mach Number, apart from an additive function of z which must be determined by conditions far from the body, which does have Mach Number dependence, and which determines the average pressure near the body. The Laplace equation cross-flow solution may be considered as the superposition of line source, dipole, quadrupole, etc., solutions, of which the source distribution solution generally predominates at moderate distances from the axis and thus determines the additional function of z. The equivalent source distribution is given only by the cross-sectional area distribution; these considerations are in accord with the supersonic slender-body theory of Ward[11] and the transonic equivalence law of Oswatitsch.[12*] The important point here is that in most cases the linear wave structure, and therefore the first-order wave structure, is determined by the cross-sectional area distribution (Fig. 4).

There are some cases, as that of a very thin wing or of a body of constant cross-sectional area whose camber line changes its angle of incidence, in which the source solution does not necessarily always predominate at moderate distances from the axis. The succeeding term, that of the dipole distribution governing lift forces, will be included here. For simplicity the basic body shape is assumed to be symmetric with respect to the planes $\theta = 0$ and $\theta = \pi/2$ in cylindrical coordinates, about a mean camber line. This mean camber line is assumed to have an angle of incidence normal to the plane $\theta = 0$ and equal to $\alpha h(z)$; if the camber line is straight and at an angle of attack α the shape function h is identical to one.

The thickness ratio is taken to be τ, as before. The aspect ratio AR appears as a transverse thickness ratio and may in most cases be replaced by τ, because geometrical conditions on the shape generally require that τ/AR be constant. In order to include the exceptional case of a slender flat body, however, the quantity is retained, with the understanding that $AR \geqq \tau$ in general. The cross-sectional area is given by $\tau AR c^2 g_0(z)$ where g_0 is a dimensionless shape function. The dipole distribution will be determined in terms of the distribution of the area corresponding to the total effective mass (including the cross-sectional area itself) of the cross section.[13] This area is expressed by $AR^2c^2g_1(z)$, where g_1 is another dimensionless shape function and satisfies the inequality $g_1 > (\tau/AR)g_0$.

The potential equation is expressed in terms of ϕ in reduced cylindrical coordinates, in the form

$$\phi_{rr} + \frac{1}{r}\phi_r + \frac{1}{r^2}\phi_{\theta\theta} - \phi_{zz} = \frac{2\Gamma M^4}{Uc(M^2 - 1)}\phi_z\phi_{zz} \tag{20}$$

In place of the transformation of Eq. (6) the transformation

$$\phi = Uc\tau AR\Phi(r, \theta, z) \tag{21}$$

is used, giving the equation

$$\Phi_{rr} + (1/r)\Phi_r + (1/r^2)\Phi_{\theta\theta} - \Phi_{zz} = 2K_{sl}\Phi_z\Phi_{zz} \tag{22}$$

where

$$K_{sl} = \Gamma M^4 \tau AR(M^2 - 1)^{-4} \tag{23}$$

is a pseudotransonic similitude parameter for slender bodies.

At moderate distances from the axis the radial derivative of the reduced potential may be expressed approximately

$$\Phi_r = \frac{\Phi_0(z)}{r} - \frac{\Phi_1(z)\sin\theta}{r^2} \tag{24}$$

The function Φ_0 may be evaluated

$$\Phi_0 = (1/2\pi)\, g_0'(z) \tag{25}$$

and, after some intervening analysis, Φ_1 may be evaluated

$$\Phi_1 = \frac{1}{2\pi}\frac{\sqrt{M^2 - 1}\,\alpha AR}{\tau} g_1(z)h(z) \tag{26}$$

The quantity $\sqrt{M^2 - 1}\ \alpha\ AR\ \tau^{-1}$ is an additional similarity parameter which determines the relative contribution of the dipole and source parts of the solution in the region away from the body where wave systems are important. If this parameter is small it

* This law states that the solution about a slender body in transonic flow may be obtained from that for any other body with the same cross-sectional area distribution by superposing the difference between the harmonic cross-flow solutions for the two bodies.

may be neglected for most body shapes. The pressure coefficient away from the body may be expressed to first-order terms

$$-(1/2)C_p = \tau AR\Phi_z \tag{27}$$

whence the functional equation may be given

$$C_p = \tau AR\, \Pi_{sl}(K_{sl}, \frac{\tau}{AR}, \frac{\sqrt{M^2-1}\ \alpha\ AR}{\tau}, r, \theta, z) \tag{28}$$

with the entropy distribution in the Trefftz plane of the form

$$T\delta S = \tau^2 AR^2(M^2 - 1)K_{sl}s_{sl}(r, \theta) \tag{29}$$

If, as has been discussed, the parameter $\sqrt{M^2-1} \times \alpha AR\tau^{-1}$ may be neglected, the variation with respect to θ in Eqs. (28) and (29) may also be neglected.

In the case of a slender planar body, for which the mean surface assumption applies, the parameter τ/AR is small and any functional dependence on it in the formulas given above may be neglected. In the case of a slender body of revolution the quantity AR may be replaced by τ in the formulas above, and $g_1 = 2g_0$.

Two-Dimensional Flow

The case of the flow on one side of a two-dimensional body is now considered, with only a single wave family present. In this case the κ term of Eq. (9) is of third order throughout the field and absolute orientation will follow the similitude; this restriction to a single wave family is not essential but is made for convenience.

Dropping the lateral variable Eq. (11) may be expressed

$$\psi_{yy} - \psi_{zz} = 2K\psi_z\psi_{zz} \tag{30}$$

The new variable

$$\zeta = z - y \tag{31}$$

is introduced in place of z, giving the equation

$$\psi_{yy} - 2\psi_{y\zeta} = 2K\psi_\zeta\psi_{\zeta\zeta} \tag{32}$$

With only the single wave family oriented along the planes ζ = constant, the term ψ_{yy} is of higher order and may be dropped. Another change of variable is made

$$\eta = Ky \tag{33}$$

and leads to the equation

$$\psi_{\eta\zeta} + \psi_\zeta\psi_{\zeta\zeta} = 0 \tag{34}$$

which will be termed the reduced wave equation. The boundary condition at upstream infinity is a null one, as before, and on the body is

$$\psi_\zeta = -f(\zeta) \qquad \text{on} \qquad \eta = 0 \tag{35}$$

The quantity K is not a fundamental similitude parameter in this case, but appears as a lateral scale factor. The extended pseudotransonic similitude of this case may be expressed: at a given Mach Number the product of the intensity of a two-dimensional wave system and the distance at which a certain first-order wave structure pattern appears is a constant. Note the close analogy here with the vortex system behavior discussed above.

Finite Systems

A finite planar system is now considered, for which the assumption is made that nonlinear effects are unimportant within a distance from the axis of several times the span or $1/\sqrt{M^2-1}$ times the chord of the system, so that the linearized wave pattern at a distance from the body can be assumed to have been approximately established. The details of this linearized wave pattern have been previously discussed by the writer in his doctoral thesis[14] in connection with the computation of the wave drag of a finite system. Since the wave system has a geometric attenuation as the inverse half power of the radius, it is convenient to make the transformation

$$\psi = r^{-1/2}\Psi \tag{36}$$

in order to be working with a function which varies relatively slightly with r. The equation for Ψ in cylindrical coordinates is

$$\Psi_{rr} + (1/4r^2)\Psi + (1/r^2)\Psi_{\theta\theta} - \Psi_{zz} = 2Kr^{-1/2}\Psi_z\Psi_{zz} \tag{37}$$

The transformation of Eq. (31) is made with r in place of y

$$\zeta = z - r \tag{38}$$

and leads to the equation

$$\Psi_{rr} + (1/4r^2)\Psi + (1/r^2)\Psi_{\theta\theta} - 2\Psi_{r\zeta} = 2Kr^{-1/2}\Psi_\zeta\Psi_{\zeta\zeta} \tag{39}$$

under a boundary condition of the form

$$\Psi_\zeta = -f(\zeta, \theta) \qquad \text{on} \qquad r = r_0$$

where r_0 is large enough so that the linearized distant wave pattern has become established but not so large that nonlinear effects have appreciably changed the wave shape. For $r \geqq r_0$ the first three terms of Eq. (39) may be dropped as being negligible. With these terms dropped the boundary condition may be displaced to $r = 0$, this process probably compensating somewhat for the errors in ignoring nonlinear effects for $r < r_0$. The variable η is defined for this case

$$\eta = 2Kr^{1/2} \tag{40}$$

and the resultant equation is the reduced wave equation

$$\Psi_{\eta\zeta} + \Psi_\zeta\Psi_{\zeta\zeta} = 0 \tag{41}$$

with the boundary condition

$$\Psi_\zeta = -f(\zeta, \theta) \qquad \text{on} \qquad \eta = 0 \tag{42}$$

in the form as Eqs. (34) and (35) except for the appearance of θ as a parameter.

The same comments are appropriate here as for the two-dimensional case, except that the product which is constant is that of the square of the intensity and the distance at which a given pattern appears. The function f is proportional to the radial velocity in the distant field and must be obtained using the coincident signal concept of the writer.[14] This method may also be applied to bodies of revolution, without the parameter θ, in which case the function f is proportional to the function $F(y)$ of Whitham.[6] No similitude for bodies of revolution other than slender ones is obtained, however, because in general f or F depends on the Mach Number and thickness ratio as well as on the body shape. Whitham's method for determining the first-order wave structure may also be applied to the finite system case, but in this paper a direct characteristic method is used.

Reduced Wave Equation

The reduced wave equation, Eq. (34) or Eq. (41), has an immediate first integral

$$\psi_\eta + (1/2)\psi_\zeta^2 = 0 \tag{43}$$

More important, however, are the characteristics determined by

$$d\zeta - \psi_\zeta \, d\eta = 0 \tag{44}$$

along which ψ_η and ψ_ζ are constant. These characteristics are straight lines in the (η, ζ) plane.

Shock waves must be treated separately but provide no difficulties. The condition that ψ must be continuous may be used to show that Eq. (44) may still be used to describe the orientation of the shock if ψ_ζ is replaced by the mean of its values on either side

$$\psi_{\zeta_m} = (1/2)(\psi_{\zeta_1} + \psi_{\zeta_2}) \tag{45}$$

The shock waves will, in general, be curved. With the boundary conditions of Eq. (35) or Eq. (42), the solution may be readily obtained by means of a characteristic construction on the (η,ζ) plane; the position and strength of any shock that appears is obtained by the solution of an ordinary differential equation. It may be noted that shocks can begin at a finite distance in the flow but that they never die out within a finite distance.

The asymptotic structure for large values of η is usually an N-wave, which is bounded front and rear by two shock waves and has a uniform expansion region in between. If ϕ returns to zero behind the wave, which is generally the case (in two-dimensions the body must be closed), the two shocks are of equal strength. The distance between the shocks varies as $\eta^{1/2}$ and hence as the square root of the intensity. In general the asymptotic pattern depends upon the extreme values of ϕ in the wave system.

In the body of revolution or finite-system case the N-wave width varies as $r^{1/4}$ and the shock strength as $r^{-3/4}$, as was first noted by DuMond et al.[5]

Cylindrical Flow

Of particular interest, because they serve to link pseudotransonic and transonic similitudes, are considerations of cylindrical flow with the normal Mach Number concept. If M_n is the normal Mach Number corresponding to a given orientation on a plan form in a supersonic flow, the quantity

$$N = [(M_n^2 - 1)/M_n^2][M^2/(M^2 - 1)] \tag{46}$$

is preserved under a Prandtl-Glauert transformation. Following the concepts of cylindrical flow the apparent thickness ratio τ_n for the normal flow component is given by

$$M_n\tau_n = M\tau \tag{47}$$

Defining the normal similarity parameter K_n with respect to normal quantities, the result is obtained

$$K_n = \Gamma M_n^4 \tau_n (M_n^2 - 1)^{-3/2} = N^{-3/2}K \tag{48}$$

and shows that K_n is preserved in any Prandtl-Glauert transformation for which the basic parameter K is preserved.

If the normal Mach Number for a given orientation is close to one, K_n becomes the usual transonic similarity parameter for the normal flow. Thus pseudotransonic similitude corresponds to normal transonic similitude in cases for which normal transonic effects are present. including noncylindrical wings for which the normal Mach Number on the leading edge is close to one. In the case of a noncylindrical wing with the normal flow past a trailing edge close to sonic, the situation is different; normal transonic effects depend upon the absolute orientation of the corresponding wave systems. This absolute orientation generally does not follow pseudotransonic similitude where the wave systems in question are not in an undisturbed part of the flow field. Thus normal transonic effects on trailing edges do not follow pseudotransonic similitude in general.

Conical Flow

In linearized supersonic conical flow the wave systems involved are of two types, of the essentially two-dimensional type occurring along the characteristic planes tangent to the Mach cone and of the conical type associated with the Mach cone itself. The first type can mostly be handled through the two-dimensional and cylindrical flow developments given above; the second type demands special attention. If the conical wave system lies in the zone of action of one of the planar wave systems, the absolute orientation is not maintained under the similitude and must be related to the local characteristic plane orientation. Since this local characteristic plane orientation may be ob-

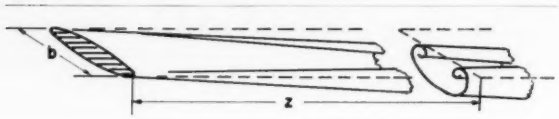

FIG 2. Rolling-up of vortex sheet.

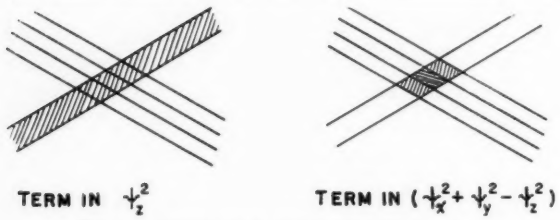

FIG. 3. Second-order terms in an intersection.

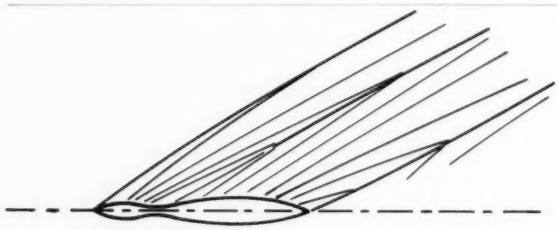

FIG. 4. Slender body of revolution.

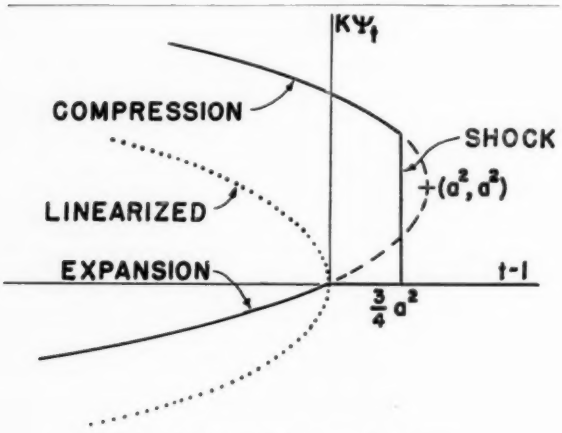

FIG. 5. Conical solutions near Mach cone.

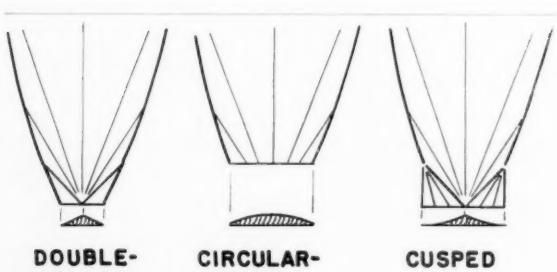

FIG. 7. Comparison of three 2-dimensional solutions.

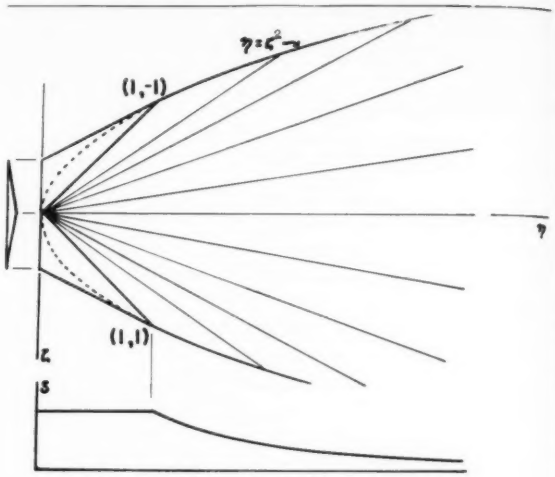

FIG. 6. Solution for double-wedge airfoil.

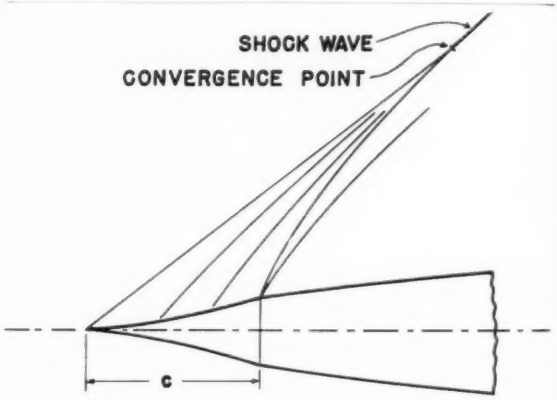

FIG. 8. Cusped nose on a body of revolution.

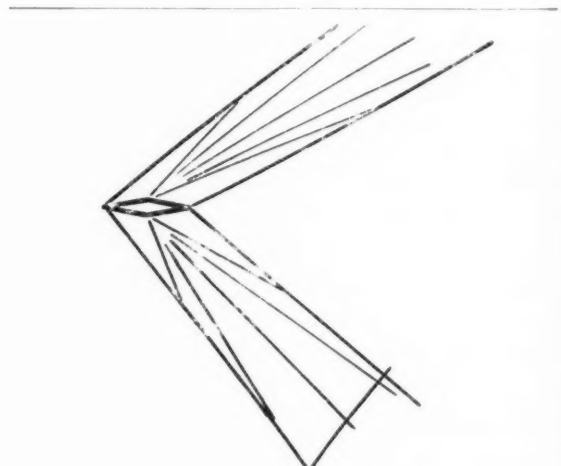

FIG. 9. Ring airfoil of high aspect ratio.

tained straightforwardly and the relative orientation does follow the similitude, attention can be restricted to the case where the conical wave lies in an undisturbed flow. In any case, since the conical property of the supersonic flow about a conical body does not depend upon linearization, the first-order wave structure must be conical over the entire field.

With the conical coordinate

$$t = r/z \tag{49}$$

introduced in place of r, and with the variable separation

$$\psi = z^n \Psi(t, \theta) \tag{50}$$

Eq. (11) becomes

$$(1 - t^2)\Psi_{tt} + (1/t)(1 - 2t^2 + 2nt^2)\Psi_t + (1/t^2)\Psi_{\theta\theta} - n(n - 1)\Psi = -2z^{n-1}K\Psi_t\Psi_{tt} \tag{51}$$

in which the contribution to the nonlinear term from waves outside the Mach cone has been neglected and this term has been approximated in the vicinity of $t = 1$. Carrying out this approximation for the linear part of the equation and considering θ as a parameter the approximate form

$$(1 - t)\Psi_{tt} + [n - (1/2)]\Psi_t + z^{n-1}\Psi_t\Psi_{tt} = 0 \tag{52}$$

is obtained, valid only near the Mach cone. Except for the special cases $n = (1/2), (3/2)$ the integral may be expressed implicitly

$$K\Psi_t = \lambda(\theta)\left[(1 - t) - \frac{z^{n-1}}{n - 3/2}K\Psi_t\right]^{n-1/2} \tag{53}$$

where λ is a function of θ, corresponding to the linear solution,

$$\Psi_t = \lambda(\theta)K^{-1}(1 - t)^{n-1/2} \tag{54}$$

The case of interest here is that of regular conical flow, for which $n = 1$. In this case Eq. (53) may be solved explicitly

$$K\Psi_t = \lambda^2 \pm \lambda\sqrt{\lambda^2 + 1 - t} \tag{55}$$

In this equation the positive sign is to be taken for a compression-type solution and the negative sign for an expansion-type solution. The latter is cut off at $t = 1$, while the limit of the compression solution is determined by the shock condition

$$t - 1 = (1/2)K\Psi_t \tag{56}$$

giving the shock at

$$t - 1 = (3/4)\lambda^2; \quad K\Psi_t = (3/2)\lambda^2 \tag{57}$$

These solutions are shown on Fig. 5 and agree with those of Lighthill.[8] This general picture of the first-order structure of the conical wave system shows that the principal effects are of the second order in the intensity. At singular lines on the Mach cone, such as where a two-dimensional wave system intersects the cone, a more complicated treatment is necessary which takes into account variations with θ. The investigation of Vincenti[9] dealt with conical wings with leading edges near the Mach cone, for which variations in θ are important.

Examples

(A) *Three Two-Dimensional Airfoils*

Three symmetric two-dimensional airfoils with the same maximum thickness τ are now treated using the reduced wave equation technique. One is a double wedge foil of chord 1 and thickness ratio τ; the other two are of chord 2 and thickness ratio $\tau/2$, one a circular arc foil and the other a cusped foil with two inverted circular arcs. These three foils have the same maximum thickness, and hence the same minimum values of the velocity potential. Only the upper sides of these foils are considered.

The first-order wave pattern for the first foil is shown in Fig. 6. With the foil lying between $[0, -(1/2)]$ and $[0, +(1/2)]$ on the (η, ζ) plane, the bow shock has a straight section from the point $[0, -(1/2)]$ to $(1, -1)$ and a parabolic section following the curve

$$\eta = \zeta^2 \tag{58}$$

to infinity. The stern shock is oriented symmetrically with respect to the η axis. From the origin extends a Prandtl-Meyer fan, which for $\eta > 1$ fills the entire space between the shocks.

The other two foils also have wave patterns which are symmetric fore and aft, and the three patterns are compared in Fig. 7. The solution for the second, the circular-arc airfoil may be obtained immediately by considering it located between $(1, -1)$ and $(1, 1)$ in the diagram of the first. The solution for the third is similar to that for the first, except that a reverse Prandtl-Meyer fan fills the triangular region $(0, -1)$, $(0, 0)$, $(1, -1)$.

It is easily seen from the entropy increase distributions that the drags of the second and third foils are equal and less than (actually two-thirds times) that of the first.

(B) *Cusped Nose on a Body of Revolution*

In order to exemplify the slender body theory, a body of revolution at zero incidence is considered which has a cusped nose whose shape may be expressed

$$r = \tau\sqrt{M^2 - 1}\, z^{3/4} \tag{59}$$

in reduced coordinates. Only the flow within the zone of action of this tip is to be considered, and the body aft of the tip is assumed to have such a shape that it will not cause interference within the region of interest. The appropriate solution is given from source methods as

$$\phi = -\frac{5}{4} Uc\tau^2 \int_r^z \frac{(z - z')^{3/2}\, dz'}{\sqrt{z'^2 - r^2}} \tag{60}$$

for which the approximate form near the axis is

$$\phi \doteq -(5/4) Uc\tau^2 z^{3/2} \ln (2z/r) \tag{61}$$

The precise quadrature involves elliptic integrals and is not necessary for the purpose of this treatment. In the vicinity of the wave system the linearized solution may be expressed

$$\phi \doteq -(15\pi/32)\, Uc\tau^2 (z - r)^2 (2r)^{-1/2} \tag{62}$$

Returning to the terminology of the finite-system analysis and replacing $\tau/\sqrt{M^2 - 1}$ by τ^2 in accordance with the slender-body theory, the boundary condition of Eq. (42) may be expressed

$$f = (15\pi/16\sqrt{2})\zeta \tag{63}$$

The solution of the reduced wave equation in this case is direct and essentially the same as that for the front half of the third airfoil of the previous example. The characteristics all converge to a point at

$$\eta = 16\sqrt{2}/15\pi \tag{64}$$

or at a value of the physical radius equal to

$$\frac{cr}{\sqrt{M^2 - 1}} = \frac{128}{225\pi^2} \frac{c(M^2 - 1)^{3/2}}{\Gamma^2 M^8 \tau^4} \tag{65}$$

Beyond this point a shock appears, whose position and strength are controlled by the body shape behind the cusped nose. This example is illustrated in Fig. 8.

(C) *Ring Airfoil of High Aspect Ratio*

A ring airfoil is now considered, with the usual quasi-cylinder assumption, and for which the chord is small compared with $\sqrt{M^2 - 1}$ times the radius of the ring (Fig. 9). This latter restriction allows the local flow about the airfoil to be considered two-dimensional and permits the approximation of the section on finite systems to be used. With the radius of the ring equal to $cr_0/\sqrt{M^2 - 1}$, the transformations

$$\psi = (r_0^{1/2}/r^{1/2})\Psi \tag{66}$$

$$\zeta = z - r - r_0 \tag{67}$$

$$\eta = 2K(r^{1/2} - r_0^{1/2}) r_0^{1/2} \tag{68}$$

yield the reduced wave equation with boundary conditions corresponding to the two-dimensional reduction. The solution of the reduced wave equation gives the first-order wave solution exterior to the ring. As before, the angle θ may be kept as a parameter, except near singular points.

For the interior of the ring the transformations may be altered by changing the sign of r and r_0 in Eq. (67), and the sign of η in Eq. (68). The waves in the interior of the ring have a focusing action, and the approximate solution loses its validity near the axis.

References

[1] Von Kármán, Th., *The Similarity Law of Transonic Flow*, J. Math. and Phys., Vol. 26, pp. 182–190, 1947.

[2] Friedrichs, K. O., *Formation and Decay of Shock Waves*, Comm. Pure and Appl. Math., Vol. 1, pp. 211–245, 1948.

[3] Lighthill, M. J., *The Energy Distribution Behind Decaying Shocks*, Phil. Mag., Ser. 7, Vol. 41, pp. 1101–1128, 1950.

[4] Pythian, J. E., *The Energy Distribution Behind a Decaying Two-dimensional Shock*, Quart. J. Mech. and Appl. Math., Vol. 5, pp. 318–323, 1952.

[5] DuMond, J. W. M., Cohen, E. R., Panofsky, W. K. H., and Deeds, E., *A Determination of the Wave Forms and Laws of Propagation and Dissipation of Ballistic Shock Waves*, J. Acoust. Soc. Amer., Vol. 18, pp. 97–118, 1946.

[6] Whitham, G. B., *The Flow Pattern of a Supersonic Projectile*, Comm. Pure and Appl. Math., Vol. 5, pp. 301–348, 1952. See also Proc. Roy. Soc. A, Vol. 201, pp. 89–109, 1950.

[7] Whitham, G. B., *The Propagation of Spherical Blast*, Proc. Roy. Soc. A, Vol. 203, pp. 571–581, 1950. See also *The Propagation of Weak Spherical Shocks in Stars*, Comm. Pure and Appl. Math., Vol. 6, pp. 397–414, 1953.

[8] Lighthill, M. J., *The Shock Strength in Supersonic "Conical Fields,"* Phil. Mag., Ser. 7, Vol. 40, pp. 1202–1223, 1949.

[9] Vincenti, W., private communication.

[10] Berndt, S. B., *Similarity Laws for Transonic Flow Around Wings of Finite Aspect Ratio*, Section 4, Technical Note KTH-AERO TN 14, Royal Institute of Technology, Stockholm, 1950.

[11] Ward, G. N., *Supersonic Flow Past Slender Pointed Bodies*, Quart. J. Mech. and Appl. Math., Vol. 2, pp. 75–97, 1949.

[12] Oswatitsch, Kl., and Keune, F., *Nichtangestellte Körper kleiner Spannweite in Unter- und Überschallströmung*, VIII Int. Congress Th. and Appl. Mech., Istanbul, August, 1952.

[13] Lamb, Sir Horace, *Hydrodynamics*, Section 72a, Sixth Edition, Cambridge University Press, 1932.

[14] Hayes, W. D., *Linearized Supersonic Flow*, Section 38, thesis, Calif. Inst. of Tech., 1947; also as North American Aviation Report AL-222, 1947.

Transition-Point Fluctuations in Supersonic Flow

JOHN C. EVVARD,* MAURICE TUCKER,† AND WARREN C. BURGESS, JR.†

Lewis Flight Propulsion Laboratory, NACA

ABSTRACT

Random movements of the transition-point location on a 10° cone were observed at supersonic speeds by means of many flash schlieren photographs. Distribution functions that statistically define the transition-point location were determined in two supersonic wind tunnels for several values of Mach Number, Reynolds Number per foot, and free-stream turbulence intensity. Concomitant temperature-recovery-factor distributions were measured for all test conditions.

The axial extent of the transition-point distribution function determined from schlieren data increased with tunnel turbulence level. Corresponding axial extensions of the transition region denoted by recovery-factor measurements were observed. The data suggest that a sharp transition from laminar to turbulent flow takes place and that this flow pattern moves randomly along the aerodynamic surfaces. With the use of the statistical distribution functions obtained from schlieren data and surface temperatures as time-averaged by the surface thermocouples, a hypothesized instantaneous surface-temperature distribution was calculated for eight sets of experimental measurements.

INTRODUCTION

SINCE THE STUDIES of Osborne Reynolds, many hundreds of experiments have been conducted to determine the cause and location of the transition region between laminar and turbulent flows. Engineering rules were formulated on the basis of these experiments both for pipes and for aerodynamic surfaces, so that quantities such as skin friction, which depend on the location of transition, could be satisfactorily predicted. The effectiveness of such rules often leads to false confidence among the general engineering profession that the transition process is well understood. Yet in spite of excellent pioneering research contributions by Tollmien and Schlichting,[1] Lees and Lin,[2, 3] G. I. Taylor,[4] and others, the transition process has not been clearly defined.

Perhaps part of the difficulty has resulted from lack of sufficiently precise instrumentation in the transition region. Certainly such visual schemes as film-drying techniques or fluorescent lacquers could only be expected to yield averaged information.

In order to obtain detailed information, exhaustive studies utilizing hot-wire equipment appear necessary. Yet, with the recently expanded interest in supersonic flow and the almost universal application of shadowgraph and schlieren photography, observations and concepts concerning transition that were not generally recognized heretofore have arisen without the use of hot-wire equipment.

One such observation contradicts the popular notion of a steady transition-point location. Schlieren and shadowgraph studies,[5–9] with short-duration exposures, have demonstrated that the transition point on bodies mounted in supersonic wind tunnels fluctuates rapidly with time along the body surface. While such fluctuations might be attributed to the turbulence of the stream, they have also been observed on models in supersonic free-flight tests conducted by Jedlicka, Wilkins, and Seiff of the NACA Ames laboratory. Likewise Schubauer (through private communication) has noted, by means of hot-wire pairs, the occurrence of transition-point fluctuations in low-speed subsonic flows.

Anticipating these experimental observations are the theoretical studies of Emmons, and Emmons and Bryson.[9, 10] They visualize the transition process as resulting from the growth of turbulent spots randomly formed in the boundary layer. The origin of these spots might arise from free-stream turbulence, from noise, or from model vibrations, as suggested in reference 10; or possibly their origin might be traced to dust particles crashing at high speeds into the boundary layer.

That turbulent spots can occur has been demonstrated by water-table experiments[9] and by schlieren photographs of models in supersonic flow, which occasionally show regions of turbulent boundary layer followed downstream by laminar flow.[8, 9] At least in the wind-tunnel experiments of Evvard, Tucker, and Burgess,[8] however, the growth of isolated turbulent spots was seldom observed on a 10° cone in supersonic flow. Rather, the transition preferred to occur abruptly, followed downstream by flow that was predominantly turbulent. The transition-point location was not steady but fluctuated longitudinally along the body surface.

Regardless of the mechanism whereby transition is initiated, the phenomenon can no longer be regarded as steady. Most published curves of skin friction, temperature-recovery factor, or heat transfer through the transition region should probably be regarded as time averages of a complicated transition state that includes fluctuating transition points, multiple laminar regions,

Presented at the Aerodynamics Session, Twenty-Second Annual Meeting, IAS, New York, January 25–29, 1954.

* Chief, Supersonic Propulsion Division.

† Aeronautical Research Scientist.

or other transient phenomena. Because such complications involve a degree of randomness, statistical studies of the transition region are suggested.

The present paper includes a statistical study of transition-point fluctuations on a thin-walled, stainless-steel 10° cone at supersonic speeds. The distribution functions for the transition-point locations have been determined by means of a multiplicity of short-exposure schlieren photographs. Concurrent temperature and recovery-factor distributions were recorded with surface thermocouples mounted along a ray of the same cone. Eight sets of measured surface temperatures and statistical distribution functions were utilized to calculate the shape of a hypothesized instantaneous surface-temperature distribution. These investigations were conducted at the NACA Lewis laboratory during the spring and summer of 1953. Special thanks should be extended to Hugo Heermann, who conducted the numerical calculations to obtain the instantaneous surface-temperature distributions.

Symbols

g = probability density; the function $g(\eta)\,d\eta$ represents the fraction of time that the transition point is located between η and $\eta + d\eta$

G = statistical distribution; the function $G(x) = \int_{\alpha}^{x} g(\eta)\,d\eta$ represents the fraction of time that transition is upstream of point x

$\bar{g}$ = average g over long time period during which flow conditions change

M = Mach Number

q = dynamic pressure

Re = Reynolds Number

r = recovery factor

r_i = instantaneous recovery factor

t = time

T = surface temperature

$\bar{T}$ = average surface temperature over long time period during which flow conditions change

x = radial distance from cone apex

α = upstream limit of transition-point movement, $g(\eta) = 0$ for $\eta < \alpha$

β = downstream limit of transition-point movement, $g(\eta) = 0$ for $\eta > \beta$

δ^* = boundary-layer displacement thickness

η = radial location from cone apex of instantaneous transition point

θ = instantaneous surface-temperature distribution function

Apparatus and Procedure

The transition studies of this report utilized two thin-walled 10° stainless-steel cones. Eight sets of test conditions were employed for which the recovery-factor distributions and the statistical distribution functions for the transition-point location were measured. The Ames cone, described in reference 11, was available for test 1 only. The Lewis cone, which was used as the model for tests 2 to 8, is similar to the Ames cone as regards included angle of 10°, wall thickness of 0.032 in., material of 18-8 stainless-steel alloy, and surface finish (maximum roughness less than 15 microin.), but is $18\,^{7}/_{16}$ in. long instead of 15 in., and internal dimensions differ somewhat near the apex as shown in Fig. 1. The two cones also differ in the number and spacing of the constantan thermocouple wires soldered into holes in the shell. A single stainless-steel wire connected to the model base completes the thermocouple circuit for each cone.

Results obtained from either cone are believed comparable. Under equilibrium conditions, the surface of these models closely simulated the ideal adiabatic surface in view of the stagnant air in the cone interior and of the thin walls and relatively poor conductivity of stainless steel.

Although the instruments used with the thermocouples have accuracies within ±0.25°F., repeatability of temperature measurements during a temperature survey was probably ±0.5°F. because of gradual changes in tunnel stagnation temperature. The change in stagnation temperature during the schlieren observations to be described was about 3°F. for tests 1 to 4. The corresponding temperature change for tests 5 to 8 was much greater, amounting to 46° for test 8. Most of the variation occurred during the first quarter of the run.

The location of the transition points for all tests was obtained by means of a multiplicity of schlieren photographs of about 1-microsec. exposure time. For tests 1 to 4, these photographs were taken at approximately uniform intervals of 20 sec. For tests 5 to 8, the time interval was about 7 sec.

Tests 1 to 4 were conducted in the Lewis 1- by 1-ft. supersonic wind tunnel, which is a continuous-flow, nonreturn, variable-pressure tunnel operating at a Mach Number of 3.12 with the specific humidity sufficiently low (about 4×10^{-5} lbs. water/lb. dry air throughout most of any given run) to eliminate condensation effects. Two cylindrical settling-chamber configurations were used to vary the stream-turbulence level.

In the original configuration (A), the flow entered parallel to the settling-chamber axis, which was transverse to the tunnel-nozzle axis. A screen having a pressure drop of $8q$, where q designates local stream dynamic pressure, was located in the settling chamber; and a screen with pressure drop of $2q$ was placed at the exit of the settling chamber. Measurements of the longitudinal turbulence intensity were made at the Mach Number 0.12 station upstream of the throat with a hot-wire probe employing tungsten wire 0.0002 in. in diameter and 0.080 in. long. An intensity of 9.4 per cent was obtained for test 1. Because configuration A resulted in a high turbulence level, the settling chamber was replaced. In the revised configuration (B), the entrance-air direction and settling-chamber axis were parallel to the nozzle axis in order to achieve a straight-through flow. Four damping screens having an overall pressure drop of $10q$ were placed in the settling chamber. A honeycomb was also installed upstream of the screens.

For configuration B, measurements of the longitudinal turbulence intensity were also made at the Mach Number 0.12 station, yielding intensities of 1.0 ,0.75, and 0.5 per cent at the pressure levels for tests 2, 3, and 4, respectively (see Table 1). Inasmuch as the same nozzle blocks were used for both configurations A and B, the upstream turbulence intensities could be used as a measure of the test-section turbulence level. Readings of the apparent intensity were also taken in the test section for configuration B. These intensities were 3.5 per cent for test 2 and 1.0 per cent for tests 3 and 4. These apparent intensities should be regarded as qualitative. Measurements of a preliminary nature revealed the presence of a peak in the energy-spectrum curve below about 40 cycles per second for both configurations A and B. The frequency range of the peak suggests that the indicated turbulence intensities include the effects of stream disturbances other than turbulence that could arise from tunnel piping resonances or from the compressor system. The amplitude of the peak was much lower, however, for configuration B, reflecting the greater effectiveness of the damping-screen arrangement.

The NACA Lewis 8- by 6-ft. supersonic wind tunnel, utilized for tests 5 to 8, has a continuous nonreturn circuit. Air is pumped through dryer beds by means of a seven-stage axial-flow compressor located about 150 ft. upstream of the test section. A large calming chamber just upstream of the throat contains a honeycomb and 1.8q screen. The location of the model was approximately 30 ft. downstream of the tunnel throat. The Mach Number of the tunnel can be varied between 1.5 and 2.0 by contouring the vertical flexible stainless-steel walls. With the $M = 1.5$ wall setting, the tunnel may also be operated subsonically at a Mach Number of 0.63.

The tunnel Reynolds Number has an approximately constant value of 4.3×10^6 per foot for all Mach Numbers. Because there is no heat exchanger in the circuit, the stagnation temperature of the air stream may vary, depending upon the tunnel Mach Number setting, the

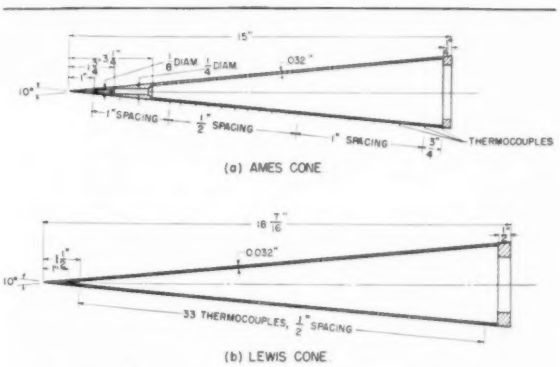

FIG. 1. Cone geometries and thermocouple locations.

TABLE 1

Test number	Tunnel	Mach number	Stagnation pressure, lb/sq in. abs	Stagnation temperature, °F	Test-section Reynolds number per foot	Number of schlieren photographs	Indicated longitudinal turbulence intensity, percent	
							Mach 0.12 station	Test section
1	1x1-A	3.12	28.55	43.9	4.8×10^6	183	9.4	---
2	1x1-B	3.12	17.67	44.0	3.0	367	1.0	3.5
3	1x1-B	3.12	29.01	46.0	4.8	272	0.75	1.0
4	1x1-B	3.12	40.11	48.8	6.6	595	0.5	1.0
5	8x6	0.63	16.8 17.05 17.01	161 144	3.5 3.6	426		
6	8x6	1.5	17.75 17.75 17.97 17.6 17.62	203.5 196 184 174 168	4.1 4.25 4.35 4.38 4.45	404		
7	8x6	1.7	20.18 19.15 19.20 19.26 19.40	161 228 223 215 205	4.95 4.0 4.1 4.2 4.3	360		
8	8x6	1.9	21.69 21.69 21.63 21.70	176 226 225 222	4.65 4.25 4.25 4.28	368		

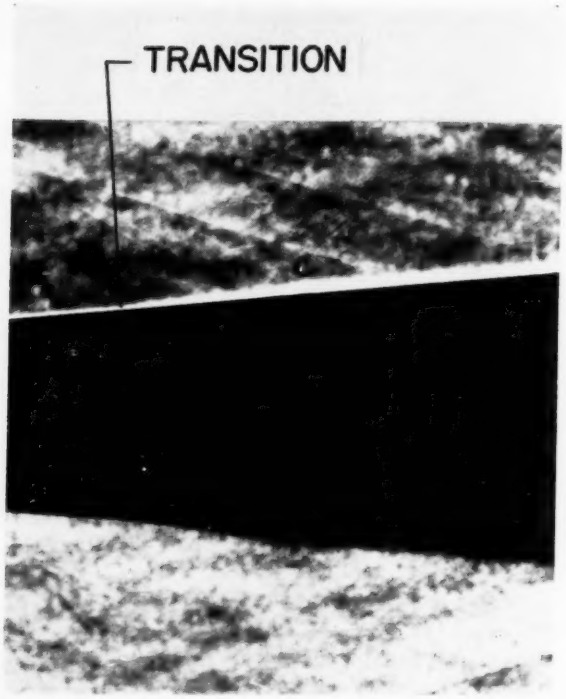

FIG. 2. Schlieren of transition on cone. Exposure, 1 microsec.

ambient-air temperature, the atmospheric humidity, and the condition of the dryer beds. The largest changes in temperature occur during a given run on hot damp summer days, which unfortunately coincided with the only period that the tests described herein could be scheduled. Approximate operating conditions and pertinent data taken during the course of the various tests are summarized in Table 1.

RESULTS AND DISCUSSION

The experimental distributions of recovery factor[11, 12] and local skin friction coefficients[13] seemingly imply that the change from laminar to turbulent flow in the boundary layer is gradual. Inasmuch as the transition point has a fluctuating location[5–8] this implication may be erroneous. High-speed schlieren photographs illustrate that transition is in fact a rather abrupt phenomenon (Fig. 2).

Many photographs of the cone flow, such as Fig. 2, were taken at each test condition. All these schlierens showed abrupt transition points, the locations of which were distributed in a random manner in the "transition region." From the data, the number of times transition occurred upstream of a given location x on the cone was obtained. Division of this number by the total number of cases (Table I) yielded the proportion of the time that transition occurred upstream of a specified point. This function $G(x)$ is known as the statistical distribution function pertaining to that location. A second statistical quantity, the probability density $g(\eta)$, may be defined. The function $g(\eta)\ d\eta$ represents the fraction of the time or the chance that the transition point is located between η and $\eta + d\eta$. The relation between the two functions is given by

$$G(x) = \int_{\alpha}^{x} g(\eta)\ d\eta \qquad (1)$$

The distribution functions and the probability densities were obtained from analysis of the schlieren data. Temperature distributions on the surface of the cone were measured concurrently with the schlieren observations and will be presented in terms of recovery factor. The rest of this paper is primarily concerned with an analysis of the data so obtained. A word of caution is perhaps warranted. Transition-point locations might be sensitive to minor changes in the cone surface or its geometry. Though considerable care was taken to prevent such changes, it is by no means certain that the results from the individual tests are comparable.

EFFECT OF FREE-STREAM TURBULENCE LEVEL

Fig. 3 compares the recovery-factor and the statistical distribution functions obtained at the two free-stream

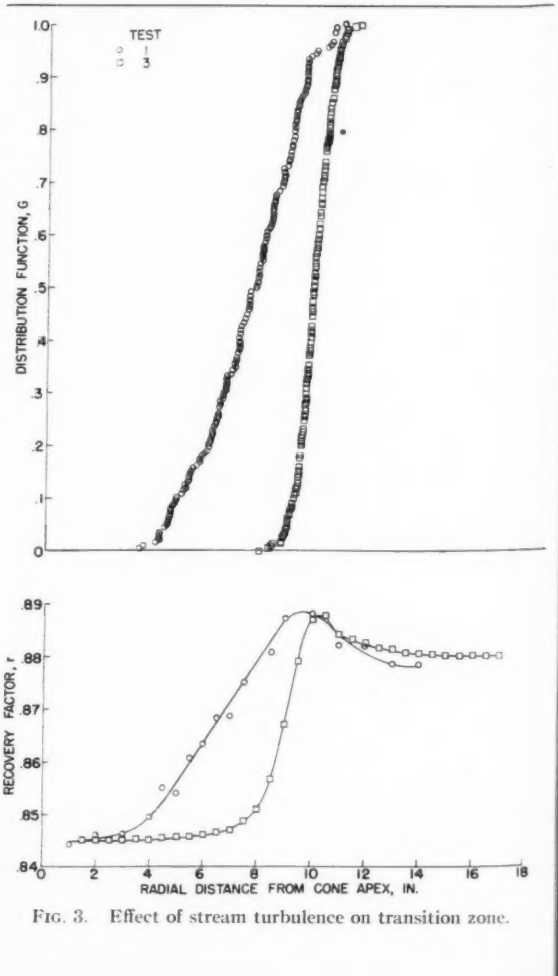

FIG. 3. Effect of stream turbulence on transition zone.

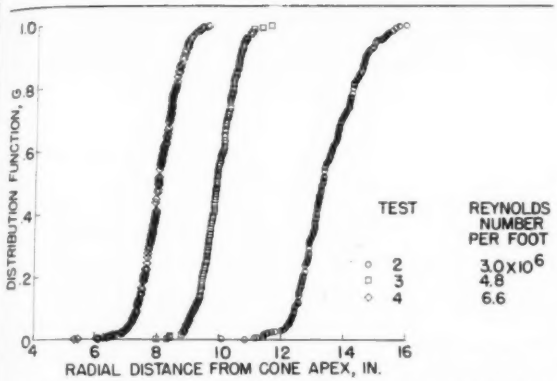

FIG. 4. Effect of Reynolds Number on transition distribution function.

turbulence levels of tests 1 and 3. In general, increasing the turbulence level increases the extent of the transition zone about the same amount for both the recovery-factor data and for the distribution functions. The indications are that the rather gradual property changes in the transition region of such time-averaged quantities as recovery factor result at least in part from the random fluctuations of the transition point. The range of fluctuation is considerably smaller if the free-stream turbulence level is low.

Also of interest is the observation that the downstream end of the transition region ($G = 1$) occurs at about the same axial distance from the cone tip for both free-stream turbulence levels. Certainly, random globs of turbulent air passing over the model would temporarily shift the instantaneous transition point forward. Likewise, random globs of turbulent-free air would allow the transition point to shift downstream. The farthest downstream position at which instantaneous transition occurs thus presumably represents the transition-point location for minimum instantaneous stream turbulence.

The peak temperature-recovery factor occurs at about the same axial location as the point of maximum slope on the distribution function, which would correspond to the most probable location of the transition point. Decay from the peak toward the equilibrium turbulent recovery factor continues downstream of the $G = 1$ or completely turbulent point. This observation demonstrates that the spread of the transition region is also partly due to causes other than transition-point fluctuations. The fact that the recovery factor has a peak higher than the equilibrium turbulent value also strengthens this conclusion.

Effect of Free-Stream Reynolds Number

Data from tests 2, 3, and 4 are included on Fig. 4 to show the influence of stream Reynolds Number on the distribution functions for the transition-point location. As shown in reference 8, the data closely approximate normal distribution functions for tests 3 and 4 but deviate somewhat for test 2. Such deviations usually increase as the axial spread of the distribution functions increases. There is perhaps little reason to suspect that the distributions should be normal with such existing flow complications as three-dimensional model effects, slight tunnel pressure gradients, sound waves in the air stream, boundary-layer damping, and so forth. As in Fig. 3, the axial spread of the distribution functions correlated closely to that of the recovery factor.

Increasing the stream Reynolds Number generally tended to move the distribution functions for the transition-point location upstream and to decrease the width of the transition zone. The change in width, however, may have been due to the change in stream-turbulence level (Table 1) between test 2 and tests 3 and 4. Based on the axial distance of the $G = 1$ point, the Reynolds Number of transition varied almost linearly from 4.12 to 5.50 $\times 10^6$ as the stream Reynolds Number was increased from 3 to 6.6 $\times 10^6$.

Effect of Mach Number

Inasmuch as the test-section Reynolds Number of the 8- by 6-ft. tunnel is nearly constant for its Mach Number range, it was hoped that the data from tests 6, 7, and 8 would indicate trends of transition Reynolds Number with Mach Number. Such interpretations should be viewed with skepticism, however, because of the variations of stagnation temperature during the course of each test and the probable changes in free-stream turbulence intensity as the compressor changed speed, pressure ratio, and mass flow from Mach Number to Mach Number. The distribution functions for the transition-point location are plotted, nevertheless, in Fig. 5. In this figure, data points close to the cone base were deleted, because they appeared to be influenced by the low base pressure.

Presumably, if the Reynolds Number varies during a given test, the transition point would occur, on the

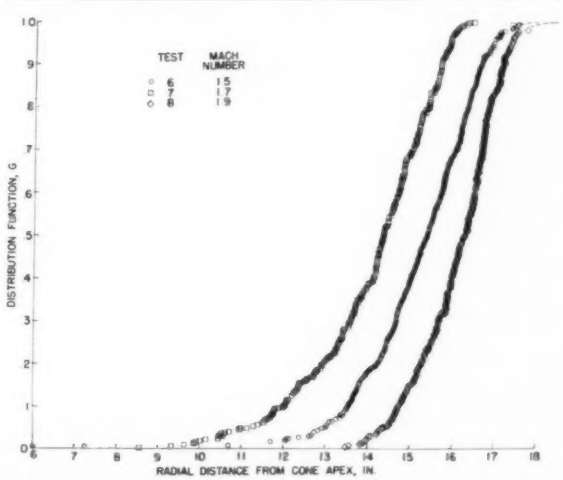

FIG. 5. Effect of Mach Number on transition distribution function.

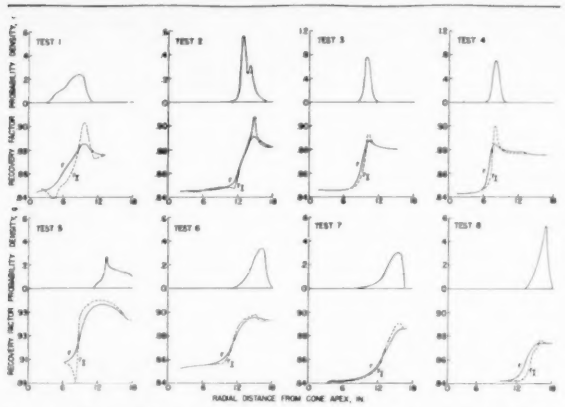

FIG. 6. Comparison of probability-density and recovery-factor distributions.

average, farthest downstream at the lowest Reynolds Number. Utilizing these lowest values and the axial locations for the $G = 1$ point gives transition Reynolds Numbers of 6.15, 5.58, and 6.55 $\times$ 10^6 for Mach Numbers 1.5, 1.7, and 1.9, respectively. One might presume from these numbers that there is little variation in transition Reynolds Number with Mach Number in this speed range. Such a presumption is somewhat contrary to the trends included in references 11 and 14. At least part of the difference is due to the manner of defining the "transition point," which by now is recognized as a rapidly fluctuating variable.

At a free-stream Reynolds Number of 4.3 $\times$ 10^6 per foot, which approximates the value of the 8- by 6-ft. tunnel tests, the $G = 1$ transition Reynolds Number of the Mach Number 3.12 data is estimated at 4.6 $\times 10^6$. The value indicates an apparent decrease in the Reynolds Number of transition as the flow Mach Number (and many other things) changes from 1.9 to 3.12. This trend of decreasing transition Reynolds Number with increasing Mach Number above 2 was suggested to the authors by Lester Lees in the spring of 1952. It likewise conforms approximately to the trends of references 6, 7, 14, and 15.

No comparison was made for the Mach Number 0.63 data of test 5, because the $G = 1$ point was apparently well off the cone surface. Also, there was reasonable assurance from linearized theory that the model surface was exposed to a favorable pressure gradient. Likewise, because of uncertainties in such quantities as the local surface Mach Number, the absolute values of recovery factor should not be trusted for this test.

Instantaneous Temperature-Recovery Factors

Temperatures measured on the surface of the cone are time-averaged by the heat capacity of the model and thermocouples. These time averages are influenced by the shape of the probability density curve $g(\eta)$. The relation between the surface temperatures and the probability density curve could be determined if the instantaneous temperatures adjacent to the surface were known.

For simplicity (as in reference 8) an instantaneous temperature distribution θ is postulated that moves with the transition-point location and is unaffected by translation of the transition point. The origin of this function will be taken at the transition point. Thus, when transition is located at a distance η from the cone apex, a thermocouple at a distance x from the apex is subjected to the instantaneous temperature $\theta(x - \eta)$ for $g(\eta)\ d\eta$ percentage of the time. Summation over all positions of the transition-point location gives the time-averaged temperature at the thermocouple:

$$T(x) = \int_{\alpha}^{\beta} \theta(x - \eta)\ g(\eta)\ d\eta \qquad (2)$$

This average should be regarded as that caused only by fluctuations of the transition-point location. The limits of integration, α and β, are chosen so that all nonzero values of g are included between them.

If the stream static temperature is subtracted from both members of equation (2) and the resulting terms are divided by the difference of the stream stagnation and static temperatures, the time-averaged recovery factor results:

$$r(x) = \int_{\alpha}^{\beta} r_1(x - \eta)\ g(\eta)\ d\eta \qquad (3)$$

The function $r_1(x - \eta)$ represents the instantaneous recovery-factor distribution.

Inasmuch as the time-averaged temperature $T(x)$ and the distribution function $g(\eta)$ were both measured, Eq. (2) represents an integral relation for evaluating the instantaneous temperature distribution θ. Before proceeding, it may be well to note, however, that there were some gradual changes in free-stream Reynolds Numbers during the course of tests 5, 6, 7, and 8. Under such conditions, even though T and g are time-averaged over a short period, they should be regarded as depending upon time over a long period. That is,

$$T(x, t) = \int_{\alpha}^{\beta} \theta g(\eta, t)\ d\eta \qquad (4)$$

Averaging both sides of eq. (4) (subject to the assumption that the function θ does not depend on transition-point location) yields:

$$\bar{T}(x) = \int_{\alpha}^{\beta} \theta \bar{g}(\eta)\ d\eta \qquad (5)$$

Thus the instantaneous temperature distribution may still be calculated even if T varies during the period for which $\bar{g}\ (\eta)$ was measured.

Instantaneous temperature distributions were calculated for all eight tests by numerical solution of the integral equation. Generally, when the calculated values of the instantaneous distributions were reinserted into the equation, the calculated and measured temperatures agreed within 0.5°F. or less over the whole curve,

indicating the approximate accuracy of the solution. Nevertheless, even though in principle Eq. (2) has a unique solution, many instantaneous temperature distributions can usually be found that, with a given probability density distribution $g(\eta)$, will yield a time-averaged temperature distribution $T(x)$ within the accuracy of the temperature measurements. The general characteristics of the instantaneous recovery-factor distribution should, therefore, be obtained from the results of many tests rather than from an isolated example.

The functions g, r, and r_I are compared in Fig. 6 for each of the eight sets of test data. On the curves, the peak of the instantaneous recovery factors was arbitrarily aligned with that of the time-averaged values.

Though plots of G may appear deceivingly close to normal distribution functions, inspection of the probability-density curves indicates that this was not generally the case. The instantaneous recovery factors for tests 3 and 4 were duplicated from reference 8. Unlike those of reference 8, the solutions for the other instantaneous recovery factors presented herein did not require the assumption of a normal distribution function.

Though some deviations are to be noted, the calculated instantaneous recovery-factor curve is steeper and reaches a higher peak than that for the measured recovery factor. Likewise the axial spread of the instantaneous values in the transition region is smaller. Like the average, the instantaneous recovery factor appears to approach an equilibrium turbulent-boundary-layer value at some distance downstream of the peak. The trend for Mach Number 0.63 (test 5) is a notable exception. This may have resulted from the observation that the probability-density curve is incomplete at the base of the cone.

The control over the tunnel flow conditions was more precise for tests 1 to 4, so that the resulting curves should be more reliable. The instantaneous recovery-factor distributions for these tests are superimposed in Fig. 7. The preliminary conclusion might be drawn from this figure that either decreases in stream Reynolds Number or increases in stream turbulence, or both, will increase the axial spread of the instantaneous transition region.

The occurrence of a peak on the recovery-factor distribution raises questions concerning its cause. Perhaps large eddies expected to form at transition yield a different proportion of heat and momentum transfer and a different form factor than that for a standard turbulent boundary layer, and a higher recovery factor might thereby result. Such a hypothesis would explain the relatively slow asymptotic approach toward usual equilibrium turbulent recovery factors. The decay process seems to be approximately exponential in character, requiring from 30 to 100 boundary-layer thicknesses for approximate completion.

A local increase in apparent recovery factor could also be attributed to the shock wave generated at transition in supersonic flow or to the tendency for the flow to stagnate at the transition point in subsonic flow. Either phenomenon would increase the local static temperature so that, if the local recovery factor were actually constant, the calculated recovery factor in terms of the free-stream conditions would increase.

Calculations were made for the Mach Number 3.12 data to see what shock strength would be required to give an apparent rise of 0.02 in the instantaneous recovery factor; a flow deflection of 13° would be necessary. While a change in $d\delta^*/dx$ at transition corresponding to this deflection is not beyond reason, the long decay period is. The expansion waves generated by a rapidly decreasing $d\delta^*/dx$ downstream of the shock should return the flow to nearly the initial conditions within a few boundary-layer thicknesses of the shock. The conclusion persists that the change in stream conditions due to the shock is not the predominant cause for the rise in the instantaneous recovery factor.

A preliminary experiment was conducted at a Mach Number of 3.12 to see what would happen to the recovery factor if a 0.03-in. diameter O-ring were placed in the fully turbulent region between the peak and the equilibrium turbulent value. The data with and without the ring are compared in Fig. 8.

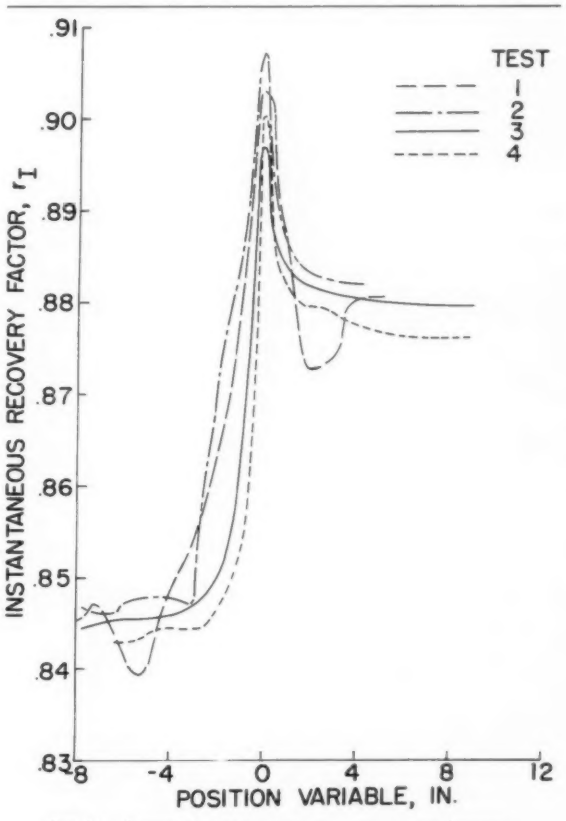

FIG. 7. Composite of instantaneous recovery factors.

As expected, there was a local rise in recovery factor just ahead of the ring, which in this case was attributed to the resulting shock. Unexpected, however, was the large drop in recovery factor just downstream of the ring with a rather gradual asymptotic approach toward the turbulent equilibrium values. It would almost seem that "partly laminar" flow was generated downstream of the O-ring. Conversion of turbulent flow to laminar has been demonstrated on cone cylinders at Mach 3 by Joseph Sternberg.

A brief test was also conducted at Mach Number 0.63 with the 0.03-in.-diameter O-ring mounted at the same place on the cone, but this time in a fully developed turbulent boundary layer—artificially tripped by a 0.02-in.-diameter O-ring placed $1^1/_2$ in. from the cone nose. The trend of the recovery factor near the O-ring was the same as in the supersonic case, but the magnitude of the incremental drop in recovery factor downstream of the ring was more than twice as great. These observations suggest the need for additional experiments including heat-transfer measurements, with possible applications in the problems associated with aerodynamic heating.

Occurrence of Multiple Transition Points

As reported in reference 8, a study of the schlieren photographs from test 3 indicated that about 2 per cent of the schlierens (6 pictures in 272) showed the obvious presence of more than one transition point. The other 98 per cent of the cases showed only one transition followed downstream by turbulent flow to the base of the cone.

A similar study of the data obtained in the 8- by 6-ft. tunnel indicated a more frequent occurrence of multiple transitions. In one case, as many as 4 clearly defined transitions were observed, with alternating turbulent and laminar regions. A summary of the multiple transition observations for tests 5 to 8 is included in the following table:

Test Number	Mach Number	Total Number of Readings	Multiple Transitions Number	Multiple Transitions Per cent	Number of Schlierens with 2 Transitions	3 Transitions	4 Transitions
5	0.63	426	68	16	56	12	...
6	1.5	404	73	18	58	14	1
7	1.7	360	45	$12^1/_2$	37	8	...
8	1.9	368	55	15	53	2	...

In analyzing the data, the influence of multiple transitions downstream of the first was ignored. The calculated instantaneous recovery factors for tests 5 to 8 are therefore somewhat in error.

The great difference between the frequency of multiple transitions in the 8- by 6- and 1- by 1-ft. tunnel data indicates a considerable difference in the character of the two air streams. As suggested in reference 8, small-scale eddies in the free stream would favor the observation of multiple transitions if such eddies are the cause of the Emmons turbulent spots. A large-scale eddy, on the other hand, would tend to brush the whole boundary layer in passing across the model surface and would probably leave in its wake only one transition point. The influence of dust particles in the air stream is also a factor. It seems physically plausible to assume that the presence of dust would increase the probability for multiple transitions.

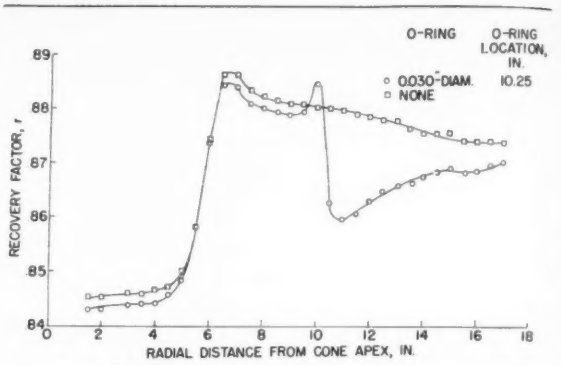

FIG. 8. Effect of disturbance in boundary layer on turbulent recovery-factor distribution. Test-section Reynolds Number per foot, 7.95×10^6.

This report has included considerable experimental evidence to demonstrate that the transition-point location is not steady, but rather fluctuates rapidly along the model surface. These fluctuations in part explain the spread of the transition region. The data suggest that an instantaneous temperature distribution moves with the transition point. Whether this hypothesized temperature distribution merely results from a mathematical definition or actually conforms to a physical process is still open to question. The authors believe that the calculated instantaneous temperature distributions do approximate a physical process but grant that the initial evaluations may be too crude, in that the influence of Reynolds Number and stream turbulence has been ignored.

References

[1] Pillow, A. F., *A Review of Hydrodynamic Stability and Its Bearing on Transition to Turbulent Flow in the Boundary* Rep. A.35, Div. Aero., Council Sci. and Ind. Res., Melbourne (Australia), May, 1945.

[2] Lees, Lester, and Lin, Chia Chiao, *Investigation of the Stability of the Laminar Boundary Layer in a Compressible Fluid*, NACA TN 1115, 1946.

[3] Lees, Lester, *The Stability of the Laminar Boundary Layer in a Compressible Fluid*, NACA Rep. 876, 1947. (Supersedes NACA TN 1360.)

[4] Taylor, G. I., *Statistical Theory of Turbulence. V—Effect of Turbulence on Boundary Layer. Theoretical Discussion of Relationship Between Scale of Turbulence and Critical Resistance of Spheres*, Proc. Roy. Soc. (London), Vol. COVI, No. A.888, ser. A, pp. 307–317, August 17, 1936.

[5] Brinich, Paul F., and Diaconis, Nick S., *Boundary-Layer Development and Skin Friction at Mach Number 3.05*, NACA TN 2742, 1952.

(*Continued on page 748*)

Generalized Aerodynamic Forces on the Delta Wing with Supersonic Leading Edges

J. WALSH,* G. ZARTARIAN,† AND H. M. VOSS‡

Bureau of Aeronautics and Massachusetts Institute of Technology

SUMMARY

It is shown on a semiphysical basis that strip theory, that is, treating each chordwise strip aerodynamically as a portion of an infinite unswept wing, is exact in determining the contribution of any flexible or rigid-body mode to the generalized aerodynamic force on any rigid-body mode. It is also seen that this result is an approximation to the correct result when the second mode involved is a flexible mode. Employing the reverse flow theorem, the exact expressions are then obtained for determining the contribution of an arbitrary flexible mode to the generalized force in a second arbitrary flexible mode for a supersonic delta wing, with each mode represented by a double polynomial series. The error involved in the use of strip theory is found analytically and comparative calculations are carried out for several cases of practical interest. It is seen that the strip theory is sufficiently accurate for problems ordinarily encountered.

LIST OF SYMBOLS

x, y	= Cartesian coordinates nondimensionalized with respect to the chord $2b$ at the root
t	= time in seconds
ω	= circular frequency of oscillation in rad./sec.
b	= semichord at the root in feet
U	= free-stream velocity in ft./sec.
M	= free-stream Mach Number
ρ	= density of the fluid medium in slugs per cu.ft.
$\Delta p(x, y)$	= pressure jump across the airfoil at point x, y
$Z_a(x, y)$	= vertical displacement of the airfoil at point x, y
Q_{ij}	= generalized force for mode j due to the pressure from mode i
$g_i(x, y, t)$	= the i-th mode
$f_i(x, y)$	= the i-th normalized mode shape
$q_i(t)$	= generalized coordinate of the i-th mode
Λ	= sweep angle of the leading edge
β	= function defined by Eq. (12)
k	= reduced frequency, $k = (\omega b)/U$
$\bar{\omega}$	= modified reduced frequency, $\bar{\omega} = (2kM^2)/\beta^2$
J_n	= Bessel function of the first kind of order n
W	= downwash distribution function defined by Eq. (14)
Γ	= the gamma function
B	= the beta function
$f_\lambda(M, \bar{\omega})$	= function defined by Eq. (46)

Presented at the Aeroelasticity Session, Twenty-Second Annual Meeting, IAS, New York, January 25–29, 1954.

* Formerly Head, Structural Dynamics Unit, Bureau of Aeronautics, Department of the Navy; now Structural Dynamics Unit, Boeing Airplane Company, Seattle Division.

† Senior Engineer, Aero-Elastic and Structures Research, Massachusetts Institute of Technology.

‡ Research Associate, Department of Aeronautical Engineering, Massachusetts Institute of Technology.

INTRODUCTION

THE TERM, GENERALIZED FORCE, is an often used, and at times abused, expression. Most generally it is the name given to the work done during a virtual displacement of any generalized coordinate and is most often encountered in minimum energy considerations.

For the purposes of this paper, only the generalized force due to aerodynamic effects will be considered. The generalized force is then defined as

$$Q_{ij} = 4b^2 \int_A \int \Delta p_i(x, y) f_j(x, y) dx dy \qquad (1)$$

where Δp_i is the local pressure difference due to a specified deflection shape $f_i(x, y)$, and $f_j(x, y)$ is the mode for which the generalized force is to be determined.

The most apparent application of this computation is in flutter analyses where the Q_{ij} correspond to the aerodynamic coupling terms in the flutter equations. That is, the flutter mode is assumed to be of the form

$$Z_a(x, y, t) = \{g_1(x, y, t) + g_2(x, y, t) + \ldots + g_j(x, y, t) + \ldots + g_n(x, y, t)\} \qquad (2)$$

where

$$g_j(x, y, t) = q_j(t) f_j(x, y) \qquad (3)$$

and $Z_a(x, y, t)$ is the vertical displacement of the wing, $f_j(x, y)$ is the vertical displacement of the wing in the j-th degree of freedom, and $q_j(t)$ is the generalized coordinate corresponding to this degree of freedom. In a formulation of the problem using Lagrange's equation of motion, it is necessary to evaluate the virtual work done by the pressure distributions due to all mode shapes for a virtual displacement, δq_j, of any of the generalized coordinates. This may be written as

$$\begin{aligned} \frac{1}{4b^2} Q_j &= \int_A \int \Delta p(x, y, t) f_j(x, y) dx dy \\ &= \int_A \int \Delta p_1 f_j dx dy + \\ &\int_A \int \Delta p_2 f_j dx dy + \int_A \int \Delta p_3 f_j dx dy + \ldots \\ &= \frac{1}{4b^2} (Q_{1j} + Q_{2j} + Q_{3j} + \ldots) \end{aligned} \qquad (4)$$

Hence, each term is of the form of Eq. (1) above.

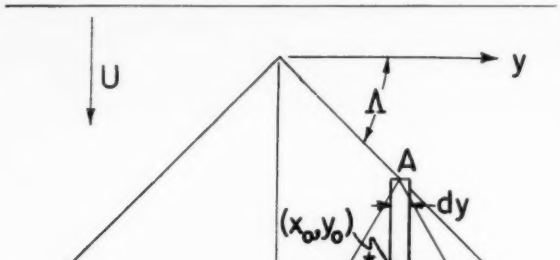

FIG. 1

Eq. (1) may, however, also be interpreted somewhat more generally: let $\Delta p_i(x, y)$ be the pressure distribution due to an arbitrary deformation of the wing and $f_j(x, y)$ be an arbitrary weighting function. Then for f_j = constant, Q_{ij} is the total lift due to an arbitrary deflection mode; for $f_j = x$, Q_{ij} is the pitching moment; for $f_j = y$, Q_{ij} is the rolling moment, etc. These quantities are often involved in determining the effect of flexibility on the aerodynamic properties of a surface.

Throughout this work, the undeformed planform is taken to be thin and initially planar, and the motions such that the disturbance velocities are everywhere small compared to the free-stream velocity; that is, linearized supersonic theory is employed. In addition, consideration is limited to planforms such that the free-stream velocity component normal to all edges is supersonic—the so-called supersonic planfom. While the strip-theory formulation holds for any supersonic planform, only the delta wing is studied in detail both for the sake of simplicity and because of its present-day usage.

The evaluation of Q_{ij} as defined by Eq. (1) for the delta planform with supersonic leading edges is then the basis of this paper. An approximate form and its limitations are first found on the basis of strip theory. The exact form of the result is then determined for the case in which two arbitrary modes are involved, each representable by a double polynomial series. It will be noted that this result includes the cases of lift and moment for the rigid-body motions obtained previously by Miles.[1]

Finally, the results of calculation are presented for several cases in which the strip-theory result is only approximate.

Strip-Theory Formulation

Consider the aerodynamic effects induced by the vertical motions in mode i of a chordwise strip of width dy, such as strip (AB) in Fig. 1. The aerodynamic forces created by strip (AB) will then lie on the area of the wing between the Mach lined from the leading edge A. It is desired to determine the contribution of these forces to the generalized force in mode j due to a mode i of the surface. This can be accomplished by determining the contribution of each spanwise strip of width dx, such as (CD) in Fig. 1, to the generalized force due to the motion of the chordwise strip (AB), and integrating over the chord. Then spanwise integration over all chordwise strips will give the total generalized force in mode j due to mode i.

Consider the contribution of the aerodynamic forces on strip CD to the generalized force due to motion of AB,

$$\left(\frac{1}{4b^2}\right)\left(\frac{dR_{ij}(x_0, y_0)}{dx_0}\right) = \int_{y_1}^{y_2} \Delta p_i'(x_0, y_0, y) f_j(x_0, y) dy \tag{5}$$

where y_1, and y_2 are the values of y at the intersections of the strip with the Mach lines, and $\Delta p_i'(x_0, y_0, y)$ is the pressure difference due only to motion of strip (AB) of differential width. Expanding $f_j(x_0, y)$ in a power series in y about y_0,

$$f_j(x_0, y) = a_0(x_0, y_0) + a_1(x_0, y_0)(y - y_0) + a_2(x_0, y_0)(y - y_0)^2 + \ldots \tag{6}$$

this becomes,

$$\left(\frac{1}{4b^2}\right)\left(\frac{dR_{ij}}{dx_0}\right) = a_0 \int_{y_1}^{y_2} \Delta p_i' dy + a_1 \int_{y_1}^{y_2} \Delta p_i'(y - y_0) dy + a_2 \int_{y_1}^{y_2} \Delta p_i'(y - y_0)^2 dy + \ldots \tag{7}$$

But $\Delta p_i'$ is symmetric in $(y - y_0)$; hence, the integrals involving an odd weighting function will vanish, i.e.,

$$\int_{y_1}^{y_2} \Delta p_i'(y - y_0) dy = \int_{y_1}^{y_2} \Delta p_i'(y - y_0)^3 dy = \ldots = 0 \tag{8}$$

and thus

$$\left(\frac{1}{4b^2}\right)\left(\frac{dR_{ij}}{dx_0}\right) = a_0 \int_{y_1}^{y_2} \Delta p_i' dy + a_2 \int_{y_1}^{y_2} \Delta p_i'(y - y_0)^2 dy + a_4 \int_{y_1}^{y_2} \Delta p_i'(y - y_0)^4 dy + \ldots \tag{9}$$

The first integral appearing on the right-hand side of Eq. (9) is just the lift per unit length chordwise on strip (CD) due to motion of (AB).

But the lift on a spanwise strip of differential width due to arbitrary motion of a chordwise strip of differential width is just equal to the lift on the differential area formed by their intersection, due to the two-dimensional motion of an infinite straight wing undergoing the same chordwise deformation. This may be reasoned as follows (see Fig. 2): The pressure at point c due to a source, steady or unsteady, at point a is exactly equal to the pressure at point b due to the same source at point d. The total pressure at c due to the motion of the entire strip (AB) is only affected by the portion of the strip forward of the Mach forecone and from the above is just equal to the pressure at b due to motion of a similar strip at the spanwise location of point c in the Mach forecone of b. This is true of any point on the spanwise strip (CD), and hence the total lift on the strip due to motion of (AB) is equal to the lift on the differential element at b due to motion of all chordwise strips bounded by the Mach forecone from b and a straight leading edge through (A), where each chordwise strip has the same motion as that of (AB). And this is just the product of the differential area and the pressure due to two-dimensional motion of an infinite straight wing.

Hence, one may replace the first integral on the right-hand side of Eq. (9) by the lift per unit area, $\Delta p^{(2)}(x_0, y_0)$, calculated from strip theory

$$\left(\frac{1}{4b^2}\right)\frac{dR_{ij}(x_0, y_0)}{dx_0} = a_0(x_0, y_0)\Delta p^{(2)}(x_0, y_0) + a_2(x_0, y_0)\int_{y_1}^{y_2} \Delta p_i'(y - y_0)^2 dy + a_4(x_0, y_0) \times \int_{y_1}^{y_2} \Delta p_i'(y - y_0)^4 dy + \ldots \quad (10)$$

But $a_0(x_0, y_0) = f_j(x_0, y_0)$ is the deflection of the Strip (AB) at y_0. Hence $a_0(x_0, y_0)\Delta p^{(2)}(x_0, y_0)$ is the contribution to the generalized force which would be calculated on the basis of straight-wing strip theory.

It may be directly concluded, therefore, that strip theory will give correct results for the total generalized forces whenever the mode shape j for which the force is being computed is at most linear in y. Thus the strip theory is exact for determining the contribution of any mode i, rigid or flexible, to the generalized force in any spanwise-rigid mode j, including roll. It would also seem plausible that strip theory should give a reasonable approximation to the result for modes j with low-order spanwise variation. This assumption is checked for several cases in Appendix A.

It may be noted that results similar to the above have been established by Miles[2, 3] with the limitation of straight-line trailing edge normal to the stream. The Miles approach is wholly mathematical and differs considerably from that presented here.

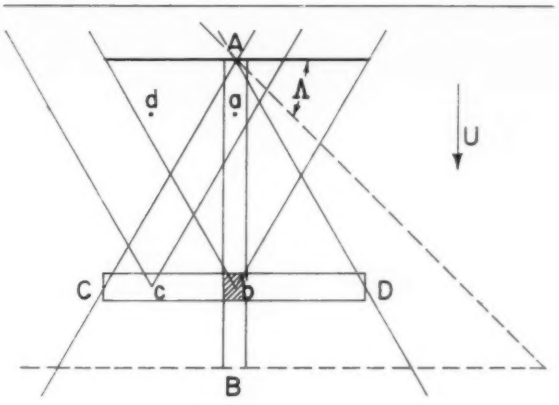

FIG. 2

Application of Strip-Theory to the Delta Plan Form in Harmonic Motion

From reference 4, one may deduce that the pressure difference in a two-dimensional unsteady flow is given, in nondimensional coordinates, by

$$\Delta p^{(2)}(x, t) = -\frac{2\rho U e^{i\omega t}}{\beta}\left[2ik\int_0^x e^{-i\bar{\omega}u}W(x-u) \times J_0\left(\frac{\bar{\omega}}{M}u\right)du + e^{-i\bar{\omega}x}W(0)J_0\left(\frac{\bar{\omega}}{M}x\right) + \int_0^x e^{-i\bar{\omega}u}\frac{\partial}{\partial x}\left\{W(x-u)\right\}J_0\left(\frac{\bar{\omega}}{M}u\right)du\right] \quad (11)$$

where U is the free-stream velocity, M is the Mach Number, ω is the circular frequency of oscillation, and

$$\beta = \sqrt{M^2 - 1} \quad (12)$$

$$k = \omega b/U \quad (13a)$$

$$\bar{\omega} = (2kM^2)/\beta^2 \quad (13b)$$

J_0 is the Bessel function of the first kind of zero order, and $W(x)$ is the downwash distribution given by

$$W(x)e^{i\omega t} = \frac{U}{2b}\left[2ik + \frac{\partial}{\partial x}\right]g(x, t) \quad (14)$$

For a chordwise mode defined by

$$g(x, t) = 2be^{i\omega t}\sum_0^N a_n(1 - x)^n \quad (15)$$

it then follows that the pressure at any point along the chord is given by

$$\Delta p^{(2)}(x, t) = -\frac{2\rho U^2 e^{i\omega t}}{\beta}\sum_0^N a_n \times \left\{\int_0^x e^{-i\bar{\omega}u}[-4k^2(1 - x + u)^n - 4ikn \times (1 - x + u)^{n-1} + n(n-1)(1 - x + u)^{n-2}] \times J_0\left(\frac{\bar{\omega}}{M}u\right)du + (2ik - n)e^{-i\bar{\omega}x}J_0\left(\frac{\bar{\omega}}{M}x\right)\right\} \quad (16)$$

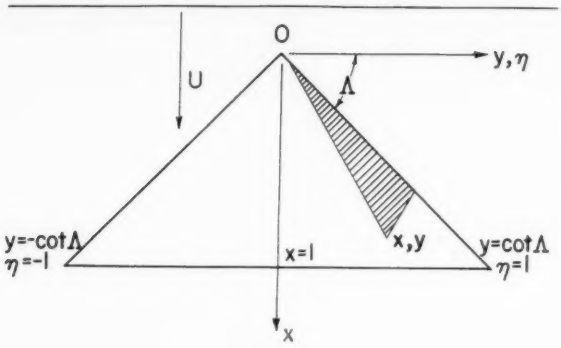

FIG. 3

It is noted that in the above the leading edge is at $x = 0$, the trailing edge at $x = 1$.

Consider now the generalized force according to strip theory due to mode i during a virtual displacement of mode j, for a delta-planform. Taking each mode as a double polynomial series (see Fig. 3 for the coordinate system and notations),

$$g_i(x, y, t) = 2be^{i\omega t} \sum_{m=0}^{M} \sum_{n=0}^{N} a_{mn}\left(\frac{y}{\cot \Lambda}\right)^m (1 - x)^n \tag{17}$$

$$g_j(x, y, t) = 2be^{i\omega t} \sum_{r=0}^{R} \sum_{s=0}^{S} b_{rs}\left(\frac{y}{\cot \Lambda}\right)^r (1 - x)^s \tag{18}$$

according to the previous section the generalized force will be given exactly or approximately (depending on r) as

$$Q_{ij}^{(2)} = 4b^2 \int_A \int \Delta p_1^{(2)}(x, y, t) f_j(x, y) dx dy \tag{19}$$

where $f_j(x, y)$ is given by the double summation of Eq. (18).

In order to normalize the variables such that, for each chordwise strip, the chordwise variable is zero at the leading edge and unity at the trailing edge, a change of variable is employed,

$$\eta = y \tan \Lambda, \qquad \xi = \frac{x - |\eta|}{1 - |\eta|} \tag{20a}$$

or

$$(1 - x) = (1 - \xi)(1 - |\eta|) \tag{20b}$$

With this change, Eqs. (17), (18), and (19) become

$$g_i(\xi, \eta, t) = 2be^{i\omega t} \sum_{m=0}^{M} \sum_{n=0}^{N} a_{mn}\eta^m (1 - \xi)^n (1 - |\eta|)^n \tag{21}$$

$$g_j(\xi, \eta, t) = 2be^{i\omega} \sum_{r=0}^{R} \sum_{s=0}^{S} b_{rs}\eta^r (1 - \xi)^s (1 - |\eta|)^s \tag{22}$$

$$Q_{ij}^{(2)} = 4b^2 \cot \Lambda \int_A \int \Delta p_i^{(2)}(\xi, \eta, t) \times f_j(\xi, \eta)(1 - |\eta|) d\xi d\eta \tag{23}$$

Then, making use of Eqs. (15–16), realizing that the two-dimensional derivation is based on the *local* semi chord, there results

$$Q_{ij}^{(2)} = -\frac{8\rho U^2 b^2 \cot \Lambda e^{i\omega t}}{\beta} \int_{-1}^{1} \int_{0}^{1} \sum_{m=0}^{M} \sum_{n=0}^{N} \sum_{r=0}^{R} \sum_{s=0}^{S} a_{mn} b_{rs} (1 - |\eta|)^{n+s} \eta^{m+r} (1 - \xi)^s \times \left\{ \int_0^{\xi} e^{-i\bar{\omega}\bar{u}} [-4\bar{k}^2 (1 - \xi + \bar{u})^n - 4i\bar{k}n(1 - \xi + \bar{u})^{n-1} + n(n - 1)(1 - \xi + \bar{u})^{n-2}] J_0\left(\frac{\bar{\omega}}{M}\bar{u}\right) d\bar{u} + (2i\bar{k} - n) e^{-i\bar{\omega}\xi} J_0\left(\frac{\bar{\omega}}{M}\xi\right) \right\} d\xi d\eta \tag{24}$$

where $\bar{k}$ and $\bar{\omega}$ are the values of k and $\tilde{\omega}$ at any spanwise station. By a slight change of variables,

$$\zeta = \xi(1 - |\eta|), \; u = \bar{u}(1 - |\eta|) \tag{25}$$

and noting that

$$\bar{k} = k(1 - |\eta|), \; \bar{\omega} = \tilde{\omega}(1 - |\eta|) \tag{26}$$

where k and $\tilde{\omega}$ are now the root values ($y = 0$), Eq. (24) may be written in a form made useful for comparison.

$$Q_{ij}^{(2)} = -\frac{8\rho U^2 b^2 \cot \Lambda \, e^{i\omega t}}{\beta} \int_{-1}^{1} \int_{0}^{1 - |\eta|} \sum_{m=0}^{M} \sum_{n=0}^{N} \sum_{r=0}^{R} \sum_{s=0}^{S} a_{mn} b_{rs} (1 - |\eta| - \zeta)^s \eta^{m+r} \times \left\{ \int_0^{\zeta} e^{-i\omega u} [-4k^2 (1 - |\eta| - \zeta + u)^n - 4ikn(1 - |\eta| - \zeta + u)^{n-1} + n(n - 1)(1 - |\eta| - \zeta + u)^{n-2}] \times J_0\left(\frac{\tilde{\omega}}{M} u\right) du + (1 - |\eta|)^n \left(2ik - \frac{n}{1 - |\eta|}\right) e^{-i\tilde{\omega}\zeta} J_0\left(\frac{\tilde{\omega}}{M}\zeta\right) \right\} d\zeta d\eta \tag{27}$$

Exact Formulation

The recent work of several authors, notably Ursell and Ward,[5] Flax,[6] and Heaslet and Spreiter,[7] along with that of their predecessors, has led to the very useful principle of the reverse flow theorem in aerodynamics. It is believed that the full usefulness of these concepts has not yet been realized, and, to the knowledge of the authors, the application to the determination of generalized forces was suggested only recently.[8] It is this approach which will be used below.

The suitable form of the reverse flow theorem states,

$$\int_A \int \Delta p_a(x, y, t) W_b(x, y) e^{i\omega t} dx dy = \int_A \int \Delta p_b(x, y, t) W_a(x, y) e^{i\omega t} dx dy \quad (28)$$

where Δp_a is the pressure difference in the forward flow due to a downwash $W_a(x, y)e^{i\omega t}$, Δp_b is the pressure difference in a reverse flow over the same planform due to a downwash $W_b(x, y)e^{i\omega t}$, and the integrals extend over the entire planform. This result holds for steady or unsteady flows, without restriction on Mach Number beyond those of the usual linearized theory.

By comparison of Eq. (28) with Eq. (1), it is seen that the generalized force can be evaluated as,

$$\left.\begin{aligned} Q_{ij} &= 4b^2 \int_A \int \Delta p_i(x, y, t) f_j(x, y) dx dy \\ &= 4b^2 \int_A \int \Delta \bar{p}_j(x, y, t) \frac{W_i(x, y)}{U} dx dy \end{aligned}\right\} \quad (29)$$

where $\Delta \bar{p}_j(x, y, t)$ is now the pressure distribution over the planform oscillating at the same frequency in a reversed flow due to a downwash distribution,

$$W_j(x, y)e^{i\omega t} = U f_j(x, y) e^{i\omega t} \quad (30)$$

From the modes defined by Eqs. (17) and (18), employing Eq. (14),

$$\frac{W_i(x, y)}{U} = \sum_{m=0}^{M} \sum_{n=0}^{N} a_{mn} \left(\frac{y}{\cot \Lambda}\right)^m \times [2ik - n(1 - x)^{-1}](1 - x)^n \quad (31)$$

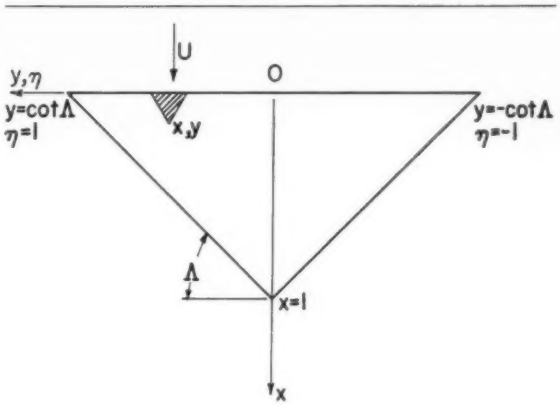

FIG. 4

$$\frac{W_j(x, y)}{U} = \sum_{r=0}^{R} \sum_{s=0}^{S} b_{rs} \left(\frac{y}{\cot \Lambda}\right)^r (1 - x)^s \quad (32)$$

For simplicity in computation, the streamwise coordinate direction may be rotated and translated,

$$(1 - x) \rightarrow x$$

such that the origin is at the leading edge of the planform in the reversed flow, and the stream direction is in the direction of increasing x (see Fig. 4). With this change the two downwash expressions become

$$\frac{W_i(x, y)}{U} = \sum_{m=0}^{M} \sum_{n=0}^{N} a_{mn} \left(\frac{y}{\cot \Lambda}\right)^m \times [2ik - nx^{-1}]x^n \quad (33)$$

$$\frac{W_j(x, y)}{U} = \sum_{r=0}^{R} \sum_{s=0}^{S} b_{rs} \left(\frac{y}{\cot \Lambda}\right)^r x^s \quad (34)$$

For the flow in this direction, the planform is purely supersonic and bounded by a straight leading edge normal to the flow. The pressure difference due to W_j can thus be evaluated with comparative ease.

It may be deduced directly from reference 4 that the pressure difference at any point will be given by

$$\Delta \bar{p}_j(x, y, t) = -\frac{2\rho U^2 e^{i\omega t}}{\pi\beta} \left(2ik + \frac{\partial}{\partial x}\right) \int_0^x \int_0^\pi \frac{W_j\left(x - u, \frac{u}{\beta} \cos \theta + y\right)}{U} e^{-i\bar{\omega}u} \cos\left(\frac{\bar{\omega}}{M} u \sin \theta\right) d\theta du \quad (35)$$

Substituting Eq. (34), the θ-integration can be carried out directly—i.e.,

$$\int_0^\pi \sum_{r=0}^{R} \sum_{s=0}^{S} b_{rs} \frac{(x - u)^s}{\cot^r \Lambda} \left(\frac{u}{\beta} \cos \theta + y\right)^r \cos\left(\frac{\bar{\omega}}{M} u \sin \theta\right) e^{-i\bar{\omega}u} d\theta = e^{-i\bar{\omega}u} \sum_{r=0}^{R} \sum_{s=0}^{S} b_{rs} \frac{(x - u)^s}{\cot^r \Lambda} \int_0^\pi \left(\frac{u}{\beta} \cos \theta + y\right)^r \cos\left(\frac{\bar{\omega}}{M} u \sin \theta\right) d\theta \quad (36)$$

Making use of the identities from reference 1,

$$\left.\begin{aligned}\int_0^\pi \cos^{2p}\theta \cos\left[\frac{\bar\omega}{M}u\sin\theta\right]d\theta &= \frac{\sqrt{\pi}\,2^p}{\left(\frac{\bar\omega}{M}u\right)^p}\Gamma\left(p+\frac{1}{2}\right)J_p\left(\frac{\bar\omega}{M}u\right)\\ \int_0^\pi \cos^{2p+1}\theta \cos\left[\frac{\bar\omega}{M}u\sin\theta\right]d\theta &= 0\end{aligned}\right\} \tag{37}$$

it follows that

$$\int_0^\pi \left(\frac{u}{\beta}\cos\theta + y\right)^r \cos\left(\frac{\bar\omega}{M}u\sin\theta\right)d\theta = \pi \sum_{p=0}^{\leq (r/2)} \left(\frac{uM}{\beta^2\bar\omega}\right)^p y^{r-2p}\frac{r!p!2^p}{(2p)!\,(r-2p)!}\frac{B\left(\frac{1}{2},\,p+\frac{1}{2}\right)}{\pi}J_p\left(\frac{\bar\omega}{M}u\right) \tag{38}$$

where $B\left(\frac{1}{2},\,p+\frac{1}{2}\right)$ is the Beta function[9] and the upper limit of summation implies the largest integer equal to or less than $r/2$.

Finally, employing Eq. (38) in Eq. (35) for the pressure difference and combining with W_i from Eq. (33) the exact form of the generalized force is given, according to Eq. (29), by

$$Q_{ij} = -\frac{8\rho U^2 b^2\cot\Lambda e^{i\omega t}}{\beta}\int_{-1}^{1}\int_0^{1-|\eta|}\left\{\sum_{m=0}^{M}\sum_{n=0}^{N}\sum_{r=0}^{R}\sum_{s=0}^{S} a_{mn}b_{rs}\sum_{p=0}^{\leq (r/2)}\eta^{m+r-2p}\frac{x^{n-1}}{\cot^{2p}\Lambda}(-n+2ikx)\times\right.$$

$$\left.\left(\frac{r!p!2^p}{(2p)!(r-2p)!}\right)\left[\frac{B\left(\frac{1}{2},\,p+\frac{1}{2}\right)}{\pi}\right]\left(\frac{M}{\beta^2\bar\omega}\right)^p\left(2ik+\frac{\partial}{\partial x}\right)\int_0^x u^p e^{-i\omega u}(x-u)^s J_p\left(\frac{\bar\omega}{M}u\right)du\right\}dx\,d\eta \tag{39}$$

wherein the change of variable

$$\eta = y\tan\Lambda \tag{20a}$$

has been made. The integrand with respect to η in Eq. (39) will be even or odd depending on whether $m+r$ is even or odd; if odd, the integral vanishes, if even

$$\int_{-1}^{1}\int_0^{1-|\eta|}\ldots dxd\eta = 2\int_0^1\int_0^{1-|\eta|}\ldots dxd\eta = 2\int_0^1\int_0^{1-x}\ldots d\eta dx \tag{40}$$

and the η-integration can be carried out:

$$Q_{ij} = -\frac{8\rho U^2 b^2\cot\Lambda e^{i\omega t}}{\beta}\sum_{m=0}^{M}\sum_{n=0}^{N}\sum_{r=0}^{R}\sum_{s=0}^{S} a_{mn}b_{rs}\sum_{p=0}^{\leq (r/2)}\frac{1}{\cot^{2p}\Lambda}\times$$

$$\left\{\left(\frac{r!p!2^p}{(2p)!(r-2p)!}\right)\left[\frac{B\left(\frac{1}{2},\,p+\frac{1}{2}\right)}{\pi}\right]\left(\frac{M}{\beta^2\bar\omega}\right)^b I\right\} \tag{41}$$

where

$$I = 2\int_0^1\left[\left\{\frac{(1-x)^{m+r-2p+1}}{m+r-2p+1}x^{n-1}(-n+2ikx)\right\}\times\right.$$

$$\left.\left\{\left(2ik+\frac{\partial}{\partial x}\right)\int_0^x u^p e^{-i\omega u}(x-u)^s J_p\left(\frac{\bar\omega}{M}u\right)du\right\}\right]dx \qquad \text{(for } m+r \text{ even)} \tag{42}$$

$$I = 0 \qquad \text{(for } m+r \text{ odd)}$$

Limiting attention to $(m+r)$ even the differentiation may be performed and the order of integration interchanged, yielding

$$I = \frac{2}{m+r-2p+1}\int_0^1\int_u^1 (1-x)^{m+r-2p+1}x^{n-1}(-n+2ikx)\left\{\begin{aligned}&2iku^p e^{-i\omega u}(x-u)^s J_p\left(\frac{\bar\omega}{M}u\right)+\\ &su^p e^{-i\omega u}(x-u)^{s-1}J_p\left(\frac{\bar\omega}{M}u\right)\end{aligned}\right\}dxdu +$$

$$\frac{2\delta(s)}{m+r-2p+1}\int_0^1 (1-u)^{m+r-2p+1}u^{n-1}(-n+2iku)u^p e^{-i\omega u}J_p\left(\frac{\bar\omega}{M}u\right)du \tag{43}$$

where $\delta(s)$ is defined as

$$\delta(s) = \begin{cases} 1 & \text{when } s = 0 \\ 0 & \text{when } s \neq 0 \end{cases} \tag{44}$$

It will be noted that the x-integrations are of the form

$$\begin{aligned} \int_u^1 (1-x)^\alpha x^\gamma (x-u)^\nu dx &= \int_u^1 \left\{ (1-x)^\alpha (x-u)^\nu \sum_{\sigma=0}^{\gamma} (-1)^\sigma \frac{\gamma!}{(\gamma-\sigma)!\sigma!} (1-x)^\sigma \right\} dx \\ &= \sum_{\sigma=0}^{\gamma} \frac{(-1)^\sigma \gamma!}{(\gamma-\sigma)!\sigma!} \int_u^1 (1-x)^{\alpha+\sigma} (x-u)^\nu dx \\ &= \sum_{\sigma=0}^{\gamma} \frac{(-1)^\sigma \gamma!}{(\gamma-\sigma)!\sigma!} B(\alpha+\sigma+1, \nu+1)(1-u)^{\alpha+\sigma+\nu+1} \end{aligned} \tag{45}$$

The remaining integration on u is then of the form

$$\int_0^1 (1-u)^\kappa u^{\rho+\tau} e^{-i\omega u} J_\rho\left(\frac{\bar{\omega}}{M} u\right) du$$

which can be expanded and reduced to combinations of the function

$$f_\lambda(M, \bar{\omega}) = \int_0^1 u^\lambda e^{-i\omega u} J_0\left(\frac{\bar{\omega}}{M} u\right) du \tag{46}$$

The functions defined by Eq. (46) are involved in the determination of the two-dimensional air forces[10] and some tabulations[1, 11, 12] as well as a ready method of evaluation[13] are available. The method of obtaining the generalized forces by the above reduction is illustrated in Appendix B.

Comparison of Strip Theory and Exact Results

Consider the term of Eq. (39) for which $p = 0$ and call it θ_{ij},

$$\theta_{ij} = -\frac{8\rho U^2 b^2 \cot \Lambda e^{i\omega t}}{\beta} \int_{-1}^{1} \int_0^{1-|\eta|} \left\{ \sum_{m=0}^{M} \sum_{n=0}^{N} \sum_{r=0}^{R} \sum_{s=0}^{S} a_{mn} b_{rs} \eta^{m+r} x^{n-1} (-n + 2ikx) \times \left(2ik + \frac{\partial}{\partial x}\right) \int_0^x e^{-i\omega u} (x-u)^s J_0\left(\frac{\bar{\omega}}{M} u\right) du \right\} dx d\eta \tag{47}$$

It will now be shown that θ_{ij} is identical to $Q_{ij}^{(2)}$ from Eq. (27). If so, since Eq. (47) is exact for $r = 0, 1$, the conclusion is reaffirmed that strip theory is exact for an arbitrary mode i which gives the pressure distribution and for a virtual displacement mode j which is arbitrary chordwise but no more than linear spanwise ($R \leq 1$).

To prove this identity, first expand θ_{ij},

$$\begin{aligned} \theta_{ij} = &-\frac{8\rho U^2 b^2 \cot \Lambda e^{i\omega t}}{\beta} \sum_{m=0}^{M} \sum_{n=0}^{N} \sum_{r=0}^{R} \sum_{s=0}^{S} a_{mn} b_{rs} \times \\ &\left\{ \int_{-1}^{1} \int_0^{1-|\eta|} \left[\eta^{m+r} x^{n-1} (-n + 2ikx) 2ik \int_0^x e^{-i\omega u} (x-u)^s J_0\left(\frac{\bar{\omega}}{M} u\right) du \right] dx d\eta + \right. \\ &\int_{-1}^{1} \left\{ \left[\eta^{m+r} x^{n-1} (-n + 2ikx) \int_0^x e^{-i\omega u} (x-u)^s J_0\left(\frac{\bar{\omega}}{M} u\right) du \right]_{x=0}^{x=1-|\eta|} \right\} d\eta - \\ &\left. \int_{-1}^{1} \int_0^{1-|\eta|} \left[\eta^{m+r} x^{n-2} [-n(n-1) + 2iknx] \int_0^x e^{-i\omega u} (x-u)^s J_0\left(\frac{\bar{\omega}}{M} u\right) du \right] dx d\eta \right\} \\ \equiv &-\frac{8\rho U^2 b^2 \cot \Lambda e^{i\omega t}}{\beta} \sum_{m=0}^{M} \sum_{n=0}^{N} \sum_{r=0}^{R} \sum_{s=0}^{S} a_{mn} b_{rs} \{ I_1 + I_2 + I_3 \} \end{aligned} \tag{48}$$

from which is obtained

$$I_1 + I_2 = \int_{-1}^{1} \int_0^{1-|\eta|} \left\{ \int_0^x \eta^{m+r} x^{n-2} [n(n-1) - 4iknx - 4k^2 x^2] e^{-i\omega u} (x-u)^s J_0\left(\frac{\bar{\omega}}{M} u\right) du \right\} dx d\eta \tag{49}$$

Inverting the order of integration, i.e.,

$$\int_0^{1-|\eta|} \int_0^x \ldots du dx = \int_0^{1-|\eta|} \int_u^{1-|\eta|} \ldots dx du \tag{50}$$

and with

$$x = 1 - |\eta| - z + u, \qquad dx = -dz \tag{51}$$

it follows that

$$I_1 + I_3 = \int_{-1}^{1}\int_{0}^{1-|\eta|} \eta^{m+r}\left\{\int_{u}^{1-|\eta|} [(1 - |\eta| - z + u)^{n-2}n(n-1) - (1 - |\eta| - z + u)^{n-1}4ikn - (1 - |\eta| - z + u)^{n}4k^2]\left[e^{-i\omega u}(1 - |\eta| - z)^{s}J_0\left(\frac{\bar{\omega}}{M}u\right)dz\right]\right\}du d\eta \tag{52}$$

Reinverting the order of integration, one finally obtains,

$$I_1 + I_3 = \int_{-1}^{1}\int_{0}^{1-|\eta|} \left\{\int_{0}^{z} \eta^{m+r}[n(n-1)(1 - |\eta| - z + u)^{n-2} - 4ikn(1 - |\eta| - z + u)^{n-1} - 4k^2(1 - |\eta| - z + u)^{n}]e^{-i\omega u}(1 - |\eta| - z)^{s}J_0\left(\frac{\bar{\omega}}{M}u\right)du\right\}dz d\eta \tag{53}$$

Also

$$I_2 = \int_{-1}^{1} \eta^{m+r}\left[x^{n-1}(-n + 2ikx)\int_{0}^{x} e^{-i\omega u}(x-u)^{s}J_0\left(\frac{\bar{\omega}}{M}u\right)du\right]_{x=0}^{x=1-|\eta|} d\eta$$
$$= \int_{-1}^{1} \left\{\eta^{m+r}[-n(1 - |\eta|)^{n-1} + 2ik(1 - |\eta|)^{n}]\int_{0}^{1-|\eta|} e^{-i\bar{\omega}u}(1 - |\eta| - u)^{s}J_0\left(\frac{\bar{\omega}}{M}u\right)du\right\}d\eta \tag{54}$$

Since I_1 and I_3 are not functions of z, z is replaced by ζ as a symbol, and since I_2 is not a function of u, u is replaced by ζ as a symbol. Then, combining Eqs. (53) and (54) and substituting into Eq. (48),

$$\theta_{ij} = -\frac{8\rho U^2 b^2 \cot \Lambda e^{i\omega t}}{\beta}\sum_{m=0}^{M}\sum_{n=0}^{N}\sum_{r=0}^{R}\sum_{s=0}^{S} a_{mn}b_{rs} \times$$
$$\left(\int_{-1}^{1}\int_{0}^{1-|\eta|} \eta^{m+r}(1 - |\eta| - \zeta)^{s}\left\{\int_{0}^{\zeta} [-4k^2(1 - |\eta| - \zeta + u)^{n} - 4ikn(1 - |\eta| - \zeta + u)^{n-1} + n(n-1)(1 - |\eta| - \zeta + u)^{n-2}]e^{-i\omega u}J_0\left(\frac{\bar{\omega}}{M}u\right)du + (1 - |\eta|)^{n}\left[2ik - \frac{n}{1 - |\eta|}\right]e^{-i\bar{\omega}\zeta}J_0\left(\frac{\bar{\omega}}{M}\zeta\right)\right\}d\zeta d\eta\right) \tag{55}$$

By comparison of Eq. (55) with Eq. (27) it is seen that the right-hand sides are indeed identical, and thus

$$\theta_{ij} = Q_{ij}^{(2)} \tag{56}$$

Then the exact expression can be written in terms of the strip-theory result,

$$Q_{ij} = Q_{ij}^{(2)} + \Delta Q_{ij} \tag{57}$$

where

$$\Delta Q_{ij} = -\frac{8\rho U^2 b^2 \cot \Lambda e^{i\omega t}}{\beta}\int_{-1}^{1}\int_{0}^{1-|\eta|} \left\{\sum_{m=0}^{M}\sum_{n=0}^{N}\sum_{r=0}^{R}\sum_{s=0}^{S} a_{mn}b_{rs}\sum_{p=1}^{\leq (r/2)} \eta^{m+r-2p}\frac{x^{n-1}}{\cot^{2p}\Lambda}(-n + 2ikx) \times \left(\frac{r!p!2^{p}}{(2p)!(r-2p)!}\right)\left[\frac{B\left(\frac{1}{2}, p + \frac{1}{2}\right)}{\pi}\right]\left(\frac{M}{\beta^2\bar{\omega}}\right)^{p}\left(2ik + \frac{\partial}{\partial x}\right)\int_{0}^{x} u^{p}e^{-i\bar{\omega}u}(x-u)^{s}J_p\left(\frac{\bar{\omega}}{M}u\right)du\right\}dx d\eta \tag{58}$$

Thus the error term involved in the use of strip theory can be evaluated explicitly. Several numerical comparisons are carried out in Appendix A. Although the number of cases is insufficient to be conclusive, it would appear that the strip-theory calculation is accurate enough for most applications.

Also, although the analysis has been carried out on the basis of unsteady flow, it is correct for the limiting case of steady flow. Thus strip theory is shown to be exact for such consideration as the effect of flexibility on the total lift, pitching moment, rolling moment in steady flow. In addition it may be noted that the reasoning behind the strip-theory formulation is also valid for the determination of these quantities in transient problems, and for more arbitrary supersonic planforms.

TABLE 1

Comparison of the Strip-Theory Results for the Generalized Force $Q_{jj}^{(2)}$ with the Exact Q_{jj}.

Mode Shape, g_j	M	$\bar{\omega}$	$\frac{Q_{jj}e^{-i\omega t}}{2\rho U^2 b^2}$	Phase Angle Degrees	$\frac{Q_{jj}^{(2)}e^{-i\omega t}}{2\rho U^2 b^2}$	Phase Angle Degrees	Percentage Error in Magnitude
$2b\left(\frac{y}{\cot \Lambda}\right)^2 e^{i\omega t}$	3/2	0.5	0.070,434,8	−92.3	0.066,090,9	−91.8	−6.2
$2b\left(\frac{y}{\cot \Lambda}\right)^2 e^{i\omega t}$	2	0.5	0.059,227,1	−91.2	0.057,648,0	−91.0	−2.7
$2b\left(\frac{y}{\cot \Lambda}\right)^2 e^{i\omega t}$	5/2	0.5	0.049,596,4	−90.8	0.048,831,8	−90.7	−1.5
$2b\left(\frac{y}{\cot \Lambda}\right)^2 e^{i\omega t}$	2	0.2	0.023,728,3	−90.5	0.023,088,4	−90.4	−2.7
$2b\left(\frac{y}{\cot \Lambda}\right)^2 e^{i\omega t}$	2	1.0	0.117,798,0	−92.4	0.114,783,5	−92.0	−2.6
$2b\left(\frac{y}{\cot \Lambda}\right)^3 e^{i\omega t}$	2	0.5	0.031,921,2	−91.0	0.030,900,4	−90.8	−3.2
$2b\left(\frac{y}{\cot \Lambda}\right)^4 e^{i\omega t}$	2	0.5	0.019,747,9	−97.5	0.019,232,6	−90.7	−2.6
$2b\left(\frac{y}{\cot \Lambda}\right)^2 (1-x)^2 e^{i\omega t}$	2	0.5	0.003,838,7	−174.4	0.003,670,7	−174.8	−4.4

Appendix A—Numerical Comparison of Strip-Theory and Exact Results

The derivation above has already shown that the strip-theory calculation will be exact as long as the virtual displacement mode is at most linear in y. However, it would also seem reasonable that the strip-theory calculation should serve as a good approximation for higher order spanwise variation of the virtual displacement mode. In an effort to check this conclusion, calculations have been carried out for several higher order modes.

For the example chosen, the sweep angle, Λ, was taken as 45°. In each case the quantity determined is Q_{jj}, that is, the contribution of the aerodynamic forces due to mode j to the generalized force due to a virtual displacement in mode j. The mode considered, the values of the remaining parameters, and the comparison of Q_{jj} and $Q_{jj}^{(2)}$ are given in Table 1.

Appendix B—Example of Evaluation of the Generalized Forces

From the foregoing it would appear that the most straightforward method of determining the generalized force using strip theory would be as follows: First determine the generalized force on spanwise strips making use of previous work and available tables, then employ a numerical spanwise integration scheme. However, as indicated in Eqs. (40) to (46), the integrations in the exact expression can be reduced to known tabulated functions. Since the strip-theory portion can be distinctly identified, this will often be a simpler and more convenient method of evaluation.

To illustrate, consider the generalized force $Q_{jj}^{(2)}$ for a mode given by

$$g_j = 2b\left(\frac{y}{\cot \Lambda}\right)^2 e^{i\omega t} \tag{B1}$$

Then, by comparison with Eqs. (17) and (18),

$$N = S = 0, \qquad M = R = 2$$
$$a_{00} = a_{10} = b_{00} = b_{10} = 0, \quad a_{20} = b_{20} = 1 \tag{B2}$$

Since the strip-theory result has been shown to correspond to the $p = 0$-term of the exact result, from Eqs. (41) and (43),

$$Q_{jj}^{(2)} = -\frac{8\rho U^2 b^2 \cot \Lambda e^{i\omega t}}{\beta} I \tag{B3a}$$

and

$$I = \frac{4ik}{5}\int_0^1 \int_u^1 (1-x)^5 \left\{2ike^{-i\omega u} J_0\left(\frac{\bar{\omega}}{M}u\right)\right\} dxdu + \frac{4ik}{5}\int_0^1 (1-u)^5 e^{-i\omega u} J_0\left(\frac{\bar{\omega}}{M}u\right) du$$
$$= \frac{4ik}{5}\int_0^1 \left\{(1-u)^5 + \frac{2ik}{6}(1-u)^6\right\} e^{-i\bar{\omega}u} J_0\left(\frac{\bar{\omega}}{M}u\right) du \tag{B3b}$$

Therefore,

$$Q_{jj}^{(2)} = \frac{32\rho U^2 b^2 \cot \Lambda k e^{i\omega t}}{5\beta} \left\{ -i(f_0 - 5f_1 + 10f_2 - 10f_3 + 5f_4 - f_5) + \frac{k}{3}(f_0 - 6f_1 + 15f_2 - 20f_3 + 15f_4 - 6f_5 + f_6) \right\} \quad \text{(B4)}$$

where f_λ is the function defined in Eq. (46).

When higher order Bessel functions are involved, it is necessary to first reduce the order, for example[14]

$$J_p(\alpha x) = \frac{2(p-1)}{\alpha x} J_{p-1}(\alpha x) - J_{p-2}(\alpha x) \quad \text{(B5)}$$

In this manner, the order can be reduced to zero and one. Finally J_1 can be eliminated by partial integration, employing either of the identities[14]

$$\frac{d}{dx}\{xJ_1(\alpha x)\} = \alpha x J_0(\alpha x) \quad \text{(B6)}$$

$$\frac{d}{dx}\{J_0(\alpha x)\} = -\alpha J_1(\alpha x) \quad \text{(B7)}$$

Thus the integrals can always be reduced to the f_λ − function.

References

[1] Miles, J. W., *On Harmonic Motion of Wide Delta Airfoils at Supersonic Speeds*, Navord Report 1234, June 13, 1950.

[2] Miles, J. W., *On Non-Steady Motion of Delta Wings*, Journal of the Aeronautical Sciences, Readers' Forum, Vol. 16, No. 9, pp. 568–569, September, 1949.

[3] Miles, J. W., *Simple Planforms in Supersonic Flow*, Journal of the Aeronautical Sciences, Readers' Forum, Vol. 17, No. 2, p. 127, February, 1950.

[4] Garrick, I. W., and Rubinow, S. I., *Theoretical Study of Air Forces on an Oscillating or Steady Thin Wing in a Supersonic Main Stream*, NACA TN 1383, July, 1947.

[5] Ursell, F., and Ward, G. N., *On Some General Theorems in the Linearized Theory of Compressible Flow*, Quarterly Journal of Mechanics and Applied Mathematics, Vol. III, Part 3, pp. 326–348, September, 1950.

[6] Flax, A. H., *Reverse Flow and Variational Theorems for Lifting Surfaces in Non-Stationary Compressible Flow*, Cornell Aeronautical Laboratory Report No. CAL-42, February, 1952.

[7] Heaslet, M. A., and Spreiter, J. R., *Reciprocity Relations in Aerodynamics*, NACA TN 2700, May, 1952.

[8] Voss, H. M., Zartarian, G., and Hsu, P. T., *Theoretical and Experimental Investigation of the Aeroelastic Behavior of Low-Aspect-Ratio Wings*, MIT Aero-Elastic and Structures Report for the Bureau of Aeronautics, Contract NOa(s) 51-109-c, June 15, 1953.

[9] Whittaker, E. T., and Watson, G. N., *A Course of Modern Analysis*, Fourth Edition, Cambridge University Press, 1950.

[10] Garrick, I. E., and Rubinow, S. I., *Flutter and Oscillating Air-Force Calculations for an Airfoil in a Two-Dimensioral Supersonic Flow*, NACA TR 846, 1946.

[11] Borbely, S. V., *Aerodynamic Forces on a Harmonically Oscillating Wing at Supersonic Velocity (Two-Dimensional Case)*, RTP Translation No. 2019, British Ministry of Aircraft Production (From Z.F.A., Bd. 22, Hft. 4, pp. 190–205, August, 1942).

[12] Schwarz, L., *Untersuchung einiger mit den Zylinderfunktionen Nullter Ordnung Verwandter Functionen*, Luftfahrtforschung, Bd. 20, Lfg. 12, pp. 341–372, February 8, 1944.

[13] Zartarian, G., and Voss, H. M., *On the Evaluation of the Function $f_\lambda(M, \bar{\omega})$*, Journal of the Aeronautical Sciences, Readers' Forum, Vol. 20, No. 11, pp. 780–781, November, 1953.

[14] Hildebrand, F. B., *Advanced Calculus for Engineers*, Prentice-Hall, Inc., New York, 1950.

Transition-Point Fluctuations . . .

(*Continued from page 738*)

[6] Lange, A. H., and Gieseler, L. P., *Measurement of Boundary-Layer Transition on a Standard Model to Determine the Relative Disturbance Level in Two Supersonic Wind Tunnels*, NAVORD Rep. 2752, U.S. Naval Ord. Lab. (Maryland), February 19, 1953.

[7] Lee, Roland E., *Measurements of Pressure Distribution and Boundary-Layer Transition on a Hollow-Cylinder Model*, NAVORD Rep. 2823, U.S. Naval Ord. Lab. (Maryland), April 28, 1953.

[8] Evvard, J. C., Tucker, M., and Burgess, W. C., Jr., *Statistical Study of Transition-Point Fluctuations in Supersonic Flow*, NACA TN 3100, 1953.

[9] Emmons, H. W., *The Laminar-Turbulent Transition in a Boundary Layer*, Part I, Journal of the Aeronautical Sciences, Vol. 18, No. 7, pp. 490–498, July, 1951.

[10] Emmons, H. W., and Bryson, A. E., *The Laminar-Turbulent Transition in a Boundary Layer*, Proc. First U.S. Nat. Cong. Appl. Mech., pp. 859–868, June, 1951.

[11] Ross, Albert O., *Determination of Boundary-Layer Transition Reynolds Numbers by Surface-Temperature Measurements of a 10° Cone in Various NACA Supersonic Wind Tunnels*, NACA TN 3020, 1953.

[12] Stine, Howard A., and Sherrer, Richard, *Experimental Investigation of the Turbulent-Boundary-Layer Temperature-Recovery Factor on Bodies of Revolution at Mach Numbers from 2.0 to 3.8*, NACA TN 2664, 1952.

[13] Coles, Donald, *Direct Measurement of Supersonic Skin Friction*, Journal of the Aeronautical Sciences, Vol. 19, No. 10, p. 717, October, 1952.

[14] Potter, J. L., *New Experimental Investigations of Friction Drag and Boundary Layer Transition on Bodies of Revolution at Supersonic Speeds*, NAVORD Rep. 2371, U.S. Naval Ord. Lab. (Maryland), April 24, 1952.

[15] Potter, J. L., *Friction Drag and Transition Reynolds Number on Bodies of Revolution at Supersonic Speeds*, NAVORD Rep. 2150, U.S. Naval Ord. Lab. (Maryland), August 20, 1950.

Effects of Certain Steady Motions on Small-Disturbance Airplane Dynamics

MALCOLM J. ABZUG*

Douglas Aircraft Company, Inc.

SUMMARY

Linearized equations of airplane motion are derived for small disturbances from flight with certain arbitrary steady motions. The conditions studied include flight with steady coordinated turning rates, steady pitching or rolling velocities, and steady longitudinal accelerations. The equations are solved to determine the effects of these maneuvers on the small-disturbance controls-fixed modes of motion of a typical fighter-type airplane. The main results indicate that the damping of the longitudinal short-period oscillation is decreased by steady rolling, but is relatively unaffected by the other conditions. The damping of the lateral oscillation (dutch-roll) is decreased by steady turning, steady positive pitching, and steady longitudinal deceleration, but is increased by steady rolling. Spiral mode divergence is experienced in turns at high bank angles. This mode is made more convergent by steady positive pitching, steady rolling, and steady longitudinal deceleration. The rolling mode, or large real lateral root, is relatively unaffected by any of the conditions studied. These results are significant with regard to the dynamic stability of both piloted and automatically-controlled flight in extreme maneuvers.

INTRODUCTION

PRESENT-DAY performance standards for automatically-controlled airplanes require that flight control systems be matched carefully to the dynamics of the airplane. The classic equations of airplane motion for small disturbances from steady straight symmetric flight[1] are generally used in system design to calculate the modes of airplane motion and airplane transfer functions.[2, 3] However, for airplanes which must be automatically controlled during extreme maneuvers, a stabilization system design based on small disturbances from steady straight symmetric flight may be inadequate. At the same time, it is desirable to avoid the difficulties inherent in using the general nonlinear equations of airplane motion for this purpose.

In this paper, linearized equations of small-disturbance motion are developed which are applicable to small disturbances from four conditions of maneuvering flight. The effects of these maneuvers on the controls-fixed modes of disturbed motion are investigated for a typical fighter-type airplane.

General small-disturbance equations of motion were previously developed by Frazer, Duncan, and Collar,[4] using matrix techniques. However, those equations involved disturbance variables in terms of earth coordinates, and are considered of less general usefulness than those of the present paper.

Received January 14, 1954.

* Design Specialist, Aerodynamics, El Segundo, Calif.

SYMBOLS

NACA stability axes[3] are used in this analysis. Vector quantities are indicated by boldface type.

$\mathbf{F}$	= aerodynamic force vector
$\mathbf{g}$	= acceleration of gravity vector
$\mathbf{H}$	= angular momentum vector
$\mathbf{Q}$	= aerodynamic moment vector
$\mathbf{V}$	= total velocity vector
$\mathbf{X}$	= disturbance rotation vector
$\boldsymbol{\Omega}$	= angular velocity vector
$\times$	= multiplication sign for vector cross-product
D	= absolute change (seen on the earth reference frame or on a reference frame in steady linear motion)
d, $d(\ )/dt$	= relative change, rate of change (seen on the airplane reference frame)
g	= acceleration of gravity
I_X, I_Y, I_Z, I_{XZ}	= moment and product of inertia about the X-, Y-, Z-, and X-Z axes
L, M, N	= rolling, pitching, and yawing aerodynamic moments
m	= mass
N_p	= $\partial N/\partial p$, etc.
n	= load factor
P, Q, R	= rolling, pitching, and yawing velocities
p, q, r	= disturbance rolling, pitching, and yawing velocities
s	= operator d/dt. s^{-1} is the operator $\int dt$
u, v, w	= disturbance velocities along the X-, Y-, and Z-axes
V	= total velocity
X, Y, Z	= longitudinal, lateral, and normal aerodynamic forces
γ	= flight path angle
ϕ	= bank angle (rotation about X-axis)

Subscript

1	= steady flight condition about which disturbances occur

DERIVATION OF EQUATIONS

General Equations of Airplane Motion

General equations of airplane motion which apply at any instant[1, 5] may be written in vector notation as:

$$\left.\begin{aligned}\mathbf{F} + m\mathbf{g} &= m(d\mathbf{V}/dt) + \boldsymbol{\Omega} \times m\mathbf{V}\\ \mathbf{Q} &= d\mathbf{H}/dt + \boldsymbol{\Omega} \times \mathbf{H}\end{aligned}\right\} \quad (1)$$

General Small-Disturbance Equations

In disturbed flight,

$$\left.\begin{aligned}\mathbf{F} &= \mathbf{F}_1 + D\mathbf{F}\\ \mathbf{g} &= \mathbf{g}_1 + D\mathbf{g} = \mathbf{g}_1\\ \mathbf{V} &= \mathbf{V}_1 + D\mathbf{V}, \text{ etc.}\end{aligned}\right\} \quad (2)$$

TABLE 1
General Equations of Small-Disturbance Airplane Motion.

		COEFFICIENT OF					
		u	v	w	p	q	r
EQUATIONS	$\Sigma dX/m + (dV/dt)_1 =$	s	$-R_1$	Q_1	0	$g\cos\gamma_1\cos\phi_1\, s^{-1}$	$-g\cos\gamma_1\sin\phi_1\, s^{-1}$
	$\Sigma dY/m =$	R_1	s	$-P_1$	$-g\cos\gamma_1\cos\phi_1\, s^{-1}$	0	$V_1-[g\sin\gamma_1+(dV/dt)_1]s^{-1}$
	$\Sigma dZ/m =$	$-Q_1$	P_1	s	$g\cos\gamma_1\sin\phi_1\, s^{-1}$	$-V_1+[g\sin\gamma_1+(dV/dt)_1]s^{-1}$	0
	$\Sigma dL =$	0	0	0	$I_X s - Q_1 I_{XZ}$	$R_1(I_Z-I_Y)-P_1 I_{XZ}$	$-I_{XZ}s+Q_1(I_Z-I_Y)$
	$\Sigma dM =$	0	0	0	$R_1(I_X-I_Z)+2P_1 I_{XZ}$	$I_Y s$	$P_1(I_X-I_Z)-2R_1 I_{XZ}$
	$\Sigma dN =$	0	0	0	$-I_{XZ}s+Q_1(I_Y-I_X)$	$P_1(I_Y-I_X)+R_1 I_{XZ}$	$I_Z s+Q_1 I_{XZ}$

where $\mathbf{F}$, $\mathbf{g}$, $\mathbf{V}$, etc., apply to disturbed flight, $\mathbf{F}_1$, $\mathbf{g}_1$, $\mathbf{V}_1$, etc., apply to the steady flight condition that existed previously and $D\mathbf{F}$, $D\mathbf{g}$, $D\mathbf{V}$, etc., are the absolute vector changes that occurred in the interval. The absolute vector changes are related to changes seen by an observer on the airplane reference frame $d\mathbf{F}$, $d\mathbf{g}$, $d\mathbf{V}$, etc., by:[6]

$$\left.\begin{aligned} D\mathbf{F} &= d\mathbf{F} + \mathbf{X}\times\mathbf{F}_1 \\ D\mathbf{g} &= d\mathbf{g} + \mathbf{X}\times\mathbf{g}_1 \\ D\mathbf{V} &= d\mathbf{V} + \mathbf{X}\times\mathbf{V}_1, \text{ etc.} \end{aligned}\right\} \tag{3}$$

Substituting Eqs. (2) and (3) into (1), neglecting the products of infinitesimals, and simplifying, the general equations of motion for small disturbances from steady flight are:

$$\left.\begin{aligned} d\mathbf{F}/m + \mathbf{X}\times[(d\mathbf{V}/dt)_1 - \mathbf{g}_1] + (d\mathbf{V}/dt)_1 &= d\mathbf{V}/dt + \boldsymbol{\Omega}_1\times d\mathbf{V} + d\boldsymbol{\Omega}\times\mathbf{V}_1 \\ d\mathbf{Q} &= d\mathbf{H}/dt + \boldsymbol{\Omega}_1\times d\mathbf{H} + d\boldsymbol{\Omega}\times\mathbf{H}_1 \end{aligned}\right\} \tag{4}$$

Eqs. (4) are given in Cartesian form in Table 1, using NACA stability axes.[3] These equations apply, in general, to small disturbances from asymmetric flight since the initial rolling and yawing angular velocities are not necessarily zero. As a result, the aerodynamic cross-derivatives such as M_p and M_r are also not necessarily identical to zero.

Classic Small-Disturbance Equations of Airplane Motion

The classic equations of airplane motion for small disturbances from steady straight symmetric flight may be obtained from Table 1 by setting the following quantities equal to zero: P_1, Q_1, R_1, ϕ_1, and $(dV/dt)_1$. In this case, the equations are separable into symmetric or longitudinal, and asymmetric or lateral sets.

Equations for Small Disturbances from Turning Flight

In steady turning flight about a vertical space axis:

$$\left.\begin{aligned} P_1 &= -\Omega\sin\gamma_1 \\ Q_1 &= \Omega\cos\gamma_1\sin\phi_1 \\ R_1 &= \Omega\cos\gamma_1\cos\phi_1 \end{aligned}\right\} \tag{5}$$

where, for coordinated turning flight (resultant aerodynamic force in the plane of symmetry), Ω_1 may be approximated by:

$$\Omega_1 = g\tan\phi_1/V_1 \tag{6}$$

Eq. (6) is valid for large absolute values of the initial flight path angle γ_1.

Equations for Small Disturbances from Steady Pitching or Rolling Flight

These equations may be obtained from Table 1 by the appropriate substitutions of Q_1 or P_1. In the former case, the equations are separable into longitudinal and lateral equations. The equations of lateral motion for small disturbances from steady pitching flight may be used to obtain a linearized representation of the rolling-pullout maneuver. The airplane's load factor is found in this case as:

$$n = Q_1 V_1/g + \cos\gamma_1 \tag{7}$$

A simplified form of the equations of motion for small disturbances from steady rolling flight has been developed by Phillips.[3]

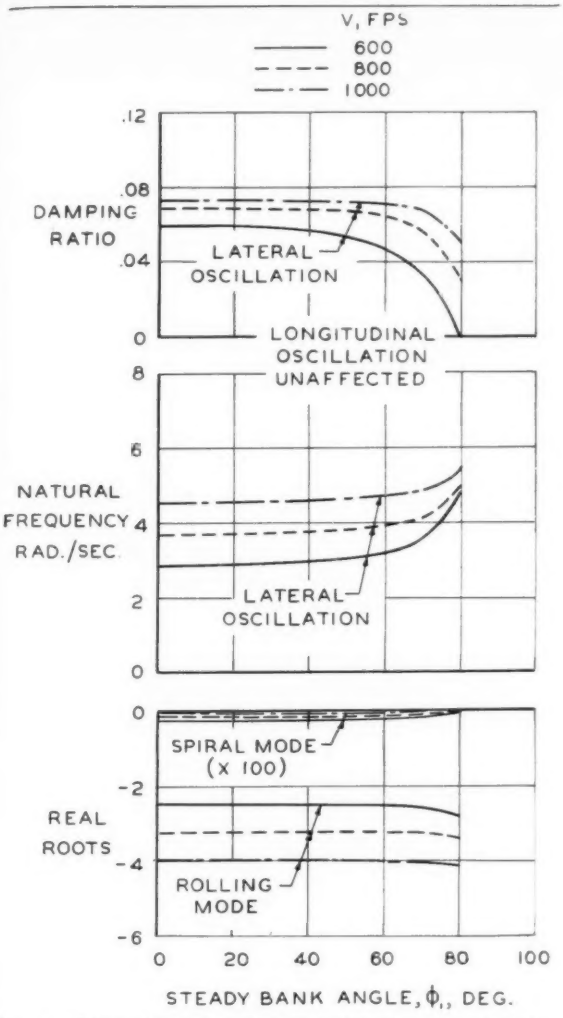

FIG. 1. Effect of steady turning on modes of motion of typical fighter-type airplane.

Equations for Small Disturbances from Longitudinally Accelerated Flight

These equations are obtained from Table 1 by letting P_1, Q_1, R_1, and ϕ_1 equal zero. The equations are then separable into longitudinal and lateral equations.

RESULTS

The effects of the conditions studied on the controls-fixed modes of motion of a typical fighter-type airplane have been determined by making numerical solutions of the equations of Table 1. These calculations were made assuming zero airspeed change during the motion, for three flight conditions. Stability derivative values used in the calculations are listed in the Appendix.

Effects of Steady Turning on Modes of Motion

The effects of steady turning on the modes of airplane motion are presented in Fig. 1, as functions of the steady bank angle. The lateral oscillatory mode becomes more lightly damped, and increases in frequency as the bank angle is increased, while the spiral mode becomes slightly more convergent at first, and then divergent at extreme bank angles. The other modes of motion are substantially unaffected, except for the long period or phugoid oscillation. Although not shown, the damping of the phugoid mode is sharply increased at high bank angles, due to the effect of increased drag.

An important result of this study is that the lateral and longitudinal modes of motion are not independent for small disturbances from steady turning flight. For example, the lateral oscillation following a sideslip angle disturbance affects measurably the angle of attack and pitching velocity variables at a high steady angle of bank. This coupling is evident in Table 1 in a number of terms involving both gravity forces and inertial forces and moments. The characteristic equation is a ninth-degree polynomial, with a single zero root representing the neutral azimuth mode.

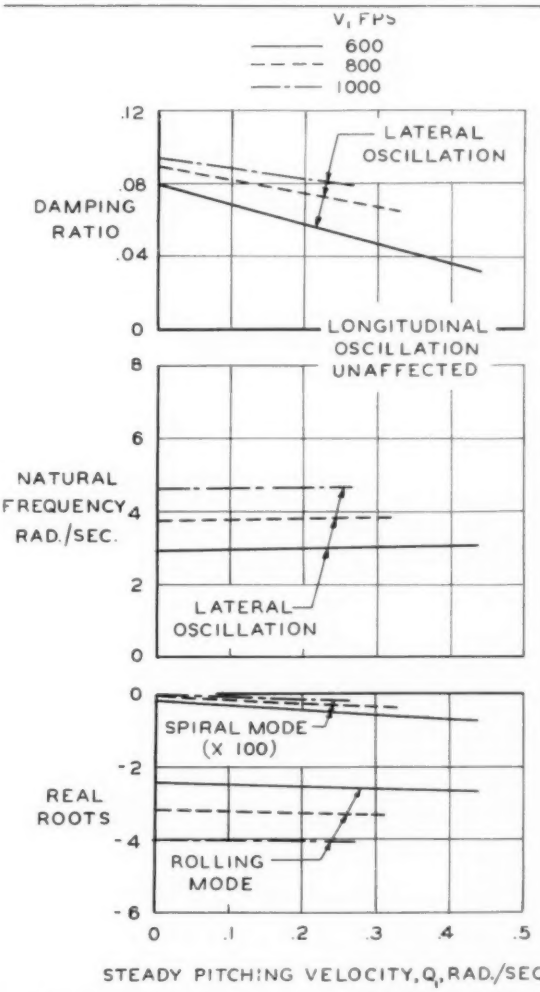

FIG. 2. Effect of steady pitching on modes of motion of typical fighter-type airplane.

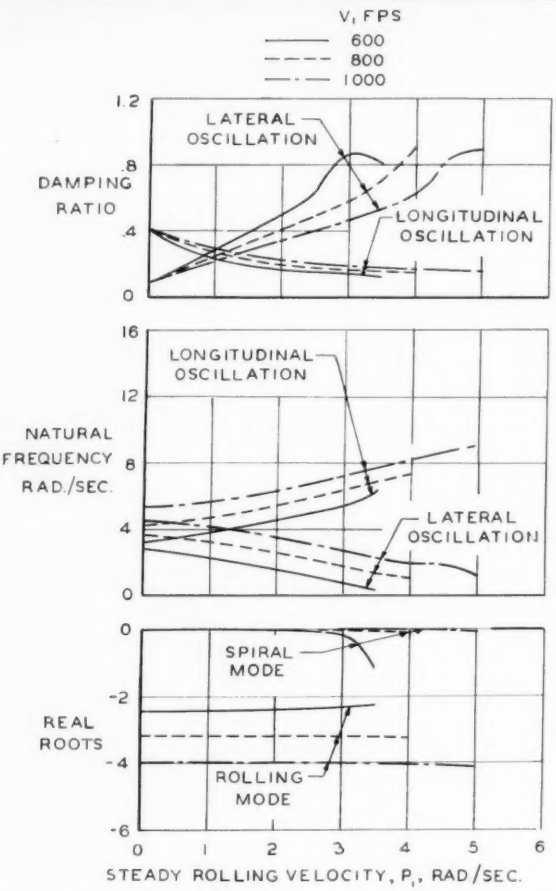

FIG. 3. Effect of steady rolling on modes of motion of typical fighter-type airplane.

Effects of Steady Pitching on Modes of Motion

The effects of steady positive pitching on the modes of motion are presented in Fig. 2 for the example airplane, as functions of the steady pitching velocity. At constant airspeed, the short-period longitudinal mode is not affected. Slight reduction in damping of the lateral oscillation is shown in Fig. 2 for positive pitching, due to a negative contribution to N_p. On the other hand, the spiral mode becomes more convergent due to a negative contribution to the derivative L_r, for the particular inertia values considered. The rolling convergence is relatively unaffected.

Effects of Steady Rolling on Modes of Motion

The effects of steady rolling on the oscillatory modes of motion shown in Fig. 3 agree substantially with the simplified calculations of Phillips,[8] for the same constants. As indicated by Phillips, the higher-frequency mode (longitudinal) increases in frequency at high rolling velocities, and conversely for the lower-frequency mode (lateral). The reduction in damping of the longitudinal oscillation shown could be serious for a highly maneuverable airplane. Steady rolling makes the spiral mode strongly convergent, for the low-speed flight condition. As in the case of small disturbances from steady turns, the longitudinal and lateral modes of motion are coupled during steady rolls.

Effects of Steady Longitudinal Acceleration on Modes of Motion

The effects of steady longitudinal acceleration on the modes of motion of the example airplane are shown in Fig. 4. The reduction in damping of the lateral oscillation shown for deceleration may be a problem on airplanes where sudden reductions in thrust or increases in drag are possible. For the same conditions, the convergence of the spiral mode is greatly increased by an outward-acting effective side force due to yaw.

CONCLUDING REMARKS

The effects of steady turning, steady pitching or rolling velocities, and steady longitudinal acceleration on the small-disturbance controls-fixed modes of motion of a typical fighter-type airplane have been investigated. From the standpoint of both piloted and automatically-controlled flight the most significant effects found were:

(*Continued on page 762*)

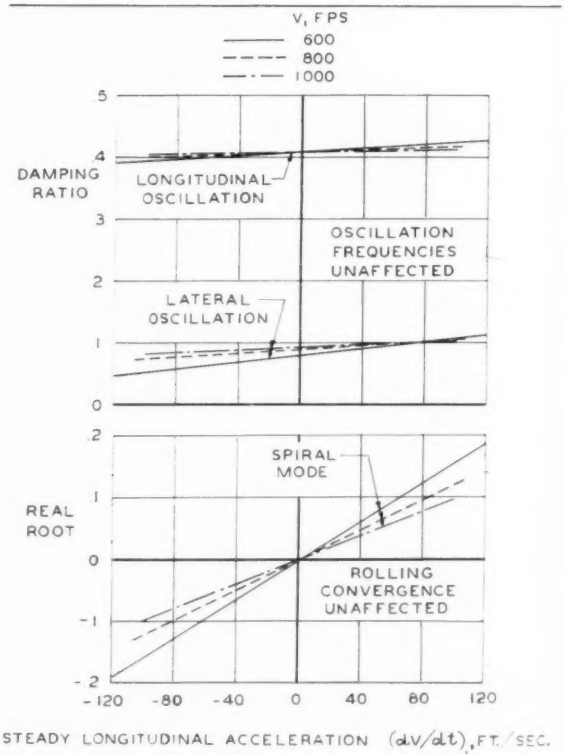

FIG. 4. Effect of steady longitudinal acceleration on modes of motion of typical fighter-type airplane.

On Structural Fatigue Under Random Loading*

JOHN W. MILES†

University of California, Los Angeles

ABSTRACT

Experience has shown that the fluctuating loads induced by a jet may cause fatigue failure of aircraft structural components. In order to throw some light on this and similar problems, the stress spectrum and the "equivalent fatigue stress" of an elastic structure subjected to random loading are studied. The analysis is simplified by assuming the structure to have only a single degree of freedom and by using the concept of cumulative damage, the results being expressed in terms of quantities that can be directly measured. As an example, a similarity expression for the probable value of the equivalent fatigue stress of a panel subjected to jet buffeting is derived.

NOTATION

A = panel area
$A(\omega)$ = resonant amplification factor, Eq. (2-12)
$C_{1,2}$ = undetermined coefficients
D = cumulative damage, Eq. (4-3)
E = Young's modulus for panel
$F(t)$ = instantaneous magnitude of force
F_0 = root mean square load—i.e., $\sqrt{\overline{F^2(t)}}$
M = subscript referring to Miner (reference 12)
$N(s)$ = number of complete stress reversals of amplitude s required to produce fatigue failure
N_i = $N(s_i)$
$P\{\ \}$ = the probability of the event $\{\ \}$
P_m = probability distribution of the envelope of $y(t)$, Eq. (3-4)
Re = Reynolds Number of jet
T_0 = period of dominant mode of oscillation
U = velocity of jet with respect to surrounding medium
Z = impedance of oscillator, Eq. (2-11)
a_0 = sonic velocity in air surrounding jet
d = jet diameter at nozzle exit
erfc = complementary error function
$f(\omega)$ = power spectral density of the force $F(t)$
$f_a(\omega)$ = see Eq. (2-8) and Fig. 4
$f_b(\omega)$ = see Eq. (2-9) and Fig. 4
g = gravitational acceleration
$g(\omega)$ = power spectral density of $y(t)$
h = panel thickness
k = a constant defined by Eq. (4-6); $k = 1$ on Miner's theory (reference 12); $k = 2$ on Shanley's theory (reference 13)
n_i = number of complete stress reversals at amplitude s_i
p_0 = static pressure of air into which jet exhausts
s = stress
$s(t)$ = instantaneous stress
s_e = equivalent or reduced fatigue stress; see Section 4
s_0 = static stress produced by F_0
s_1 = stress level (hypothetical) at which fatigue failure occurs in one complete cycle
t = time
w = specific weight of panel material
x = distance from source (jet exhaust) of aerodynamic noise to panel
$y(t)$ = instantaneous displacement of oscillator
y_0 = static displacement that would be produced by the root mean square load (F_0)
$\overline{y^2(t)}$ = mean square displacement
Γ = Gamma function; $\Gamma(n+1) = n!$ if n is an integer
α = see Eq. (4-1) and Fig. 8
δ = damping of dominant mode expressed as a fraction of critical damping and equal to logarithmic decrement divided by 2π (if $\delta << 1$)
ρ_0 = mass density of air
Φ = an arbitrary function
ψ_0 = mean square value of displacement or stress
ω = angular frequency
ω_0 = angular frequency of dominant mode of oscillation
ω_1 = characteristic frequency of input spectrum $f(\omega)$; equal to frequency of $f_{max.}$ unless $f_{max.}$ at $\omega = 0$, in which case ω_1 designates (approximately) half power point, Eq. (2-7).

Presented at the Aeroelasticity Session, Twenty-Second Annual Meeting, IAS, New York, January 25–29, 1954.

* The present paper differs in several respects from IAS Preprint No. 435 and Douglas Aircraft Report SM-14795 (June, 1953), both of which were titled "An Approach to the Buffeting of Aircraft Structures by Jets."

† Associate Professor of Engineering; also Consultant, Douglas Aircraft Company, Inc., Santa Monica, Calif.

(1) INTRODUCTION

THE PROBLEM OF DETERMINING the stresses resulting from random loading and the consequent possibility of fatigue failure appears to have received but little attention in structural design. However, recent advances in both the statistical techniques[1, 2] and the basic physical concepts[3–8] render possible an approximate analysis of some of the more important features of the problem. The statistical techniques, at least in their modern form, are due primarily to Rice[1] and Wiener.[2] The physical concepts underlying the phenomena to be considered have recently been reviewed and expounded by Liepmann[3, 4] and by Luskin and Lapin[5]; the present work may be regarded as an extension of that of Liepmann.[3] Reference also may be made to the fundamental work of Lin,[6] Uhlenbeck and his students,[7] and Graham and Rodriguez.[8] In addition to these references, the writer is indebted to H. Klein, H. W. Liepmann, and H. Luskin for frequent discussions of this problem.

The present investigation was prompted by the possibility of panel failure under the fluctuating pressure (i.e., buffeting) of a jet exhaust (Fig. 1), a special case of the more general problem of structural fatigue under random loading. A second example of aero-

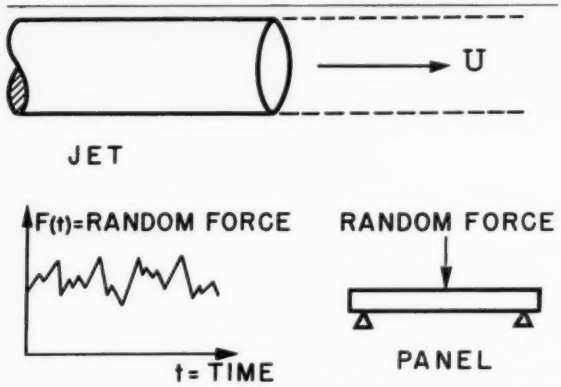

FIG. 1. A panel subjected to a random force resulting from the fluctuating pressure field of an adjacent jet. In the analysis of the text it is assumed that the force may be considered to act at a single point.

nautical interest is repeated gust loading of a wing. The general problem can be resolved into three more or less distinct parts:

(a) The statistical description of the random loading.

(b) The statistical description of the dynamical response of the prescribed structure under this loading.

(c) The determination of the probability of fatigue failure associated with this response.

Problem (a) will not be treated in the present study, although two representative statistical descriptions of the loading will be considered. In general, this information must be obtained experimentally (Fig. 2), but theoretical considerations also may be valuable. If the excitation is aerodynamic noise (as for the jet exhaust already cited), there exists the recent theory of Lighthill,[9] which has received some experimental verification.[10] Gust loading and related problems have been discussed extensively in references 3, 4, 5, and 11 and also in the references cited therein.

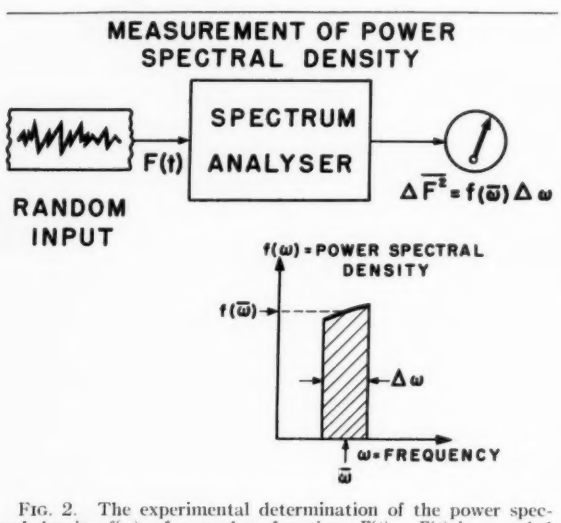

FIG. 2. The experimental determination of the power spectral density $f(\omega)$, of a random function, $F(t)$. $F(t)$ is recorded (e.g., on a tape) and fed into a spectrum analyzer that transmits only those components within the pass band $\bar{\omega} \pm (1/2)\Delta\omega$. The intensity (to which the power is proportional) of the output in the pass band—viz., $\Delta\overline{F^2}$—is recorded on a mean square meter, and the power spectral density at $\bar{\omega}$ is determined by dividing $\Delta\overline{F^2}$ by $\Delta\omega$. Thus, the meter reading, $\Delta\overline{F^2}$, appears in the power spectral density *vs.* frequency plane as an increment of area of width $\Delta\omega$ and mean ordinate $f(\bar{\omega})$.

The determination of the response of a dynamical system under random loading has been considered in references 3–8. The model selected for the present study is a single degree of freedom (lightly damped) oscillator loaded at one point, for which the analysis is similar to that of references 3 and 6. This model exhibits the essential feature that distinguishes the dynamic response of an elastic system from the corresponding static response—namely, the relatively sharp (frequency) selectivity associated with resonance. On the other hand, a distributed structure has an infinite set of resonant frequencies and a (possibly several) characteristic length(s) that must be compared with some characteristic length of the excitation in order to establish a measure of the phase differences among loads at various points. The former shortcoming of the single degree of freedom model is not believed to be serious, since one mode usually will dominate the dynamic response of a distributed structure, but the effects of distributed loading would appear to justify further investigation.

At the present time, the description of fatigue appears to rest on an almost entirely phenomenological basis, and analytical work on the subject is slight. The present analysis will be based on Miner's concept of "cumulative damage,"[12] and on Shanley's extension[13] of this concept. It is the writer's opinion (cf. references 12, 13, 17, 19, and 20) that the cumulative damage concept is probably adequate in the sense that presently available data do not permit the prediction of fatigue life to better than a factor of two (indeed on statistical grounds, this may never be possible *for a single sample*); however, an alternative approach is discussed in the Appendix, and it is concluded that the assumption of a representative type of nonlinear accumulation of damage leads to only an insignificant change in fatigue life when, as in the present study, stress amplitudes are distributed continuously over a wide range.

(2) Response of a Simple Oscillator

A simple oscillator can be characterized by ω_0, its resonant frequency, δ, the ratio of the actual damping to critical damping (and equal to the logarithmic decrement of the free oscillations divided by 2π provided that this decrement is small), and y_0, the static response to some reference input F_0. If the mechanical model of Fig. 3, having mass m, spring constant k, and viscous damping constant c, is adopted, then

$$\omega_0 = \sqrt{k/m} \tag{2-1}$$

$$\delta = c/2\sqrt{km} \tag{2-2}$$

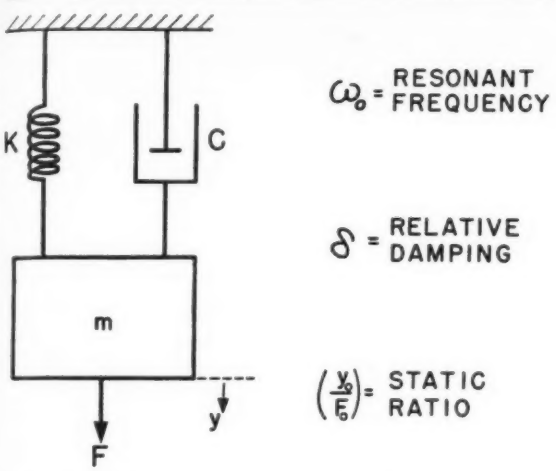

FIG. 3. A *model* of a single degree of freedom oscillator, characterized by its resonant frequency, relative damping, and static ratio.

$$y_0 = F_0/k \tag{2-3}$$

but, irrespective of the actual model, the parameters ω_0, δ and (y_0/F_0), being more amenable to generalization and subject to experimental determination, are preferable to such a set as (m, c, k).

Let $y(t)$ represent the displacement of the oscillator from its position of static equilibrium (mg/k for the model of Fig. 3); then the differential equation governing its response to the input $F(t)$ is, in dimensionless form,

$$\left(\frac{\ddot{y}}{\omega_0^2 y_0}\right) + 2\delta\left(\frac{\dot{y}}{\omega_0 y_0}\right) + \left(\frac{y}{y_0}\right) = \frac{F(t)}{F_0} \tag{2-4}$$

which, for the model of Fig. 3, is equivalent to the more familiar form

$$m\ddot{y} + c\dot{y} + ky = F(t) \tag{2-5}$$

However, the dimensionless form, Eq. (2-4), is to be preferred in the present study, not only in being independent of the particular model but also in that, by virtue of Hooke's law, the displacement $y(t)$ may be replaced by the stress $s(t)$ provided that y_0 also is replaced by s_0, the static stress produced by F_0.

Now suppose that $F(t)$ is a random function having the power spectral density $f(\omega)$. The latter can be broadly characterized by two parameters: the mean square value of $F(t)$, given by

$$\overline{F^2(t)} = \int_0^\infty f(\omega)\, d\omega \tag{2-6}$$

and some characteristic frequency, here designated as ω_1. If $f(\omega)$ is a monotonically decreasing function of ω, it is convenient to choose $\omega_1 = \omega_{1/2}$ where $\omega_{1/2}$ defines (at least roughly) the "half power point"—viz.

$$\int_0^{\omega_{1/2}} f(\omega)\, d\omega \simeq \int_{\omega_{1/2}}^\infty f(\omega)\, d\omega \tag{2-7}$$

If, on the other hand, $f(\omega)$ exhibits a peak at some frequency ω_m that is appreciably greater than zero it is convenient to choose $\omega_1 = \omega_m$.

Examples of these two possible types of power spectral density are given by

(a) Monotonic:

$$f_a(\omega) = (2\overline{F^2}/\sqrt{\pi}\,\omega_1)e^{-(\omega/\omega_1)^2} \tag{2-8}$$

(b) Peaked:

$$f_b(\omega) = (4\overline{F^2}/\sqrt{\pi}\omega_1)\,(\omega/\omega_1)^2\, e^{-(\omega/\omega_1)^2} \tag{2-9}$$

and are plotted in Fig. 4. The half power point for f_a occurs approximately at $\omega = 0.48\,\omega_1$. It is, of course, conceivable that $f(\omega)$ could exhibit several maxima, but $f_a(\omega)$ and $f_b(\omega)$ may be considered to be adequate representations (for the present investigation) of the more important types.

The response of the oscillator at a particular frequency ω is governed by its force-displacement impedance,* $Z(\omega)$, and the power spectral density of this response is given by (reference 3)

$$g(\omega) = f(\omega)/|Z(\omega)|^2 \tag{2-10}$$

In terms of the parameters defined above, $|Z|^2$ is given by

$$|Z(\omega)|^2 = \left(\frac{F_0}{y_0}\right)^2\left\{\left[1 - \left(\frac{\omega}{\omega_0}\right)^2\right]^2 + 4\delta^2\left(\frac{\omega}{\omega_0}\right)^2\right\} \tag{2-11}$$

The "power amplification curve," or the square of the usual resonance curve, is given by

* $Z(\omega)$ is defined such that if $F(t) = e^{i\omega t}$, $y(t) = e^{i\omega t}/Z(\omega)$.

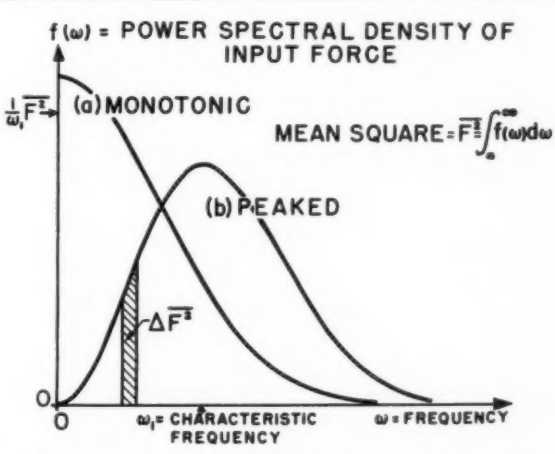

FIG. 4. Typical power spectral densities, as given by Eqs. (2-8) and (2-9). Such curves usually are determined experimentally, a single reading of the type illustrated in Fig. 2 leading to an increment of area such as that shown under curve (b).

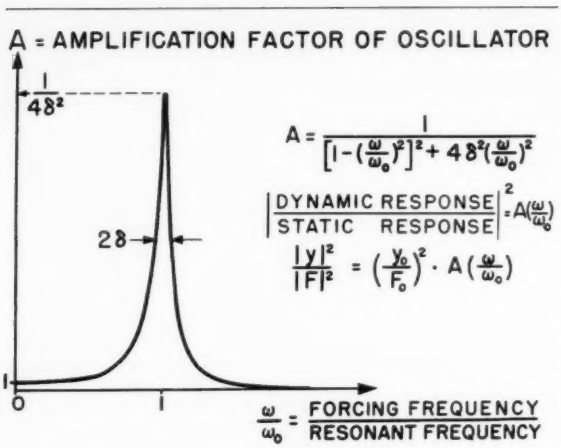

FIG. 5. The power amplification curve of a single degree of freedom oscillator, as given by Eq. (2-12).

$$A(\omega) = \left(\frac{F_0}{y_0}\right)^2 |Z(\omega)|^{-2} = \frac{1}{[1 - (\omega/\omega_0)^2]^2 + 4\delta^2(\omega/\omega_0)^2} \tag{2-12}$$

and is plotted in Fig. 5 for $\delta = 0.1$.

If $(\delta\omega_0/\omega_1) = 0(1)$, as illustrated in Fig. 6, the response of the oscillator is essentially resonant and it receives appreciable loading only in the neighborhood of resonance, in which neighborhood its power spectral density is approximated by

$$g(\omega) \simeq \frac{f(\omega_0)}{|Z(\omega)|^2} = \left(\frac{y_0}{F_0}\right)^2 f(\omega_0)A(\omega), \qquad \frac{\delta\omega_0}{\omega_1} = 0(1) \tag{2-13}$$

and (*in the neighborhood of* ω_0) has the same shape as the (power) resonance curve of Fig. 5. If, on the other hand, $(\delta\omega_0/\omega_1) >> 1$, the response of the oscillator would be essentially static ($A \simeq 1$), and its power spectral density would be given approximately by

$$g(\omega) \simeq \frac{f(\omega)}{|Z(0)|^2} = \left(\frac{y_0}{F_0}\right)^2 f(\omega), \qquad \frac{\delta\omega_0}{\omega_1} >> 1 \tag{2-14}$$

and would have the same shape as the power spectral density of the loading.

The first of these two possibilities is technically the more interesting, since the amplification associated with resonance is generally large. Thus, resonance appears to be an essential factor in the fatigue failure of a panel subjected to jet buffeting. On the other hand, the loading of a wing by randomly encountered gusts might be considered to be essentially static (but the motion of the airplane as a rigid body may be important) in consequence of the relatively low frequency (compared with, say, the fundamental wing bending frequency) at which gusts of appreciable magnitude are met.

The subsequent analysis is directed primarily toward the problem of essentially resonant response, since it is not only of greater practical interest but also is mathematically simpler by virtue of the concentration of the power spectral density of the response in the neighborhood of the resonant frequency.

(3) Statistical Properties of the Response

The complete statistical description of a random function $y(t)$ requires the specification not only of its power spectral density $g(\omega)$, giving its frequency distribution, but also its probability distribution in time. The distribution most commonly encountered and also most amenable to analysis (*cf.* references 1 and 2) is designated as normal (or Gaussian) and gives as the probability that $y(t)$ may be found between the prescribed values y and $y + dy$

$$P\{y < y(t) < y + dy\} = e^{-y^2/2\psi_0} dy \,/\, \sqrt{2\pi\psi_0} \tag{3-1}$$

where ψ_0 designates the mean square value of $y(t)$—viz.,

$$\psi_0 = y^2(t) = \int_0^\infty g(\omega)\, d\omega \tag{3-2}$$

Certain results of practical interest may be calculated directly from Eq. (3-1) without the necessity of further assumptions. Thus, replacing the displacement y by the stress s and regarding ψ_0 as the mean square stress, the probability of static failure, defined by $|s(t)| > s_f$, where s_f is some arbitrarily prescribed value (e.g., elastic limit or yield point), is obtained by integrating Eq. (3-1)—viz.,

$$P\{|s(t)| > s_f\} = 2\int_{s_f}^{\infty} \frac{e^{-s^2/2\psi_0} ds}{\sqrt{2\pi\psi_0}} \tag{3-3a}$$

$$= \operatorname{erfc}(s_f/\sqrt{2\psi_0}) \tag{3-3b}$$

$$= 2\sqrt{\frac{\psi_0}{2\pi s_f^2}}\, e^{-s_f^2/2\psi_0}\left[1 - \left(\frac{\psi_0}{s_f^2}\right) \cdots\right] \tag{3-3c}$$

However, the calculation of such quantities as probable fatigue life demands that additional information and/or assumptions be introduced.

The analysis of the essentially resonant response is especially simple in that it is *completely* characterized by the resonant frequency ω_0 and the mean square response ψ_0 (*cf.* the *broad* characterization of $F(t)$ by ω_1 and F^2). Moreover, whatever the statistical distribution (in time, not frequency) of the input $F(t)$, the response $y(t)$ tends to a normal distribution as its bandwidth becomes small compared with that of $f(\omega)$—i.e., as $(\delta\omega_0/\omega_1)$ tends to zero.*

* It is generally argued that this result follows directly from the central limit theorem (see also reference 14).

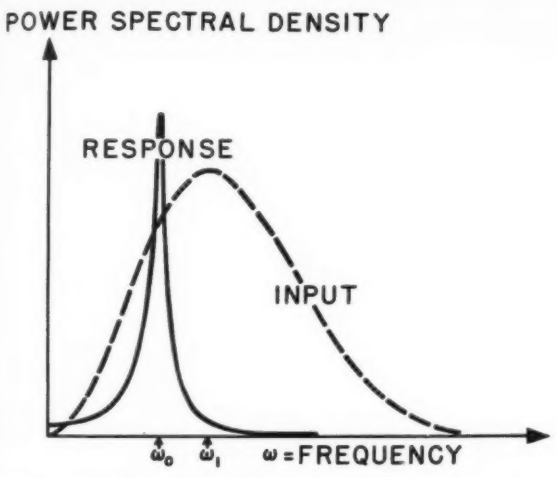

FIG. 6. Illustrating the approximation, Eq. (2-13), based on the relatively narrow bandwidth of the oscillator amplification factor compared with the bandwidth of the input [assumed as $f_0(\omega)$ in the sketch, but the result would be essentially similar for an input spectrum of the monotonic type f_a].

A qualitative picture of the essentially resonant response to a random input may be formed by noting that a lightly damped oscillator acts as a narrow band filter, passing only those frequencies in the neighborhood $\omega_0 \pm \delta\omega_0$ [cf. Eq. (2-13) and Fig. 5]. Then, recalling the phenomenon of "beats,"[15] wherein the synthesis of two harmonic waves of approximately the same frequency gives rise to a wave oscillating with the mean of the two frequencies and having an amplitude envelope that fluctuates at a rate equal to the difference frequency, it may be inferred that the synthesis of a large number (tending to infinity) of harmonic waves having frequencies in the approximate band $\omega_0 \pm \delta\omega_0$ and randomly distributed phases will give rise to a wave oscillating with frequency ω_0 and having an amplitude envelope that exhibits a random fluctuation, the rapidity of which must be of the order of $2\delta\omega_0$.

The probability distribution of this envelope (as opposed to the distribution of the instantaneous response) may be determined by synthesizing it from the randomly oriented vectors representing the individual harmonic waves. This problem, known as the two-dimensional "random walk," was first solved by Rayleigh[16] and may be regarded as *the* antecedent to modern, physical applications of stochastic methods.* Rayleigh's analysis gives as the probability that the envelope $y_m(t)$ lies between y and $y + dy$

$$P\{y < y_m(t) < y + dy\} = P_m\, dy = e^{-y^2/2\psi_0} y\, dy/\psi_0 \tag{3-4}$$

This quantity P_m, known as a Rayleigh distribution density, is plotted in Fig. 7.

In applying the results of Eqs. (3-1), (3-3), and (3-4) to the essentially resonant response of a simple oscillator, an approximate calculation of ψ_0 may be carried out along the lines of Eq. (2-13)—viz.,

$$\psi_0 \simeq \left(\frac{y_0}{F_0}\right)^2 f(\omega_0) \int_0^\infty \frac{d\omega}{\left[1 - \left(\frac{\omega}{\omega_0}\right)^2\right]^2 + 4\delta^2\left(\frac{\omega}{\omega_0}\right)^2}, \qquad \frac{\delta\omega_0}{\omega_1} = 0(1) \tag{3-5a}$$

$$\psi_0 = \left(\frac{\pi}{4\delta}\right)\left[\frac{\omega_0 f(\omega_0)}{F_0^2}\right] y_0^2\,[1 + 0(\delta^2)] \tag{3-5b}$$

The fact that the mean square response is inversely proportional to δ (rather than δ^2) is a consequence of the fact that the fraction of the total power accepted by the oscillator is proportional to the product of the "bandwidth," $2\delta\omega_0$, of the resonance curve (cf. Fig. 5) and its peak value $(1/4\delta^2)$, rather than simply to the latter as in the case of resonance under monochromatic excitation.

If $g(\omega)$ were given by Eq. (2-14), ψ_0 would be given by

$$\psi_0 = \left(\frac{y_0}{F_0}\right)^2 \int_0^\infty f(\omega)\, d\omega, \qquad \frac{\delta\omega_0}{\omega_1} \gg 1 \tag{3-6a}$$

$$= (\overline{F^2}/F_0^2)\, y_0^2 \tag{3-6b}$$

$$= y_0^2 \text{ for } F_0 = \sqrt{\overline{F^2}} \tag{3-6c}$$

Thus y_0 would appear as the *static* displacement that would be produced by the root mean square loading $F_0 = \sqrt{\overline{F^2(t)}}$ in the absence of dynamic effects. Similarly, s_0 may be defined as the static stress produced by F_0. These *definitions* will be adopted throughout the remainder of the analysis; however it should be remarked that these choices of y_0, F_0 and s_0 are made

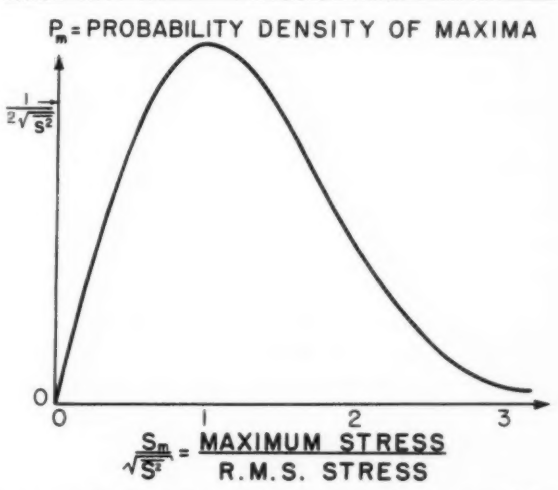

FIG. 7. The probability density of the maxima for essentially resonant loading, as defined by Eq. (3-4).

* The statistical interpretation of a sine wave having a randomly varying envelope in terms of Rayleigh's problem is due originally to Rice (unpublished lectures, California Institute of Technology, May 8, 1952); cf. also Section 3.7 of reference 1.

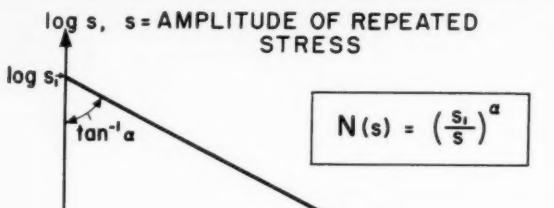
log s, s = AMPLITUDE OF REPEATED STRESS
log s_1
$\tan^{-1}\alpha$
$N(s) = \left(\frac{s_1}{s}\right)^{\alpha}$
log N
N = NUMBER OF CYCLES OF LOADING THAT WILL PRODUCE FATIGUE FAILURE

FIG. 8. Logarithmic plot of typical (s, N) curve, as given by Eq. (4-2).

purely in the interest of convenience and in no way imply the approximations of Eqs. (2–14) and (3–6).

(4) PROBABLE TIME AND EQUIVALENT STRESS FOR FATIGUE FAILURE

The usual s, N curve gives the number of cycles (N) of complete stress reversal (i.e., $-s$ to $+s$) of fixed amplitude (s) required to produce failure for a given structure. For this type of loading, it is sometimes found that there exists a minimum stress, designated as the endurance limit (s_e), below which fatigue failure never occurs (i.e., $N = \infty$ if $s < s_e$). However, the existence of an endurance limit depends on certain beneficial changes in the material produced by alternating stress at a low level ($s < s_e$), and intermediate excursions to higher stress levels may counteract these changes; moreover, it appears that only a few materials (notably steel) possess well-defined endurance limits. Thus, it seems reasonable to ignore the possibility of an endurance limit when, as in the problem at hand, stress amplitudes are distributed over a wide range. [In any event, the introduction of an endurance limit has no important effect on the results of Section (5), provided that the root mean square stress is large compared with this limit.]

Experimental data usually exhibit a wide scatter on an s, N plot,* but within the limits of this scatter an adequate approximation is furnished by (cf. reference 13)

$$N(s) = (s_1/s)^{\alpha} \tag{4-1}$$

where s_1 is the stress at which Eq. (4-1) predicts failure occurs in one complete cycle [although such an extrapolation of the approximation, Eq. (4-1), is unwarranted, so that this interpretation of s_1 is essentially hypothetical]. On the assumption of an endurance limit s_e, s could be replaced by $(s - s_e)$ in Eq. (4-1).

* Indeed, it appears that N is itself a stochastic function of s.[17, 18]

It is customary to plot the s, N curve on semi-log paper, but the approximation of Eq. (4-1) is more conveniently plotted as the straight line

$$\log s = \log s_1 - (1/\alpha) \log N \tag{4-2}$$

the slope of which is α^{-1}, as shown in Fig. 8. A typical value of the exponent α is 10, although it may range as high as 25 (reference 13).

In order to determine the conditions for fatigue failure under random loading, it is necessary to establish the "damage" done by a number of stress reversals (n) less than the number (N) that produces failure at a given level (s). The most common assumption ("Miner's rule"[12]) is that the damage accumulates linearly, so that if a structure is subjected to n_i stress reversals at a level s_i the partial damage is $n_i/N(s_i)$, and the cumulative damage (D) is given by

$$D_M = \sum_i \left(\frac{n_i}{N_i}\right), \qquad N_i = N(s_i) \tag{4-3}$$

with fatigue failure occurring at $D = 1$. Assuming the (s, N) law of Eq. (4-1), Eq. (4-3) becomes

$$D_M = \sum_i n_i (s_i/s_i)^{\alpha} \tag{4-4}$$

Miner's hypothesis, Eq. (4-3), is subject to such objections as the fact that it ignores the temporal sequence of loadings. Various alternative hypotheses have been offered,[19] but it may be argued that presently available fatigue data scarcely warrant the additional complications insofar as the prediction of the fatigue life of a *single sample* is concerned. Moreover, as shown in the Appendix, the introduction of cumulative damage hypotheses more closely in accord with appropriately averaged experimental results has no appreciable effect when, as in the present application, the stress amplitudes are continually distributed over a wide range.

In formulating design criteria, it is convenient to introduce an equivalent stress (often called "reduced stress"), s_r, which would produce the same fatigue damage as the spectrum (n_1, s_1), (n_2, s_2)...after the same (total) number of cycles of loading. On Miner's hypothesis, it follows from Eq. (4-4) that

$$s_{rM} = [\sum_i n_i s_i^{\alpha} / \sum_i n_i]^{1/\alpha} \tag{4-5}$$

It is evident that, without postulating or otherwise determining an expression for cumulative damage, one might regard Eq. (4-5) as a working hypothesis in which the weighting constant could be determined either empirically or on the basis of some physical model (with or without direct reference to the slope of the s, N curve). Thus, Shanley's theory of fatigue[13] leads to the replacement of α by 2α in Eq. (4-5). However, presently available data are not sufficiently precise to sharply delimit the weighting constant, and it there-

fore seems advantageous in the present analysis to write

$$s_r = [\sum_i n_i s_i^{k\alpha} / \sum_i n_i]^{1/k\alpha} \qquad (4\text{-}6)$$

and leave the choice of k open, with 2 as a (probably) conservative upper limit.

In the present calculation of probable fatigue life of a lightly damped structure under random loading,* the probable number of cycles of loading having an amplitude in the range $(s, s + ds)$ is obtained by multiplying the total number of cycles (at frequency $\omega_0/2\pi$) by $P_m(s)\, ds$. It then follows from Eq. (4-6) that the probable equivalent stress is given by

$$s_r = \left[\int_0^\infty s^{k\alpha} P_m(s)\, ds / \int_0^\infty P_m(s)\, ds \right]^{1/k\alpha} \qquad (4\text{-}7)$$

The (angular) frequency at which the equivalent stress s_r may be supposed to oscillate is, of course, ω_0.

(5) Fatigue Failure of Resonant Structure

If the probability distribution P_m for a resonant structure is substituted in Eq. (4-7) from Eq. (3-4), the resulting equivalent stress is

$$s_r = \left[\int_0^\infty s^{k\alpha+1} e^{-s^2/2\psi_0}\, ds / \int_0^\infty s e^{-s^2/2\psi_0}\, ds \right]^{1/k\alpha} \qquad (5\text{-}1)$$

Introducing the Gamma function (Γ) integral

$$\Gamma(z+1) = 2^{-z} \int_0^\infty x^{2z+1} e^{-(1/2)/x^2}\, dx \qquad (5\text{-}2)$$

Eq. (5-1) goes over to

$$s_r = [\Gamma(k\alpha/2 + 1)]^{1/k\alpha} (2\psi_0)^{1/2} \qquad (5\text{-}3)$$

Here and subsequently $\psi_0^{1/2}$ represents $\sqrt{\bar{s}^2}$, the root mean square stress.

If (since α is always large) the Gamma function is approximated by Stirling's formula—viz.,

$$\Gamma(z+1) \simeq e^{-z} z^{z+(1/2)} \sqrt{2\pi}, \qquad z \gg 1 \qquad (5\text{-}4)$$

the equivalent stress becomes

$$s_r = (\pi k\alpha)^{(1/2k\alpha)} \left(\frac{k\alpha \bar{s}^2}{e} \right)^{1/2} \simeq \left(\frac{k\alpha \bar{s}^2}{e} \right)^{1/2}, \qquad \alpha \gg 1 \qquad (5\text{-}5)$$

It appears from the foregoing that the determination of the equivalent stress under random loading depends essentially on the determination of the root mean square stress produced by the same loading. If the static displacement y_0 of Sections 2 and 3 is now replaced by the stress (s_0) that would be produced by the root mean square force F_0 under static loading conditions, the mean square stress produced in a resonant structure by the random loading is given by Eq. (3-5b) as

$$\bar{s}^2 = \psi_0 = \left(\frac{\pi}{4\delta} \right) \left[\frac{\omega_0 f(\omega_0)}{F_0^2} \right] s_0^2 \qquad (5\text{-}6)$$

The ratio of equivalent to static stress then is given by Eq. (5-5) as

$$\frac{s_r}{s_0} = \left[\frac{k\pi\alpha}{4e\delta} \cdot \frac{\omega_0 f(\omega_0)}{F_0^2} \right]^{1/2} \qquad (5\text{-}7)$$

which may be regarded as the central result of the foregoing analysis.

In order to form some estimate of the magnitudes given by Eq. (5-7), the equivalent stresses based on the representative power spectral density distributions of Eqs. (2-8) and (2-9) will be evaluated. Substituting these distributions, where now $\bar{F}^2 = F_0^2$, in Eq. (5-7) yields

$$\left(\frac{s_r}{s_0} \right)_a = \frac{\pi^{1/4}}{(2e)^{1/2}} \left(\frac{k\alpha}{\delta} \right)^{1/2} \left(\frac{\omega_0}{\omega_1} \right)^{1/2} e^{-(1/2)(\omega_0/\omega_1)^2} \qquad (5\text{-}8)$$

$$\left(\frac{s_r}{s_0} \right)_b = \frac{\pi^{1/4}}{e^{1/2}} \left(\frac{k\alpha}{\delta} \right)^{1/2} \left(\frac{\omega_0}{\omega_1} \right)^{3/2} e^{-(1/2)(\omega_0/\omega_1)^2} \qquad (5\text{-}9)$$

These results are plotted in Fig. 9.

It is probable that Eq. (5-9) can be accepted as representative of random load distributions of the type encountered in practice. The corresponding upper bound for the equivalent stress is given by

$$(s_r/s_0)_{\max.} \simeq 0.51(k\alpha/\delta)^{1/2} \qquad (5\text{-}10)$$

For $\alpha = 10$, $k = 2$, and $\delta = 0.02$ (a typical value for structural damping of a panel) this last result yields 16, while for $\alpha = 25$, $k = 2$, and $\delta = 0.01$ (probably the worst possible case that could be obtained, even under laboratory conditions) the ratio is 36.

(6) Jet Buffeting of a Panel

The results of the preceding sections now will be illustrated by application to the specific problem of a panel

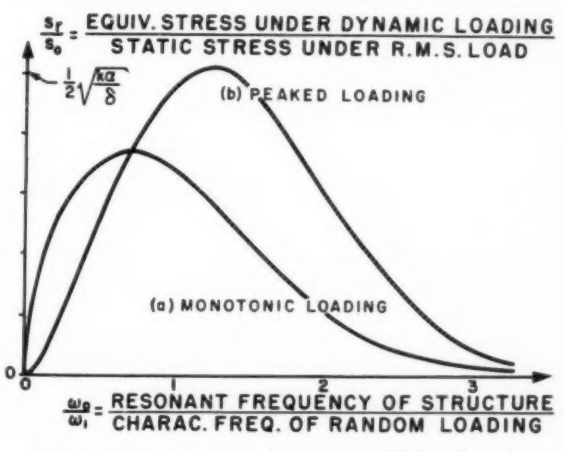
$\frac{s_r}{s_0}$ = EQUIV. STRESS UNDER DYNAMIC LOADING / STATIC STRESS UNDER R.M.S. LOAD
$\frac{1}{2}\sqrt{\frac{k\alpha}{\delta}}$
(b) PEAKED LOADING
(a) MONOTONIC LOADING
0
1
2
3
$\frac{\omega_0}{\omega_1}$ = RESONANT FREQUENCY OF STRUCTURE / CHARAC. FREQ. OF RANDOM LOADING

FIG. 9. The stress ratios given by Eqs. (5-8) and (5-9).

* The implied assumption of completely reversed loading is consistent with the result that the rate of fluctuation of the envelope is of the order of $2\,\delta\omega_0$, so that successive maxima and minima can differ only by a fraction of order δ.

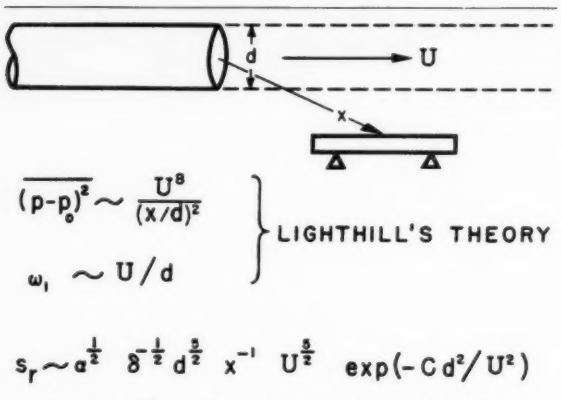

FIG. 10. The configuration discussed in Section (6).

excited by aerodynamic noise (as from a jet). Probably the most reliable procedure for determining the equivalent stress would be to make a direct measurement of the root mean square stress in the panel under the random loading of the jet (or other source) and substitute in Eq. (5-5). If this is not possible, it might be possible to measure or estimate the parameters ω_0, δ, and $f(\omega_0)$, calculate the corresponding values of F_0 and s_0, and substitute in Eq. (5-7). However, it generally would be difficult to estimate the power spectral density of the jet *in the neighborhood of the panel*, and its measurement there probably would be even more difficult than the direct measurement of the root mean square stress that it produces. Accordingly, it appears worth while to formulate an approximate similarity expression for the equivalent stress on the basis of the foregoing results and on Lighthill's theory[9] of aerodynamic noise generation.*

According to Lighthill's results, the density variations arising in an aerodynamically generated noise field (Fig. 10) are asymptotically ($x >> d$) proportional to $\rho_0(U/a_0)^4\ (d/x)$ where U is the jet velocity (with respect to the surrounding medium), d a characteristic length (e.g., the jet diameter), x is the distance from the source (say the jet orifice, although directional effects also must be considered), ρ_0 is the mass density of the medium into which the sound is radiated, and a_0 is the sonic velocity in this medium. Accordingly, the root mean square pressure may be expected to vary like

$$\sqrt{(p - p_0)^2} \sim (U/a_0)^4\ (d/x)\ p_0 \qquad (6\text{-}1)$$

(Lighthill's theory is not valid if $U > a_0$.†) The corresponding static stress in a thin plate of thickness h and area A then will vary like

$$s_0 \sim \sqrt{(p - p_0)^2}\left(\frac{A}{h^2}\right) \sim \left(\frac{U}{a_0}\right)^4\left(\frac{d}{x}\right)\left(\frac{A}{h^2}\right) p_0 \qquad (6\text{-}2)$$

The resonant frequency of a plate of thickness h, area A, Young's modulus E, and specific weight w will vary like

$$\omega_0 \sim (h/A)\ (gE/w)^{1/2} \qquad (6\text{-}3)$$

while the characteristic frequency of the jet will vary approximately like‡

$$\omega_1 \sim U/d \qquad (6\text{-}4)$$

whence

$$(\omega_0/\omega_1) \sim (hd/A)\ (gE/wU^2)^{1/2} \qquad (6\text{-}5)$$

Substituting Eqs. (6-2) and (6-5) in Eq. (5-7) yields [since $\omega_0 f(\omega_0)/F_0^2$ depends only on ω_0/ω_1]

$$\frac{s_r}{p_0} = \left(\frac{k\alpha}{\delta}\right)^{1/2}\left(\frac{A}{h^2}\right)\left(\frac{d}{x}\right)\left(\frac{U}{a_0}\right)^4 \Phi\left[\left(\frac{gE}{wU^2}\right)^{1/2}\left(\frac{hd}{A}\right)\right] \qquad (6\text{-}6)$$

where Φ is an undetermined function.

On the basis of both theory and experiment,[10] it appears that the power spectral density of the jet has approximately the distribution $f_0(\omega)$ given by Eq. (2-9). Thus, if s_0 and ω_0/ω_1 from Eqs. (6-2) and (6-5) are posed in Eq. (5-9), Eq. (6-6) takes the more explicit form

$$\frac{s_r}{p_0} = C_1\left(\frac{k\alpha}{\delta}\right)^{1/2}\left(\frac{gE}{wa_0^2}\right)^{3/4}\left(\frac{d^{5/2}}{A^{1/2}h^{1/2}x}\right)\left(\frac{U}{a_0}\right)^{5/2} \times \exp\left[-C_2\left(\frac{gE}{wU^2}\right)\left(\frac{hd}{A}\right)^2\right] \qquad (6\text{-}7)$$

where C_1 and C_2 are undetermined, positive constants (v.i.).

The principal shortcomings of the expressions (6-6) and (6-7) probably are due to the omission of the (spacewise) phase effect in determining the loading of the single degree of freedom structural model and in the neglect of directional and Reynolds Number effects in the description of the jet noise. These factors can be taken into account by introducing the scale factor $dA^{-1/2}$ in Φ and C_1 (so that the latter is no longer constant) and the jet Reynolds Number and the angle between the jet axis and the line joining the jet exhaust and the panel in Φ, C_1, and C_2. It also should be noted that directional effects become more important when referred to a moving reference frame, as with an aircraft in flight (cf. reference 9).

Having s_r, the fatigue life of the panel is given by $N(s_r)\ T_0$, where T_0 is the period of the resonant mode.**

* It should be emphasized that, in the absence of further experimental data, the results of this section must be regarded as rather less reliable than the results of Sections (2)–(5).

† Preliminary results (reference 9, Part II) indicate that jet noise may increase much more rapidly with jet velocity when the latter exceeds a_0.

‡ Experimental results yield roughly $\omega_1 = \pi U/d$ (reference 9, Part II).

** Thus Eq. (6-7) would predict a fatigue life proportional to $U^{-5\alpha/2}\exp(+\text{constant}\cdot U^{-2})$. This extremely rapid decrease of fatigue life with jet velocity has received qualitative confirmation in at least one case, where the fatigue life of a panel decreased from approximately 100 hours to 20 min. with a nominal increase of jet power.

In view of the great sensitivity of N to small changes of s_r (and, therefore, to small changes in each of the parameters affecting s_r), it appears to be more expedient to base design criteria on s_r. Moreover, it should be specifically remarked that the decrease in T_0 due to stiffening the panel (e.g., by increasing h) usually would have a negligible effect on the fatigue life NT_0 compared with the large reduction of s_r. Thus, while T_0 is inversely proportional to the panel thickness h, $N(s_r)$ varies like $h^{+\alpha/2} \exp(+ C \alpha h^2)$, where C is a positive constant.

The damping of a vibrating panel will be due primarily to radiation and structural hysteresis, but, insofar as δ is expressed as a fraction of the critical damping and is small, the end results should not be too sensitive to the particular mechanism. If g_s is the usual structural damping factor [such that the effective stiffness is multiplied by the factor $(1 + ig_s)$ for harmonic motion], then

$$\delta = (1/2)g_s \tag{6-8}$$

Radiation damping is more complex, but for a panel it may be approximated by

$$\delta \simeq (2/\pi^2)\,(\rho_0 g\sqrt{A}/wh) \tag{6-9}$$

The effective value of δ then should be obtained by adding Eqs. (6-8) and (6-9)—viz.

$$\delta \simeq (g_s/2) + (2/\pi^2)\,(\rho_0 g\sqrt{A}/wh) \tag{6-10}$$

Appendix

Suppose that fatigue damage accumulates according to

$$D = \sum_i (n_i/N_i)^{x_i} \tag{A-1}$$

where the exponent x_i depends on the amplitude of stress reversal. Then the probable damage per cycle resulting from a probability distribution $P_m(s)$, the total integral of which is unity, is given by

$$D_1 = \int_0^\infty \frac{\partial D}{\partial n} P_m\, ds \tag{A-2a}$$

$$= \int_0^\infty \frac{x(s)\, D^{1-[1/x(s)]}}{N(s)} P_m(s)\, ds \tag{A-2b}$$

The damage rate, $\dot{D}$, may be obtained by dividing Eq. (A-2) by the period T_0. In particular, if x is assumed to be independent of s, Eq. (A-2b) yields

$$\frac{\partial D}{\partial t} = \left(\frac{1}{T_0}\int_0^\infty \frac{P_m\, ds}{N}\right) x\, D^{1-(1/x)} \tag{A-3}$$

Integrating this result between $D = 0$ and 1, the probable fatigue life is given by (using a zero superscript to denote that x has been assumed independent of s)

$$T_F^{(0)} = T_0\left(\int_0^\infty \frac{P_m ds}{N}\right)^{-1}\int_0^1 \frac{1}{x} D^{(1/x)-1}\, dD \tag{A-4a}$$

$$= T_0\left(\int_0^\infty \frac{P_m ds}{N}\right)^{-1} \tag{A-4b}$$

independently of the value of x.

A more realistic assumption as to the dependence of x on s is furnished by recent results of Marco and Starkey,[20] which suggest that

$$x = 2, \qquad s < s_c \tag{A-5a}$$

$$x = 1, \qquad s > s_c \tag{A-5b}$$

where s_2 is a certain critical stress level (35,000 lbs. per sq.in. for 76S-T61 aluminum) at which a change in the type of fracture occurs. Substituting Eq. (A-5) in Eq. (A-2) and dividing by T_0 then yields

$$\frac{\partial D}{\partial t} = \frac{1}{T_0}\left(\int_{s_c}^\infty \frac{P_m ds}{N}\right) + \frac{2}{T_0}\left(\int_0^{s_c} \frac{P_m ds}{N}\right) D^{1/2} \tag{A-6}$$

which may be rewritten

$$\partial D/\partial t = (1/T_F^{(0)})\,[A + 2(1 - A)D^{1/2}] \tag{A-7}$$

where $T_F^{(0)}$ is given by Eq. (A-4), and

$$A = \int_{s_c}^\infty \frac{P_m ds}{N} \Big/ \int_0^\infty \frac{P_m ds}{N} \tag{A-8}$$

Integrating (A-7) then yields for the fatigue life

$$T_F = T_F^{(0)} \int_0^1 \frac{dD}{A + 2(1 - A)D^{1/2}} \tag{A-9a}$$

$$= T_F^{(0)}\,(1 - A)^{-1}\left[1 - \frac{A}{2(1 - A)} \ln\left(\frac{2 - A}{A}\right)\right] \tag{A-9b}$$

The expression for A given by Eq. (A-8) may be evaluated explicitly in terms of incomplete Gamma functions if P_m and N are substituted from Eqs. (3-4) and (4-1), but, whatever the actual forms of P_m and N (except, of course, that they must be positive), A must lie between 0 and 1. In this range Eq. (A-9b) yields the following values:

$A =$	0	0.1	0.2	0.4	0.6	0.8	0.9	1.0
$1 - \frac{T_F}{T_F^{(0)}} =$	0	0.071	0.100	0.104	0.089	0.055	0.033	0

In view of the relatively small change in fatigue life (compared with experimental scatter) associated with the assumed, representative variation in exponent of fatigue accumulation, it is evident that Miner's hypothesis ($x \equiv 1$), which leads to the fatigue life $T_F^{(0)}$, may be regarded as adequate for the prediction of probable fatigue life of a structure subjected to random loading. Further, it should be emphasized that this conclusion is independent of the distribution P_m insofar as the latter is continuous [otherwise the differentiation $(\partial D/\partial n)$ in Eq. (A-2) would be invalid]. This conclusion is also valid for other possible variations of the exponent x; for example, if 2 is replaced by (1/2) in Eq. (A-5a),

the end effect is only to replace A by $(1 - A)$ in predicting T_F.

REFERENCES

[1] Rice, S. O., *Mathematical Analysis of Random Noise*, Bell Syst. Tech. Jour., Vol. 23, pp. 282–332, 1944 and Vol. 24, pp. 46–156, 1945; reprinted as Bell Tel. Syst. Monograph B-1589.

[2] Wiener, N., *Extrapolation, Interpolation and Smoothing of Stationary Time Series;* John Wiley & Sons, Inc., New York, 1950.

[3] Liepmann, H. W., *On the Application of Statistical Concepts to the Buffeting Problem*, Journal of the Aeronautical Sciences, Vol. 19, No. 12, pp. 793–800, December, 1952.

[4] Liepmann, H. W., *An Approach to the Buffeting Problem from Turbulence Considerations*, Rep. SM-13940, Douglas Aircraft Company, Inc., Santa Monica, 1951.

[5] Luskin, H., and Lapin, E., *An Analytical Approach to the Fuel Sloshing and Buffeting Problems of Aircraft*, Journal of the Aeronautical Sciences, Vol. 19, No. 4, pp. 217–228, April, 1952.

[6] Lin, C. C., *On the Motion of a Pendulum in Turbulent Flow*, Q. Appl. Math., Vol. 1, p. 43, 1943.

[7] Uhlenbeck, G. E., and Wang, M. C., *On the Theory of Brownian Motion—II*, Rev. Mod. Ph., Vol. 17, pp. 323–342, 1945.

[8] Graham, E. W., and Rodriguez, A. M., *Response of Some Linear Systems to Random Forces with Reference to Aircraft Buffeting*, Douglas Aircraft Report SM-14517, 1952.

[9] Lighthill, M. J.: *On Sound Generated Aerodynamically*, Proc. Roy. Soc. Lon. (A), Vol. 211, pp. 564–587 (1952); *ibid.*, Vol. 222, pp. 1–32, 1954.

[10] Westley, R., and Lilley, G. M., *An Investigation of the Noise Field from a Small Jet and Methods for its Reduction*, Rep. 53, Coll. of Aeronautics, Cranfield, U.K., 1952.

[11] Taylor, J., *Measurement of Gust Loads in Aircraft*, J. Roy. Aero. Soc., Vol. 57, pp. 78–88, 1953.

[12] Miner, M. A., *Cumulative Damage in Fatigue*, J. Appl. Mech., Vol. 12, pp. 159–164, 1945.

[13] Shanley, F. R., *A Theory of Fatigue Based on Unbonding During Reversed Slip*, RAND Rep. P-350, Santa Monica, Calif., 1952.

[14] Mazelsky, B., *Extension of Power Spectral Methods, Etc.*, Journal of the Aeronautical Sciences, Vol. 21, No. 3, pp. 145–153, March, 1954.

[15] Lord Rayleigh, *Theory of Sound*, Vol. 1, Article 30; Dover Publications, New York, 1945.

[16] *ibid*, Article 42a.

[17] Weibull, W., *The Statistical Aspect of Fatigue Failures and Its Consequences* from *Fatigue and Fracture of Metals* (edited by W. M. Murray), Technology Press, M.I.T., 1952.

[18] Yokobori, T., *Fatigue Fracture from the Standpoint of Stochastic Theory*, J. Phys. Soc Japan, Vol. 8, pp. 265–268, 1953; also see *ibid.*, Vol 6, p. 81, 1951, and other references given by Yokobori.

[19] Newmark, N. M., *A Review of Cumulative Damage in Fatigue* from *op. cit.* reference 17.

[20] Marco, S. M., and Starkey, W. L., *A Concept of Fatigue Damage*, Trans. A.S.M.E., Vol. 76, 627–632, 1954.

Effects of Certain Steady Motions . . .

(*Continued from page 752*)

(1) The lateral oscillation becomes more lightly damped and the lateral and longitudinal modes of motion are coupled at high steady turning rates.

(2) The lateral oscillation is better damped but the damping of the longitudinal short-period oscillation becomes seriously reduced for high steady rolling rates. The lateral and longitudinal modes of motion are coupled also in steady rolls.

(3) Damping of the lateral oscillation is reduced by high values of steady longitudinal deceleration.

REFERENCES

[1] Durand, W. F., *Aerodynamic Theory*, 1st Edition, Vol. 5, pp. 121–135; Julius Springer, Berlin, 1934.

[2] Jones, Arthur L., and Briggs, Benjamin R., *A Survey of Stability Analysis Techniques for Automatically Controlled Aircraft*, NACA TN 2275, January, 1951.

[3] Bollay, W., *Aerodynamic Stability and Automatic Control*, Journal of the Aeronautical Sciences, Vol. 18, No. 9, pp. 577–589, 611–613, September, 1951.

[4] Frazer, R. A., Duncan, W. J., and Collar, A. R., *Elementary Matrices*, 1st edition, pp. 284–287; Cambridge University Press, Cambridge, England, 1938.

[5] Milne-Thomson, L. M., *Theoretical Aerodynamics*, 1st edition, pp. 322–326; Macmillan and Co., London, 1948.

[6] Goldstein, H., *Classical Mechanics*, 1st Edition, pp. 132–134; Addison-Wesley Press, Cambridge, Mass., 1950.

[7] Mokrzycki, G. A., *Application of the LaPlace Transformation to the Solution of the Lateral and Longitudinal Stability Equations*, NACA TN 2002, January, 1950.

[8] Phillips, William H., *Effect of Steady Rolling on Longitudinal and Directional Stability*, NACA TN 1627, January, 1948.

APPENDIX—STABILITY DERIVATIVES USED IN SAMPLE CALCULATIONS

The stability derivatives used in the sample calculations of this paper are listed in Table 2. These values apply to a typical fighter-type airplane in horizontal flight at three values of airspeed. All aerodynamic cross-derivatives such as C_{m_p} and C_{m_r} are assumed equal to zero. For convenience, standard NACA dimensionless notation[7] is used in this listing.

TABLE 2
Stability Derivatives Used in Sample Calculations

Flight Condition	V_1	τ
1	600	1.000
2	800	0.750
3	1,000	0.600

$K_{X_\theta} = 0.1448$
$K_{Y_\theta} = 0.4299$
$K_{Z_\theta} = 0.2686$

$\epsilon = 1.22°$

$\alpha = C_L/2.60$
$C_{L_\alpha} = 2.60$
$C_D = 0.010 + 0.264\ C_L^2$
$C_{m_\alpha} = -0.10$
$C_{L_q} = 1.30$
$C_{m_q} = -1.00$
$C_{m_{D\alpha}} = 0$

$C_{l_\beta} = -0.023 - 0.20\ C_L$
$C_{n_\beta} = 0.060 + 0.050\ C_L$
$C_{Y_\beta} = -0.40$
$C_{l_r} = 0.035 + 0.180\ C_L$
$C_{n_r} = -0.090$
$C_{Y_r} = 0.10$
$C_{l_p} = -0.20$
$C_{n_p} = 0.020 - 0.220\ C_L$
$C_{Y_p} = 0$

An Experimental Determination of Flat Plate Recovery Factors for Mach Numbers Between 1.90 and 3.14*

R. H. SHOULBERG,† J. A. F. HILL,‡ AND M. A. RIVAS, JR.**

Massachusetts Institute of Technology

ABSTRACT

An experimental investigation of temperature recovery factors on a flat plate was carried out in a continuous type wind tunnel at the Naval Supersonic Laboratory of the Massachusetts Institute of Technology. The Mach Number range for the tests lay between 1.90 and 3.14, and the Reynolds Number based on the plate length extended to 17×10^6. The stagnation temperature was nominally 110°F., while stagnation pressures were varied from 6 to 31 psia. The test results can be summarized as follows: (1) The recovery factor for the laminar boundary layer on a flat plate is independent of Mach Number and equal to 0.850 ± 0.007, a value about 1% higher than the square root of the Prandtl Number based on the plate surface temperature and 2% lower than the square root of the Prandtl Number based on the stream temperature. (2) The recovery factor for the turbulent boundary layer on a flat plate is independent of Mach Number, but decreases slightly with Reynolds Number from a value of 0.882 at a Reynolds Number of 5×10^6 to a value of 0.880 at a Reynolds Number of 10^7. These values of the recovery factor are about 1% lower than the cube root of the Prandtl Number based on wall temperature. A maximum systematic error of ± 0.003 is possible, but this error would not affect the slight decrease of recovery factor with Reynolds Number. (3) The beginning of boundary layer transition occurs on the plate at Reynolds Numbers between 1.0 and 2.5×10^6. The recovery factors in the transition zone are higher than those of the laminar and turbulent regimes, but never exceed 0.90.

NOMENCLATURE

A = area, ft.²
c_p = specific heat at constant pressure, B.t.u./lb. °F.
h = convective heat-transfer coefficient, B.t.u./hr. ft.² °F.
k = thermal conductivity of air, B.t.u./hr. ft. °F.
l = fixed distance from leading edge measured in x direction, ft.
M = Mach Number
p = static pressure, psia
p_0 = stagnation pressure, psia
Pr = Prandtl Number = $c_p\mu/k$
q = rate of heat transfer, B.t.u./hr.
r = recovery factor = $(T_{aw} - T_1)/(T_{01} - T_1)$
Re_x = Reynolds Number = $\rho ux/\mu$
t = excess temperature of heated nose, °F.
T = static temperature, °F. abs.
T_{aw} = adiabatic wall temperature, °F. abs.
T_i = temperature indicated by probe, °F. abs.
T_0 = stagnation temperature, °F. abs.
T_w = surface temperature downstream of heated length of plate, °F. abs.
u = velocity parallel to plate surface, ft./hr.
x = distance from leading edge along plate surface, ft.
y = distance perpendicular to plate surface, ft.
γ = ratio of specific heats
δ = boundary-layer thickness, ft.
δ^* = boundary-layer displacement thickness, ft.
θ = boundary-layer momentum thickness, ft.
μ = absolute viscosity, lb./hr. ft.
ρ = density, lb./ft.³

Subscripts

$( )_1$ = free stream condition
$( )_{aw}$ = an adiabatic wall condition

Superscripts

$( )'$ = boundary layer property behind normal shock

INTRODUCTION

THE SUBJECT OF aerodynamic heating has received so much attention in the recent literature that further discussion of its importance seems almost unnecessary. Suffice it to say that wind tunnels are being planned with stagnation temperatures of 1,500°F. at high Mach Numbers, and that aircraft are being built whose body surfaces, unless cooled by radiation or internal refrigeration, would reach steady-state temperatures of more than 200°F. Missile skin temperatures, of course, far exceed this value. In order to predict cooling requirements for the tunnel walls and the aircraft and missile surfaces, accurate knowledge of thermal effects at high speeds is necessary. Indeed, an acute need is currently felt for such information by virtually everyone interested in supersonic aerodynamics.

At the present time extensive theoretical treatments of thermal effects in the laminar boundary layer are

Received November 11, 1953. Revised and received March 1, 1954.

* The work described in the preceding paper has been carried out as a part of a program sponsored by the Office of Air Research (Contract No. AF33(038)-23165) under the direction of Professors J. R. Markham and M. Finston of the Aeronautical Engineering Department and Professor J. Kaye of the Mechanical Engineering Department of the Massachusetts Institute of Technology.

The authors wish to acknowledge with sincere appreciation the very able assistance of Robert E. Kendall of the Mechanical Engineering Department, Herman Bockstruck of the Adhesives Laboratory of the Department of Building Construction, and of the many members of the Naval Supersonic Laboratory staff who were associated with this project, especially Don H. Ross, Francis S. Harrow, J. Thomas Egan, and Robert D. Taylor.

† Instructor in Mechanical Engineering; now with M. W. Kellogg Company.

‡ Research Engineer, Naval Supersonic Laboratory.

** Research Assistant in Mechanical Engineering.

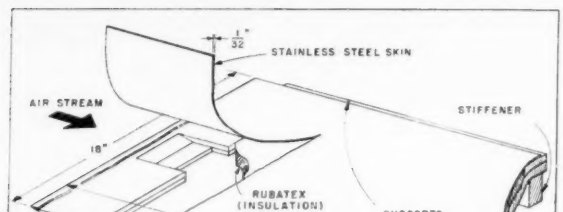

FIG. 1. Adiabatic Flat Plate

obtainable. The theory of turbulent boundary layers is much more restricted in nature, and theories of transition are quite rare. Although many experimental programs are now in existence, the amount of published experimental data relating to heat transfer at high speeds is greatly limited, as was pointed out by Kaye[1] in a recent survey of friction factors, recovery factors, and heat transfer coefficients for supersonic flow.

The work which is described in the present report represents the first part of a research program undertaken at the Naval Supersonic Laboratory of the Massachusetts Institute of Technology to investigate certain aspects of aerodynamic heating of importance in wind tunnel design. The initial effort pertains to the temperature of insulated flat surfaces in high-speed flow or to the so-called "adiabatic wall temperature." This temperature is customarily related to the stagnation temperature and static temperature of the undisturbed (free stream) flow by means of a dimensionless recovery factor, r, where

$$r = \frac{T_{aw} - T_1}{T_{01} - T_1} \tag{1}$$

Reference 1 showed that certain discrepancies exist in the recovery-factor data available in the current literature, notably the disagreement between the values of the recovery factor measured for laminar boundary layers on cones and on flat plates, and the wide range of values of the recovery factor in the boundary-layer transition region reported on plates, cones, and cone-cylinders. It was with the hope of clarifying some of this conflicting data, as well as of extending the Mach and Reynolds Number ranges for which recovery-factor data are available, that the flat-plate recovery-factor tests described herein were initiated.

Experimental Apparatus

Wind Tunnel: The tests were conducted at the Naval Supersonic Laboratory of the Massachusetts Institute of Technology, in a continuous type wind tunnel having an 18- by 24-in. cross section for Mach Numbers less than or equal to 2.5 and an 18- by 18-in. section for higher Mach Numbers. The nominal stagnation temperature was maintained at 110°F, while stagnation pressures were varied between 6 and 31 psia. The Mach Number range covered in the tests lay between 1.90 and 3.14; the Reynolds numbers based on distance from the leading edge of the plate extended to 17×10^6. Complete details of the tunnel and its operation are given in a descriptive manual.[2]

Adiabatic Flat Plate: The design of the flat-plate model used in the recovery-factor tests was undertaken with four major objectives in view: (1) Conduction of heat through and along the measuring surface was to be minimized, the ultimate goal, of course, being the condition of zero heat transfer. (2) The measuring surface was to be a smooth, flat, continuous plane. (3) The model was to be mounted in such a fashion that its angle of attack could be rapidly altered, in order to set it in such a position that the strength of the bow wave was minimized or to change appreciably the Mach Number over the measuring surface for any set of nozzle blocks. (4) Thermocouples were to be mounted as close as possible to the measuring surface. In addition to these considerations it was necessary to make the plate sufficiently strong to withstand the maximum foreseeable air loading. All these requirements were satisfied by a model with a sandwich-type construction, mounted in a pair of rotatable disks fitted into two windows on opposite sides of the tunnel test section.

The model construction, shown in Fig. 1, consists of a $^1/_2$-in. steel plate which provides a rigid supporting surface for a $^1/_2$-in. layer of Rubatex, a multicellular plastic insulating material having a thermal conductivity of 0.023 B.t.u./hr. ft. °F. and a compressive strength of 200 psi. The Rubatex insulates a $^1/_{32}$-in. sheet of polished stainless steel, which provides a smooth continuous measuring surface, while the combination of rubatex and stainless steel reduces heat transfer in a direction parallel to the air flow to negligible proportions. The stainless steel sheet is fastened to the rubatex and to a steel frame surrounding the rubatex with a catalytically cured high-strength bonding material, Shell Chemical Corporation's Epon VI. The nose of the model consists of a 15° wedge of steel and Textolite.

The plate is supported by two rotatable steel discs, which replace the tunnel windows ordinarily used for observation purposes. The discs permit a variation of ±5° in the model's angle of attack, and three windows in the discs allow observation of the model and Schlieren pictures of the bow wave. A view of the model as seen through the open test section door appears in Fig. 2. Further details of the construction and mounting of the plate appear in reference 3.

Three sets of nozzle blocks were used in the tests, giving nominal test section Mach Numbers of 2.0, 2.5, and 3.0. By varying the angle of attack of the plate, within certain limits, surface Mach Numbers other than

the nominal test section Mach Numbers could be obtained.

Instrumentation: Temperature measurements on the plate surface were made with 30 copper-constantan thermocouples soldered on the bottom side of the stainless steel sheet. Twenty-two of these couples were used to obtain data on the centerline of the plates; the other eight served to check the spanwise temperature distribution. Three thermocouples between the steel bed plate and the Rubatex were used to measure the temperature gradient in the Rubatex at three locations on the plate centerline. Twelve thermocouples mounted on a screen in the tunnel stilling section were used to determine the average stagnation temperature of the air stream.

The static-pressure distribution over the plate surface was measured with twenty-one 0.020-in. pressure taps. Thirteen taps were used to obtain data in the region of the plate's centerline; eight taps, to determine the spanwise pressure distribution.

Two movable boundary-layer probes were used to measure boundary-layer profiles. One probe, fitted with an external drive, was permanently mounted on the plate centerline with its two tips, one for impact pressure measurement and the other for stagnation temperature measurement, 28 in. from the leading edge; it may be seen in Fig. 2. The other probe, fitted with a tip for measuring impact pressure, could be inserted in the tunnel sidewall. The tip was located 6 in. downstream of the plate's leading edge and 3 in. from its centerline.

The stagnation-temperature probe was fashioned after a design of Spivack.[4] It consists essentially of an iron-constantan thermocouple made of 36 gage wire, located in an 0.020-in. I.D. tube which is vented to allow a low velocity flow past the thermocouple junction. After calibration in streams of known properties, the instrument can be used to determine local stagnation temperature as a function of indicated temperature, Mach Number, and Reynolds Number.

Discussion of Results

A total of 38 tests, in which recovery temperatures were measured, were made at various Mach Numbers and stagnation pressures. During 15 of these tests boundary-layer profiles were also measured, and during the final three tests a portion of the plate surface was artificially roughened to thicken the boundary layer in an effort to simulate flow at higher Reynolds Numbers than could be investigated with the available range of stagnation pressure and temperature. Since the major purpose of the report is to present recovery-factor data, the boundary-layer profiles (which were measured primarily to identify laminar and turbulent boundary layers) are considered in Appendix A, and the roughness tests in Appendix B. Before discussing in detail the results of the recovery-factor tests, a few general comments are in order concerning such matters as the turbulence level of the tunnel, the dew point in the test section, and certain other relevant items.

At the present time no measurement of either the intensity or scale of turbulence has been made anywhere in the tunnel. Schlieren pictures of the boundary layers on tangent ogive-cylinders with well polished surfaces have indicated transition at Reynolds Numbers of 4×10^6. The beginning of transition on the flat plate occurred at Reynolds Numbers between 10^6 and 2.5×10^6, which is in fair agreement with the summary of flat plate wind tunnel data given by Gazley.[5]

The dew point in the tunnel was not low enough to eliminate the possibility of moisture condensation effects, and measurements in the tunnel indicated that condensation did occur. The principal effect of condensation (so far as the measurement of recovery factors is concerned) is a rise in stagnation temperature proportional to the latent heat of the amount of water vapor condensing. This change in stagnation temperature can be computed approximately. The effect on plate surface temperature is *a priori* unknown since there exists the possibility of re-evaporation in the boundary layer. It was found that data obtained at different dew points could be correlated (with regard to recovery factor) by assuming that no re-evaporation occurred. The only correction applied for humidity to all the data was a change in T_0. The effect of such corrections on the laminar recovery factors is shown in Table 1, which is discussed later. The maximum

Table 1
Laminar Recovery Factors

Run	M	P_0	r Lowest Measured Value. T_0 Uncorrected for Dew Point	Dew Point Correction	Radiation and Conduction Correction	Nose Heating Correction	r Asymptotic Value
3	1.90	6	0.866	−0.008	−0.003	−0.008	0.847
7	1.97	6	0.865	−0.003	−0.004	−0.006	0.852
26	2.00	6	0.872	−0.007	−0.003	−0.010	0.852
13	2.43	6	0.864	−0.002	−0.005	−0.007	0.850
31	2.46	6	0.874	−0.007	−0.004	−0.009	0.854
9	2.56	6	0.872	−0.009	−0.005	−0.007	0.851
16	2.73	6	0.876	−0.002	−0.008	−0.017	0.849
53	2.75	6	0.867	−0.011	+0.001	−0.012	0.845
35	2.91	6	0.869	−0.003	−0.006	−0.008	0.852
47	3.01	9	0.872	−0.007	−0.005	−0.009	0.851

change in the turbulent recovery factor resulting from such a correction was 0.008.

Another comment concerns the general problem of measuring recovery temperatures on a surface which is not truly adiabatic. Since perfect insulators do not exist, one is forced to work with materials in which heat conduction is inevitable, especially near the nose of the plate where the recovery temperature differs on two sides of a steel wedge as a result of the different Mach Numbers. Radiation between the plate and the tunnel walls also tends to make the plate nonadiabatic. However, if heat transfer in directions parallel to the plate surface is neglected, and if the temperature gradient normal to the plate surface, the plate surface emissivity, the temperature and emissivity of the surface "seen" by the plate, and the convective heat-transfer coefficients are known, the heat transfer from the plate by convection and by radiation can be separately computed. Since

$$q(\text{convection}) = hA(T_w - T_{aw}), \tag{2}$$

T_{aw} can be determined if q, h, and T_w are known. The convective heat-transfer coefficients were taken from Johnson and Rubesin.[6] The maximum change in recovery factor caused by these corrections was 0.008 for the laminar region. In the turbulent-flow regime, since the maximum correction would not affect the recovery factor by as much as 0.001, no corrections were applied.

Some typical Mach Number distributions over the plate surface along the plate's centerline are shown in Fig. 3. They indicate clearly that the flow is essentially one with zero-pressure gradient. The measurements of pressure and temperature in the regions outside the longitudinal central zone of the plate indicated that the flow could also be considered as essentially two-dimensional. In certain of the runs temperature gradients of a few degrees per foot existed in a spanwise direction, but in a majority of the tests the spanwise variations were very small, and no consistent patterns of nonuniformity were noted.

Computation of the Recovery Factor

Assuming that the free-stream flow in the nozzle and test section is isentropic and that air can be treated as a perfect gas, it can be easily shown that

$$M_1 = \sqrt{\frac{2}{\gamma - 1}\left[\left(\frac{p_{01}}{p_1}\right)^{\frac{\gamma - 1}{\gamma}} - 1\right]} \tag{3}$$

and

$$\frac{T_{01}}{T_1} = 1 + \left(\frac{\gamma - 1}{2}\right) M_1^2 \tag{4}$$

Eq. (4) combined with the definition of the recovery factor leads to

$$r = \frac{T_{aw}}{T_{01}}\left[1 + \frac{2}{(\gamma - 1)M_1^2}\right] - \frac{2}{(\gamma - 1)M_1^2} \tag{5}$$

which is the equation used for computing the recovery factor.

Laminar Recovery Factors

The recovery factor distributions along the plate centerline for some typical runs at a nominal Mach Number of 2.0 are plotted against Reynolds Number in Fig. 4. These values of the recovery factor have been computed from data corrected only for the effect of humidity. They also represent quite well the data collected at other Mach Numbers.

As is shown in the sections of this report dealing with transitional recovery factors and with boundary-layer profiles, the initial decreasing portion of the curves corresponds to a laminar boundary layer. In all cases the recovery factor appears to decrease slowly with Reynolds Number until the sharp rise at a Reynolds Number of approximately 2×10^6, which is associated with transition. It is known, however, both from the theoretical work of Pohlhausen[7] and Crocco[8] and from test data such as those of Stine and Scherrer[9] and des Clers and Sternberg,[10] that the laminar recovery factor is almost certainly independent of Reynolds Number.

The nonconstant laminar recovery-factor data of the present tests can be explained as follows. Referring to Fig. 1, note that the Rubatex insulation begins 1 in. downstream of the leading edge of the plate. Forward of this point the plate construction is such as to allow a relatively large amount of heat transfer between the top and bottom of the wedge-shaped nose. Since the Mach Number is lower on the under side of the nose than on the upper side, the adiabatic wall temperature is some 10° to 20°F. higher on the under nose surface than on the upper surface. These conditions at the nose are similar to those analyzed by Korobkin,[11] who shows that the entire nose wedge assumes a uniform temperature appreciably higher than the adiabatic wall temperature corresponding to the airstream conditions on the upper surface. It is not the nose heating itself, however, but its influence on the boundary layer downstream which is of interest. The wall-temperature excess over the adiabatic value cannot vanish instantly as soon as the heat transfer from the bottom of the plate becomes very small. The boundary-layer temperature profile adjusts itself over a length of plate which is many multiples of the heated length and only gradually approaches the profile which would exist on a plate perfectly insulated all the way from the leading edge.

If it is assumed that the recovery factor does not depend on Reynolds Number, it follows that the experimental data would approach a horizontal asymptote as the Reynolds Number approached infinity, if transition were delayed indefinitely. The asymptotic value would be equal to the constant value of the recovery factor which would be measured on a completely insulated surface. If it is not assumed that the recovery factor is independent of the Reynolds Number,

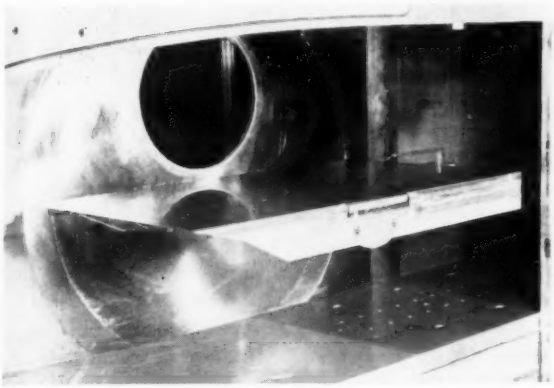

FIG. 2. Adiabatic flat plate.

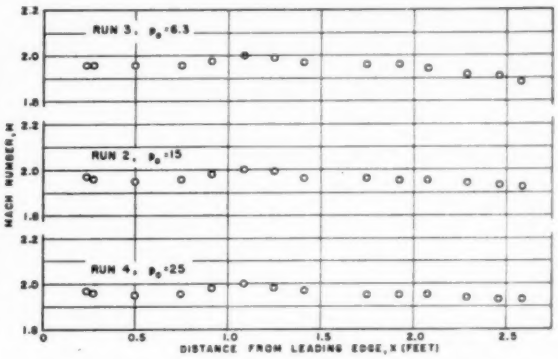

FIG. 3. Mach Number distribution along plate surface.

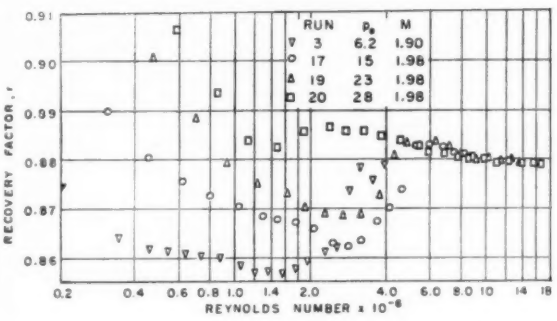

FIG. 4. Recovery factor as a function of Reynolds Number at a nominal Mach Number of 2.0.

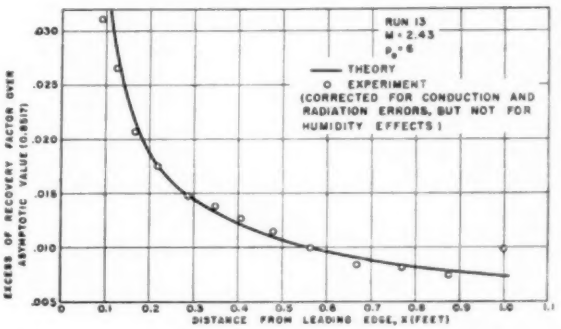
RUN 13
M = 2.43
p_0 = 6
THEORY
EXPERIMENT
(CORRECTED FOR CONDUCTION AND RADIATION ERRORS, BUT NOT FOR HUMIDITY EFFECTS)
EXCESS OF RECOVERY FACTOR OVER ASYMPTOTIC VALUE (0.8617)
DISTANCE FROM LEADING EDGE, X (FEET)

FIG. 5. Comparison of theory and experiment, decay of excess recovery factor.

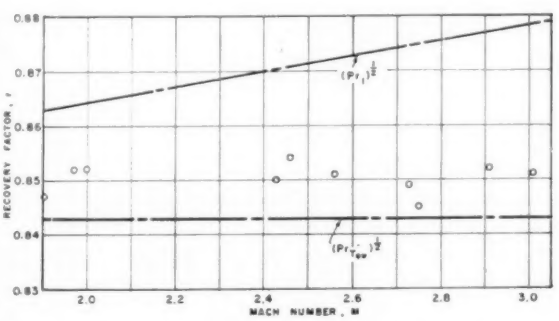

FIG. 6. Laminar recovery factor as a function of Mach Number.

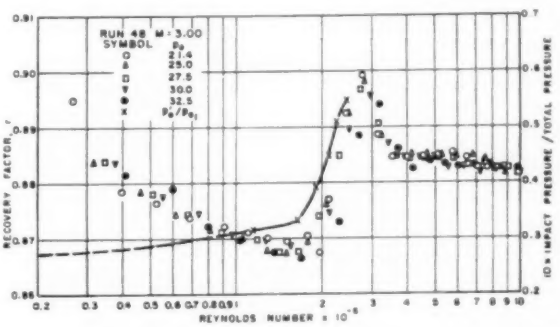

FIG. 7. Recovery factor and ratio of impact pressure to total pressure as a function of Reynolds Number.

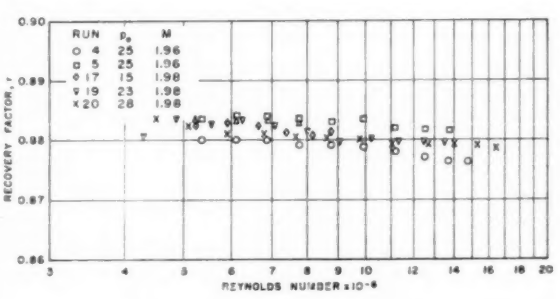

FIG. 8. Turbulent recovery factor as a function of Reynolds Number at a nominal Mach Number of 2.0.

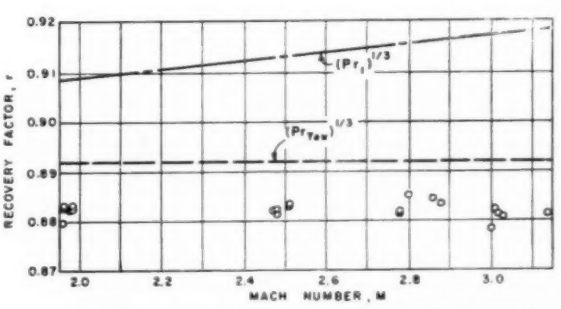

FIG. 9. Turbulent recovery factor as a function of Mach Number at a Reynolds Number of 5×10^6.

and if the variation of recovery factor with the Reynolds Number is not known, there is no way of finding such a variation from the present data, since it could not be separated from the effect of the heated nose.

In view of the theoretical and experimental evidence and the difficulty of any other course, it has been assumed that the laminar recovery factor is independent of Reynolds Number. With this assumption it is possible to calculate the asymptotic value of such data as appear in Fig. 5. Such a calculation may be based on a theoretical solution of the following idealized problem. A flat-plate flow is specified with a constant wall temperature ($T_{aw} + t$) for a short length downstream of the leading edge, $0 \leq x \leq l$. For $x > l$ the condition of zero heat transfer is specified and it is required to find the temperature distribution in this region. The solution was accomplished by a numerical procedure based on Lighthill's[12] equations for the heat transfer from a flat plate with nonuniform wall temperature, the details of which are given in reference 3. A comparison with the experimentally observed decay of excess temperature is shown in Fig. 5.

The asymptotic values of the recovery factors for all runs with an appreciable length of laminar boundary layer are shown in Fig. 6, where they are plotted against Mach Number. These data have been corrected for conduction and radiation errors and for the effects of any water vapor condensation. Within the accuracy of the tests it is not possible to detect any variation of recovery factor with Mach Number. The mean value of all experimental results is 0.850, which is about one per cent higher than the square root of the Prandtl Number based on the adiabatic wall temperature and two per cent lower than the square root of the Prandtl Number based on the free-stream temperature, using the relation between Prandtl Number and temperature of Kaye, et al.[13] The magnitude of the correction due to the heated nose is indicated in Table 1 where the lowest measured values of recovery factor are compared with the calculated asymptotic values. An analysis which takes into account the inaccuracies in the measurements and the errors in the corrections applied to the data shows that the possible error in the final value of the recovery factor is about ± 0.007.

Transition Recovery Factors

An examination of Fig. 4 shows that in each run, after the initial decreasing portion of the recovery-factor curve, the recovery factors rise rather rapidly to some peak value, then decrease, and finally level off to an almost constant value. The rapidly changing portion of the curve which centers around the peak value corresponds, as is shown later, to the region of transition from a laminar to a turbulent boundary layer. Every investigator who has recorded recovery factors measured in the transition region has noted similar peaks, although the reported magnitude of the difference between the peak value and the values corresponding to the turbulent boundary layer have varied from 0.01 to 0.08. In the present tests the highest value of the recovery factor is never more than two per cent greater than the turbulent recovery factor and does not exceed 0.90.

It is interesting to note that transition begins anywhere from a Reynolds Number of 10^6 to 2.5×10^6. It is possible that the turbulence level in the test section varies with stagnation pressure, Mach Number, and/or the amount of heating or cooling of the air. It is also possible that pressure oscillations in the stilling section have a role in initiating transition which becomes increasingly important with decreasing stagnation pressure.

The transition data are in good agreement with those of Stalder et al.,[14] who record a peak transition recovery factor of 0.89 at a Mach Number of 2.4. The only other flat-plate data extant are those of Slack,[15] who extrapolated flat-plate heat-transfer data at a Mach Number of 2.4 to the case of zero heat transfer and found transition recovery factors as high as 0.98. It might be reasoned from these results that a large temperature peak does exist for the flat plate, but that heat conduction along the plate "smooths out" the peak. This possibility has been investigated, and an analysis of the longitudinal heat transfer (given in detail in reference 3) indicates that the recovery factor at such a peak, if it existed, could have a value no greater than 0.906 as compared to a measured value of 0.900.† The results of Stine and Scherrer[9] and of des Clers and Sternberg,[10] who found no values of the recovery factor greater than 0.90 in the transition region, are in good agreement with those of the present investigation.

In order to dispel any doubt that the velocity profile changed at the same location at which temperature measurements indicated transition, an impact pressure probe was placed adjacent to the plate surface and temperature distributions and impact pressures were measured simultaneously as the stagnation pressure was raised. The results of this test are shown in Fig. 7 where recovery factors and the ratio of impact to free-stream total pressures are plotted as functions of Reynolds Number. The sudden change in the slope of the pressure-ratio curve indicates a change in the velocity profile which coincides closely with the recovery-factor rise associated with transition.

Turbulent Recovery Factors

Some typical recovery-factor data for the turbulent portion of the boundary layer appear in Figs. 8 and 9. Fig. 8 shows the recovery factor as a function of Reynolds Number at a nominal Mach Number of 2.0;

† This analysis clearly indicates that longitudinal heat transfer may safely be neglected in all but those portions of the plate very close to the nose or in the center of the transition region, thus justifying some of the assumptions made earlier.

Fig. 9, the recovery factor as a function of Mach Number at a Reynolds Number of 5×10^6. The latter figure also indicates values of the cube root of the Prandtl Number based on the adiabatic wall temperature and on the local free-stream temperature.

It is apparent that there is no recovery-factor variation with Mach Number at a given Reynolds Number. At a fixed Mach Number there appears to be a slight decrease of recovery factor with increasing Reynolds Number (from 0.882 at $Re_x = 5 \times 10^6$ to 0.880 at $Re_x = 10^7$) which is also apparent in the data taken at other Mach Numbers, but this effect may be a consequence of boundary-layer changes in the transition region, and it might gradually disappear at very high Reynolds Numbers. An analysis which takes into account the inaccuracies in the measurements and the errors in the corrections applied to the data shows that the possible error in the final value of the turbulent recovery factor is about ± 0.003.

The data are in good agreement with those of references 9, 10, 14, and 16 and in fair agreement with those of references 15 and 17. They also lie slightly below Ackermann's[18] theoretical value of $(Pr)^{1/3}$, which applies strictly only to incompressible flow. Tucker and Maslen,[19] predict that in a compressible flow the recovery factor decreases with Mach Number at fixed Reynolds and Prandtl Numbers, as does Elser.[20] This result is not confirmed by these tests.

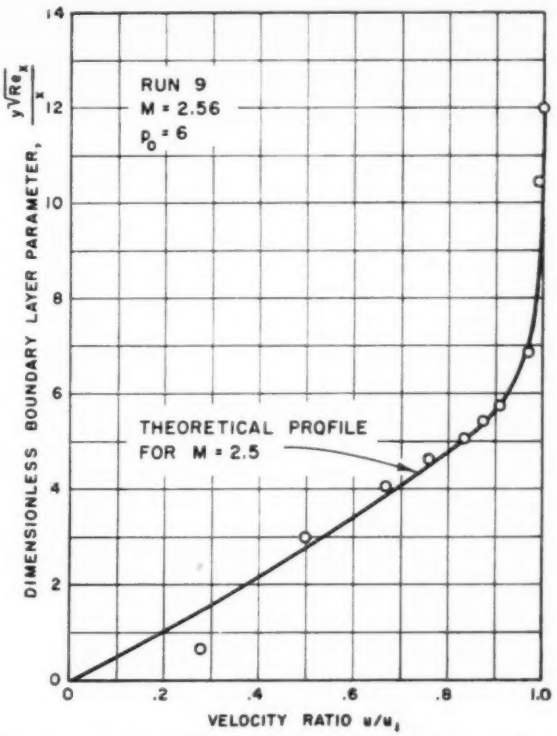

FIG. 10. Velocity profile in the laminar boundary layer at $M = 2.6$.

CONCLUSIONS

In deriving conclusions from an examination of the experimental data one must remember that the variation of wall temperature with Mach Number in these tests was very small. This situation is common to all wind-tunnel test programs run at a fixed stagnation temperature but is very different from the situation occurring in flight at a given altitude. The variation in recovery factor is probably tied closely to the variation of Prandtl Number at the wall. In flight the variation of recovery factor with Mach Number might be much larger than that observed here. The following conclusions apply directly only to flows with (Pr_{aw}) essentially fixed at approximately 0.71.

(1) For a Mach Number range of 1.90 to 3.14 the recovery factor for laminar boundary layers is 0.850 ± 0.007, a value about 1% higher than the square root of the Prandtl Number based on the adiabatic wall temperature and 2% lower than the square root of the Prandtl Number based on the free-stream temperature. This value is in excellent agreement with the available data on cones and bodies of revolution for supersonic flow. The discrepancy between flat plate and body of revolution data noted by Kaye[1] and Gruenewald[16] is now resolved.

(2) For a Mach Number range from 1.90 to 3.14 and for Reynolds Numbers up to 17×10^6 the recovery factor for turbulent boundary layers is independent of Mach Number. It decreases slightly but consistently with Reynolds Numbers, from a value of 0.882 at a Reynolds Number of 5×10^6 to a value of 0.880 at a Reynolds Number of 10^7. These values of the recovery factor are about 1% lower than the cube root of the Prandtl Number based on wall temperature. A maximum systematic error of ± 0.003 is possible, but this error would not affect the decrease of recovery factor with Reynolds Number.

(3) Recovery factors in the transition zone, which starts at Reynolds Numbers between 1.0×10^6 and 2.5×10^6, are higher than those in the laminar and turbulent regimes but never exceed 0.90.

Appendix A

BOUNDARY-LAYER PROFILES

Boundary-layer profiles were measured during several of the tests in order to verify that laminar velocity profiles corresponded to (supposedly) laminar recovery factors and turbulent velocity profiles to turbulent boundary layers. Most of these tests were made in turbulent boundary layers, but a sufficient number of laminar profiles were taken to verify that a laminar flow did correspond to the "laminar" recovery factors.

One of the few laminar velocity profiles measured is shown in Fig. 10, where it is compared with a theoretical profile interpolated from the curves of Van Driest.[21] Except near the plate surface the agreement is good,

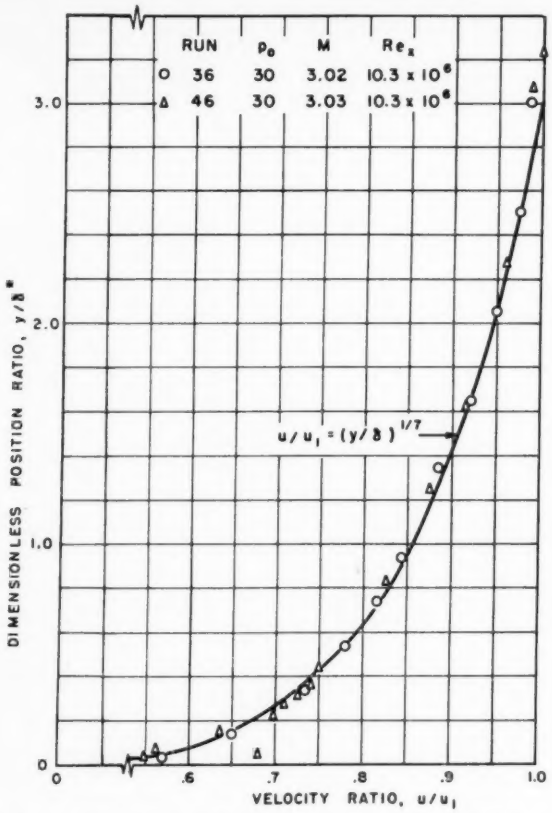

FIG. 11. Velocity profiles in the turbulent boundary layer at $M = 3.0$.

which may be fortuitous, inasmuch as the zero height position of the side-wall probe was difficult to determine.

Some turbulent velocity profiles are shown in Fig. 11. These profiles, which have been computed assuming a constant stagnation temperature across the boundary layer, show good agreement with a $^1/_7$-power curve.

The measurements of stagnation temperature in the boundary layer yielded results of considerable interest, although of somewhat questionable accuracy. The stagnation temperature probe was calibrated in the tunnel free stream and the probe calibration factor, defined as $(T_i - T)/(T_0 - T)$, had shown small but consistent variations with Mach Number and stagnation pressure. In an effort to reduce these variations, which presumably resulted from conduction errors, a nylon tip was made and used in the measurements with the intent of calibrating it after the tests were completed. Unfortunately it was damaged before calibration was completed. The stagnation temperature profiles, two of which appear in Fig. 12, were therefore computed assuming that the probe calibration factor measured in the free stream was constant. Fortunately any error introduced by the assumption diminishes with decreasing boundary-layer Mach Number. The profiles, which agree quite well with those of Spivack,[4] show that the stagnation temperature in the boundary layer reaches a peak value which is about 1% higher than the free-stream stagnation temperature. This peak occurs at a distance from the plate surface equal to about three quarters of the velocity boundary-layer thickness.

Appendix B

Roughness Tests

The final part of the test program consisted of an effort to simulate flow at high Reynolds Numbers by coating the upstream portion of the plate with particles of sand, thereby causing earlier transition and a thicker boundary layer than if transition were allowed to occur naturally. Only three tests could be made, and the results are inconclusive, but seem interesting enough to merit discussion.

In these tests sand was cemented to part of the measuring surface with a mixture of Duco cement and acetone. Recovery factors for the unsanded length and velocity profiles near the trailing edge of the plate were then measured simultaneously. The velocity profiles for the 3- and 6-in. sanded lengths fit a $^1/_7$-power curve quite closely, as do the turbulent velocity profiles measured at the same Mach Number when transition occurred naturally. This suggests that a fully developed flow of the natural transition type has

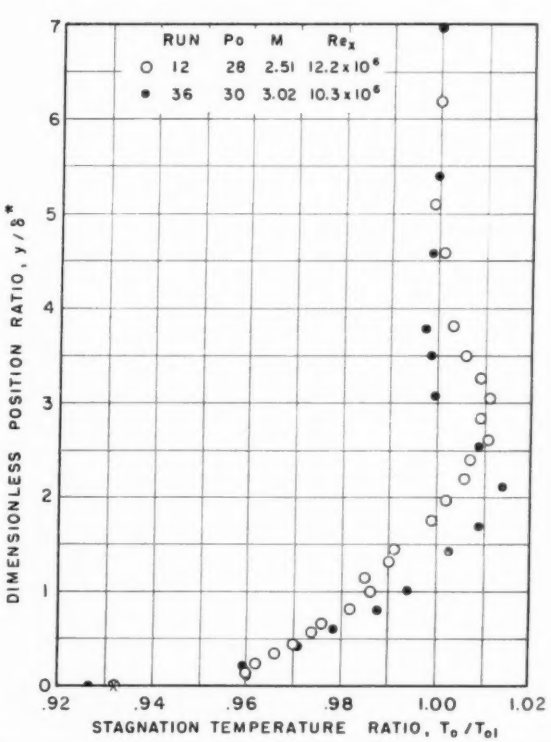

FIG. 12. Stagnation temperature distributions in turbulent boundary layers.

TABLE 2

Run	M	P_0	Sand, in.	r	δ^*, in.	θ, in.	Re_θ
46	3.03	30	0	0.880	0.124	0.0231	825
57	3.01	25	6	0.879	0.224	0.0414	3100
58	3.01	25	3	0.883	0.204	0.0385	2610

been reached.† The recovery factor data, shown in Fig. 13, suggest the same conclusion. In order to compare the results of the tests where transition was "forced" with those where transition occurred "naturally," the displacement and momentum thicknesses of the boundary layer at the aft probe position for certain of the runs are given in Table 2.

Table 2 suggests that the recovery factor may reach a constant value (or even increase) at high Reynolds Number. However, the evidence is too scanty for more than speculation.

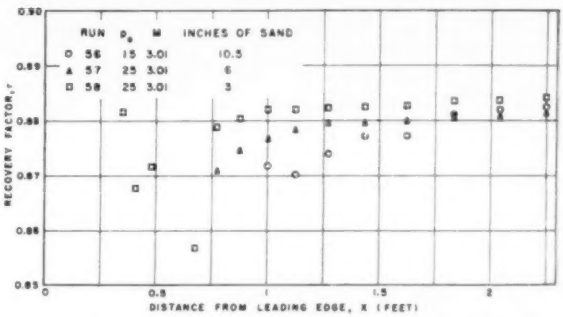

FIG. 13. Recovery factor with artificially induced transition as a function of distance from leading edge.

REFERENCES

[1] Kaye, J., *Survey of Friction Coefficients, Recovery Factors, and Heat-Transfer Coefficients for Supersonic Flow*, presented at the Institute of Aeronautical Sciences Meeting, New York, January, 1953.

[2] *Performance Information and Model Requirements, 18 Inch × 24 Inch Variable Density Supersonic Tunnel*, Massachusetts Institute of Technology, Naval Supersonic Laboratory, February, 1951.

[3] Shoulberg, R. H., Hill, J. A. F., and Rivas, M. A., *An Experimental Investigation of Flat Plate Recovery Factors for Mach Numbers Between 1.90 and 3.14*, Wind Tunnel Report No. 36, Naval Supersonic Laboratory, Massachusetts Institute of Technology, 1952.

[4] Spivack, H. M., *Experiments in the Turbulent Boundary Layer of a Supersonic Flow*, North American Aerophysics Laboratory, Report CM-615, January, 1950.

[5] Gazley, C., Jr., *Boundary-Layer Stability and Transition in Subsonic and Supersonic Flow*, Journal of the Aeronautical Sciences, Vol. 20, No. 1, pp. 19–28, January, 1953.

[6] Johnson, H. A., and Rubesin, M. W., *Aerodynamic Heating and Convective Heat Transfer—Summary of Literature Survey*, Trans. ASME, Vol. 71, No. 5, pp. 447–456, July, 1949.

[7] Pohlhausen, E., *Der Wärmeaustausch zwischen festen Körpern und Flussigkeiten mit kleiner Reibung und kleiner Wärmeleitung*, Zeit. für Angew. Math. Mech., Bd. 1, p. 115, 1921.

[8] Crocco, L., *Lo Strato limite laminare nei gas*, Monografie scientifiche di aeronautica, No. 3, 1946 (Rome); translated as Aerophysics Laboratory Report CF-1083 NAA, and RAE Library Translation No. 218.

[9] Stine, H. A., and Scherrer, R., *Experimental Investigation of the Turbulent-Boundary-Layer Temperature-Recovery Factor on Bodies of Revolution at Mach Numbers from 2.0 to 3.8*, NACA TN 2664, March, 1952.

[10] des Clers, B., and Sternberg, J., *On Boundary-Layer Temperature Recovery Factors*, Journal of the Aeronautical Sciences, Vol. 19, No. 9, pp. 645–646, September, 1952.

[11] Korobkin, I., *Apparent Recovery Factors on the Leading Edge of a Flat Plate in Supersonic Laminar Flow*, Journal of the Aeronautical Sciences, Vol. 20, No. 8, pp. 578–579, August, 1953.

[12] Lighthill, M. J., *Contributions to the Theory of Heat Transfer Through a Laminar Boundary Layer*, Proc. Roy. Soc., Vol. A202, pp. 359–77, August, 1950.

[13] Kaye, J., Keenan, J. H., Klingensmith, K., Ketchum, G. M., and Toong, T. Y., *Measurement of Recovery Factors and Friction Coefficients for Supersonic Flow of Air in a Tube*, Journal of Applied Mechanics, Vol. 19, No. 1, pp. 77–96, March, 1952.

[14] Stalder, J. R., Rubesin, M. W., and Tendeland T., *A Determination of the Laminar-, Transitional-, and Turbulent-Boundary-Layer Temperature Recovery Factors on a Flat Plate in Supersonic Flow*, NACA TN 2077, June, 1950.

[15] Slack, E. G., *Experimental Investigation of Heat Transfer Through Laminar and Turbulent Boundary Layers on a Cooled Flat Plate at $M = 2.4$*, NACA TN 2686, April, 1952.

[16] Gruenewald, K. H., *Temperature Recovery Factors in the Transitional and Turbulent Boundary Layer on a 40-Degree Cone-Cylinder at Mach Number 2.9*, U.S. Naval Ordnance Laboratory, NAVORD Report 2742, 1953.

[17] Brinich, P. F., and Diaconis, N. S., *Boundary Layer Development and Skin Friction at Mach Number 3.05*, NACA TN 2742, July, 1952.

[18] Ackermann, G., *Plattenthermometer in Strömung mit Grosser Geschwindigkeit und Turbulenter Grenzschicht*, Forschung a.d. Gebiet d. Igenieurwesens, Vol. 13, p. 226, 1942.

[19] Tucker, M., and Maslen, S. H., *Turbulent Boundary Layer Recovery Factors in Two-Dimensional Supersonic Flow*, NACA TN 2296, February, 1951.

[20] Elser, K., *Reibungstemperaturfelder in turbulenten Grenzschichten*, Mitteilungen aus dem Institut für Thermodynamik und Verbrennungsmotorenbau Nr. 8, Leemann, Zürich, 1949.

[21] Van Driest, E. R., *Investigation of Laminar Boundary Layer in Compressible Flow Using the Crocco Method*, NACA TN 2597, January, 1952.

[22] Klebanoff, P. S., and Diehl, Z. W., *Some Features of Artificially Thickened Fully Developed Turbulent Boundary Layers with Zero Pressure Gradient*, NACA TN 2475, October, 1951.

† Klebanoff and Diehl[22] showed that in a similar subsonic case, when the velocity profiles for natural and artificial transition agreed, the distribution of turbulence intensity and frequency also agreed, and the two boundary layers were fully equivalent.

On Inelastic Thermal Stresses in Flight Structures

ALFRED M. FREUDENTHAL*

Columbia University

SUMMARY

Conventional design for thermal stresses is based on an elastic analysis of the stresses and their comparison with a limiting creep-rate or creep-strain and a time-dependent fracture-stress, which both are characteristic manifestations of inelastic behavior. This contradiction between the premises of the stress analysis and of the strength analysis necessarily leads to design procedures of considerable unreality.

The effect, on the level of thermal stresses, of inelastic behavior of the structural material, with constant and with temperature-dependent parameters, is investigated; the results are compared with those of the elastic analysis. The importance of design for inelastic thermal stresses is discussed.

(I) NOTATION

a, A	= parameters
c	= constant
C	= specific heat, centigrade
d	= thickness
D, D_c	= plate stiffness
e	= volumetric strain
e_c	= Hencky's "strain intensity"
E	= Hooke's modulus
f	= function
G	= shear modulus
h	= surface heat transfer coefficient
i, j	= tensor subscripts
k	= thermal conductivity
K	= bulk modulus
K_n	= nonlinear plate parameter
M	= bending moments
M_{FL}	= flow moment of plate
Q	= activation energy
R	= gas constant
s	= hydrostatic stress
s_c	= Hencky's "stress intensity"
t	= time (variable)
t_0	= time-parameter
T	= temperature difference (variable)
T^*	= absolute temperature (variable)
T_s, T_a, T_m, T_c, T_w, T_0	= surface, average, melting, critical, wall, ambient temperature
x, y	= variables, coordinates
w	= deflection
z	= distance from middle plane, coordinate
α	= coefficient of linear thermal expansion
β	= surface heat transfer parameter, h/k
γ	= inverse time parameter
δ_{ij}	= Kronecker delta
ϵ, ϵ_{ij}	= strain components
ξ	= ratio of boundary of plastic zone to $d/2$
η, η_1	= coefficient of viscosity
ϑ	= time parameter, Cd^2/k
λ, λ_r	= coefficient of viscous traction
ν	= Poisson's ratio
ρ	= radius of curvature, density
σ, σ_{ij}	= stress components
σ_0	= yield stress
τ	= relaxation time, η/G or λ/E
φ, ψ	= functions
$\dot{w}$, $\dot{T}$	= time derivative of w, T
w_x, w_{xx} / w_y, w_{yy}	= first, second derivative with respect to x or y

Presented at the Structures Session, Twenty-Second Annual Meeting, IAS, New York, January 25–29, 1954.

* Professor, Department of Civil Engineering.

(II) INTRODUCTION

IT IS WELL KNOWN that aerodynamic heating of the boundary layer surrounding a flight-structure in supersonic flight produces high temperatures. The nonuniform temperature distribution in this structure resulting from the heating of the skin may cause thermal stresses of considerable severity; it has been shown that transient elastic thermal stresses are likely to attain and exceed the yield limit of the material after several minutes of flight.[1] Yielding will necessarily modify the stress distribution and relieve the peak stresses; it will, however, also induce residual stresses on cooling which, under certain conditions, may be high enough to cause yielding of opposite sign. In a structural material which is perfectly elastic to the yield point and ideally plastic beyond it, such heating and cooling cycles are accompanied by rather severe cycles of alternating plastic straining which, by gradually reducing the ductility of the metal, lead to failure after a relatively small number of thermal cycles. This phenomenon of thermal cycling has recently been studied under the simplest stress conditions.[2]

It is, however, generally recognized that metals at elevated temperatures show pronounced viscosity and can therefore not be considered elastic below the yield point; the importance of this deviation from elasticity increases rapidly with increasing temperature. Such recognition is expressed in the specification of a limiting creep rate or a limiting amount of creep deformation as the principal design criterion for high temperature equipment such as heat exchangers. At the same time, however, the stresses which presumably cause such creep, including the thermal stresses, are computed on the basis of elastic analysis. While such contradiction between the basis of stress analysis and of design necessarily leads to discrepancies in high temperature design of predominantly load-

carrying elements, it results in a completely unrealistic design of elements subject to severe temperature gradients or variations. This is due to the fact that the inelastic response of the structural material only affects the *distribution* of the load stresses, the resultant of which is independent of such response, while it is the *intensity* of the self-equilibrating thermal stresses which is itself primarily determined by this response.

In the analysis of the stability of columns at elevated temperatures, as well as in the analysis of load stresses in beams and rotating discs the effect of creep has been investigated for various forms of the creep law; in thermal stress design, elastic analysis is still the rule. Rational design for thermal stresses, however, should be based on a stress analysis consistent with the behavior of real materials and with the design assumptions concerning their deformation and strength at elevated temperatures.[3]

(III) Types of Inelastic Behavior

The deformational response of structural metals at elevated temperatures is a combination of elastic, quasiviscous and plastic components.[4] The three mechanical constants associated with these components of deformation—the elastic modulus, the coefficient of viscosity, and the yield stress—are temperature-dependent, and so are the thermal constants which determine the level of the thermal stresses: the coefficients of linear expansion and of thermal conductivity.

Of the mechanical constants the temperature variation of the elastic modulus is relatively unimportant, particularly in relation to the very rapid change with temperature of the coefficient of viscosity. It is also quite likely that the apparent, rather slow reduction of the modulus of elasticity with increasing temperature is, at least partly, due to the difficulty to observe the true elastic response of a material in the presence of creep and that, therefore, the elastic modulus is, in fact, even less temperature-dependent than suggested by test results obtained in conventional experiments.

The coefficient of viscosity is the most temperature-sensitive of the mechanical constants. The relation

$$\eta = \eta_0 \exp(Q/RT^*)/\exp(Q/RT_0^*) = \eta_0 \exp\left[Q/RT_0^*\left(\frac{T_0^*}{T^*} - 1\right)\right] \quad (1)$$

or

$$\ln(\eta/\eta_0) = Q/RT_0^*\left(\frac{T_0^*}{T^*} - 1\right) = Q/RT_0^* \frac{\mp T/T_0^*}{1 \pm T/T_0^*} \quad (1a)$$

is generally used[5] to describe the change of this coefficient from its value η_0 at the absolute (Kelvin) temperature T_0^* to its value η at the temperature $T^* = T_0^* \pm T$. For temperature changes that are small with respect to T_0^* Eq. (1a) can be approximated by

$$\ln(\eta/\eta_0) \doteq Q/RT_0^*[\mp T/T_0^* + (T/T_0^*)^2] \doteq \mp Q/RT_0^*(T/T_0^*) \quad (1b)$$

For metals the ratio (Q/R) (Q in cal. per mole and $R = 2$ cal. per mole,°C.) is of the order of magnitude 10^4 to 10^5.

The change of yield stress with temperature varies with the material. It is very slow for high-temperature alloys such as Inconel, moderate for titanium alloys, but rather rapid for the more conventional structural materials such as 75S-T6, SAE-4340 steel or stainless steel W. A relatively simple expression by which the observed change[6] can be roughly approximated is of the form

$$\sigma_0 = \bar{\sigma}_0[1 - (2T/T_m)^2] \quad (2)$$

where $\bar{\sigma}_0$ is the yield stress at the reference temperature $T = 0$, and T_m the melting temperature.

The coefficient of thermal expression generally increases with temperature; the relation can be roughly represented by the function

$$\alpha = \alpha_0 + \Delta\alpha\sqrt{T/T_m} \quad (3)$$

where α_0 is the coefficient at the reference temperature $T = 0$ and $\Delta\alpha$ the total range of variation between $T = 0$ and the melting point.

The thermal conductivity decreases for certain metals, while it increases for others; thus low-carbon steel at 1450°F. shows a decrease to one-half of its room temperature conductivity, while Inconel X doubles its conductivity over the same range; the variations may be assumed as roughly linear.

The use, in thermal stress analysis, of the initial, constant coefficient of expansion results in an underestimate of the stresses due to heating, and in an overestimate of the stresses due to cooling. In the case of the thermal conductivity decreasing with temperature, the use of the initial conductivity coefficient overestimates the rate of heat flow and might therefore underestimate the early transient stresses; the opposite trend in the variation of the conductivity will produce transient thermal stresses smaller than those computed on the basis of the initial coefficient of conductivity. While the effect, on the thermal stresses, of the temperature-sensitivity of both thermal coefficients may thus be significant, the consideration of this variation in the heat transfer and thermal stress equations makes their solution rather difficult. The use of intermediate constant values will improve the accuracy of the approximate solutions.

The simplest idealization of the mechanical behavior of structural materials at elevated temperatures is the assumption of viscoelastic response with creep up to the yield limit and ideal plastic or visco-plastic response above this limit. The viscous component of the deformation is usually nonlinear; this complicates

the solution of even simple visco-elastic stress problems to such an extent that it appears expedient, particularly in a general discussion of the effect of creep in design, to consider first a linear visco-elastic response. This response can be assumed to roughly represent the behavior of metals either at relatively low stresses or at very high temperatures; at stresses in the vicinity of the yield limit and within the range of moderately elevated temperatures the nonlinearity of the viscous response must be introduced.

The linear visco-elastic stress-strain relations for a material with creep (Maxwell body) have the general form

$$2G(\epsilon_{ij} - e\delta_{ij}) = \left(\frac{\partial}{\partial t} + \frac{1}{\tau}\right)(\sigma_{ij} - s\delta_{ij}) \qquad (4)$$

where the relaxation time $\tau = \eta/G$.

Nonlinear viscous steady-state creep equations of different forms have been proposed; the simplest form is that of a power function

$$\frac{\partial}{\partial t} e_r = (s_r/\lambda_r)^n \qquad (5)$$

where s_r and e_r denote Hencky's stress and strain intensities which are proportional to the square root of the second invariant of the deviators of stress I_2 and strain J_2, respectively[7]

$$s_r = \sqrt{3I_2} \quad \text{and} \quad e_r = \frac{2}{\sqrt{3}}\sqrt{J_2} \qquad (6)$$

λ_r and $n > 1$ are constants because of the desired symmetry of the stress-strain rate relation n should be an odd integer.

For stresses exceeding the yield point the yield condition

$$s_r = \sigma_0 \qquad (7)$$

determines the state of stress in the ideal plastic region of the material.

In the linear visco-plastic material the general relation between the components of the stress deviator and the strain-rate deviator

$$2\eta_1 \frac{\partial}{\partial t}(\epsilon_{ij} - e\delta_{ij}) = \left(1 - \frac{\sigma_0}{s_r}\right)(\sigma_{ij} - s\delta_{ij}) \quad (s_r > \sigma_0) \qquad (8)$$

For $s_r < \sigma_0$ the visco-plastic strain rate vanishes; the behavior is then governed by the visco-elastic relation (4), the simplifying assumption for establishing Eq. (8) being that the visco-elastic strain rates are negligibly small in relation to the visco-plastic strain rates. If this assumption cannot be made, Eqs. (4) and (8) must be combined for $s_r > \sigma_0$.

For all materials the relation between e and s has the form $e = s/3K$.

For the discussion of thermal stresses in plates the above equations of inelastic response can be simplified by the assumptions $\sigma_{xx} = \sigma_{yy} = \sigma$, $\sigma_{zz} = 0$ and therefore $\epsilon_{xx} = \epsilon_{yy} = \epsilon$. Under this condition the following relations are obtained.

Linear visco-elastic material

$$\frac{\partial}{\partial t}\epsilon = \left(\frac{\partial}{\partial t} + \frac{1}{\tau}\right)\frac{\sigma}{6G} + \frac{2}{9K}\frac{\partial \sigma}{\partial t} + \frac{\partial}{\partial t}(\alpha T) =$$

$$\left(\frac{1 - \nu}{1 + \nu}\frac{\partial}{\partial t} + \frac{1}{3\tau}\right)\frac{\sigma}{2G} + \frac{\partial}{\partial t}(\alpha T) \qquad (4a)$$

Nonlinear viscous material

$$\frac{\partial}{\partial t}\epsilon = \frac{1}{2}(\sigma/\lambda_r)^n + \frac{2}{9K}\frac{\partial \sigma}{\partial t} + \frac{\partial}{\partial t}(\alpha T) \qquad (5a)$$

Nonlinear visco-elastic material

$$\frac{\partial}{\partial t}\epsilon = \frac{1 - \nu}{1 + \nu}\frac{1}{2G}\frac{\partial \sigma}{\partial t} + \frac{1}{2}(\sigma/\lambda_r)^n + \frac{\partial}{\partial t}(\alpha T) \qquad (5b)$$

Ideal plastic material beyond the yield point

$$\sigma = \sigma_0 \qquad (7a)$$

Linear visco-plastic material beyond the yield point

$$\frac{\partial}{\partial t}\epsilon = (\sigma - \sigma_0)\frac{1}{6\eta_1} + \frac{2}{9K}\frac{\partial \sigma}{\partial t} + \frac{\partial}{\partial t}\alpha T \qquad (8a)$$

Linear visco-elastic visco-plastic material beyond the yield point

$$\frac{\partial}{\partial t}\epsilon = \left(\frac{1 - \nu}{1 + \nu}\frac{\partial}{\partial t} + \frac{1}{3\tau}\right)\frac{\sigma}{2G} + \frac{1}{6\eta_1}(\sigma - \sigma_0) + \frac{\partial}{\partial t}(\alpha T) \qquad (8b)$$

The above equations are somewhat simplified if incompressibility of the material can be assumed [$K \to \infty$ and $\nu \to (1/2)$].

(IV) Surface Stresses in Plates Subject to Rapidly Changing Ambient Temperatures

(a) Instantaneous Change of Temperature (Thermal Shock)

Considering an infinite slab of thickness d or a curved slab the radius of curvature of which is large in relation to its thickness, with one face exposed to a rapidly changing ambient temperature, the other face insulated or $(\partial T/\partial z) = 0$, the temperature-distribution problem is one-dimensional and equivalent to that of a plate of thickness $2d$ exposed at both faces to symmetrically changing ambient temperature. If the plate is not restrained along the edges, the thermal stresses at any distance z from the center plane will be the difference between the stresses suppressing the local thermal expansion depending on $T(z)$, and the uniformly distributed stresses due to the forces at infinity re-establishing the force-free edges. For the linear elastic or visco-elastic plate with temperature-independent parameters, in which the thermal stress intensity is directly proportional to the temperature, this stress difference is proportional to the difference $(T_a - T)$

between the local temperature $T(z)$ and the average temperature T_a. For nonlinear behavior the stresses must be computed by setting $(d\epsilon/dt) = 0$, and subtracting, from the resulting stress $\sigma_T(z)$ the uniform stress $\sigma_{T0} = (1/2d) \cdot \int_{-d}^{d} \sigma_T dz$, produced by the force which re-establishes the free boundary. The maximum stress $\sigma = \sigma_{T0} - \sigma_T$ (compression for increasing, tension for decreasing ambient temperature) will usually be at the surface. Consideration of the variation with temperature of α and k may, however, shift the maximum stress toward the interior of the plate.

In order to compute the surface stress not only the surface temperature, but also the full temperature distribution over the thickness of the plate must be known. The solutions of the transient heat-transfer problem giving the distribution in terms of an infinite series

$$(T/T_0) = 1 - \sum_{0}^{\infty} \varphi_k(t) \cdot \psi_k(z) \tag{9}$$

is well known; the time functions are negative exponentials $\varphi_k(t) = \exp(-a_k^2 t/\vartheta)$, $\vartheta = Cd^2/k$ is a time parameter and a_k are the roots of the transcendental equation $a_k \cdot \tan a_k = \beta$, where $\beta = dh/k$ is the surface heat transfer parameter.

To compute the stresses σ_T and σ_{T0} in nonlinear inelastic materials by combining Eq. (9) with any of the nonlinear Eqs. (4) to (8), numerical methods must be applied. In a first approximation it may, however, be assumed that in both linear and slightly nonlinear materials the stress $\sigma = \sigma_{T0} - \sigma_T$ is proportional to the temperature difference $(T_a - T)$; in this case, therefore, the critical difference, as a function of (t/ϑ) for different values of the parameter β, obtained from a numerical evaluation of Eq. (9) for the surface at which $T = T_s$, determines the surface stress. If the peak values of $(T_a - T_s)$ and the dimensionless time of their occurrence (t_0/ϑ), taken from plotted $(T_a - T_s)$ versus (t/ϑ) functions, can be related to the parameter by fitting simple functions to the points $[(T_a - T_s)_{max.}, \beta]$ and $[(t_0/\vartheta), \beta]$ respectively, and if the general shape of the plotted functions can be reproduced by a relatively simple, easily integrable function, the effect of the inelasticity of the material on the thermal stresses can be roughly analyzed.

On the basis of published numerical evaluations of Eq. (9) for various parameters β[8] it appears that a function of the type

$$(y/y_0)^n = x \cdot \exp(1 - x) \tag{10}$$

where $y = (T_a - T_s)/T_0$, $y_0 = y_{max.}$, $x = t/t_0$ reproduces the shape of the theoretical functions fairly well; by curve fitting the following approximate relations, valid for $5 < \beta < 25$ have been obtained:

$$y_0 = 1/(1 + \sqrt{5/\beta}); \qquad t_0/\vartheta = 0.18/\sqrt{\beta}; \qquad n = 4 \tag{11}$$

Introducing (11) into (10) the equation for the transient change $y(t/\vartheta)$

$$y = (T_a - T_s)/T_0 = -A(\beta)(t/\vartheta)^{1/4} \exp[-a(\beta)t/\vartheta] \tag{12}$$

where

$$A = 1.96 \sqrt[4]{\beta}/(1 + \sqrt{5/\beta}) \text{ and } a = 1.39\sqrt{\beta} \quad (5 < \beta < 25) \tag{13}$$

The effect of the inelasticity of the material on the thermal stresses under conditions of thermal shock can now be discussed by introducing the difference between the rate of deformation due to T and the rate of deformation due to the negative force restoring the free edge and roughly proportional to T_a: $\frac{\partial \epsilon}{\partial t} - \frac{\partial}{\partial t}(\alpha T) \doteq \frac{\partial}{\partial t}(T_a - T_s)$ into the inelasticity equations. Thus, for instance, for the simplest case of linear viscoelastic response the differential equations for the stress at the surface σ_S

$$\left(\frac{\partial}{\partial t} + \frac{1+\nu}{1-\nu}\frac{1}{3\tau}\right)\sigma_S = -2G\alpha \frac{1+\nu}{1-\nu}\frac{\partial}{\partial t}(T_a - T_S) \tag{14}$$

Assuming a temperature-independent relaxation time $\tau_1 = 3\tau(1 - \nu)/(1 + \nu)$ and introducing $(T_a - T_S)$ according to Eq. (12), the solution of (14) can be written in the form of a series

$$\sigma_S = -2G\alpha T_0 \frac{1+\nu}{1-\nu} A e^{-at/\vartheta} (t/\vartheta)^{1/4} \left[1 - \frac{1}{5}\left(\frac{4\vartheta}{\tau_1}\right) \times (t/\vartheta) + \frac{1}{5.9}\left(\frac{4\vartheta}{\tau_1}\right)^2 \left(1 - \frac{\tau_1 a}{\vartheta}\right)(t/\vartheta)^2 - \frac{1}{5.9.13} \times \left(\frac{4\vartheta}{\tau_1}\right)^3 \left(1 - \frac{\tau_1 a}{\vartheta}\right)^2 (t/\vartheta)^3 + \ldots\right] \tag{15}$$

or

$$\sigma_s = (\sigma_S)_{\text{elastic}}\left[1 - \frac{1}{5}\left(\frac{4t}{\tau_1}\right) - \frac{1}{5.9}\left(\frac{\tau_1}{4t_0} - 1\right)\left(\frac{4t}{\tau_1}\right)^2 - \frac{1}{5.9.13}\left(\frac{\tau_1}{4t_0} - 1\right)^2\left(\frac{4t}{\tau_1}\right)^3 - \frac{1}{5.9.13.17}(\quad)^4 \ldots\right] \tag{15a}$$

where $(\sigma_S)_{\text{elastic}}$ is the expression in front of the bracket in Eq. (15). For the maximum temperature difference at $t = t_0$ the surface stress

$$\sigma_S = (\sigma_{S max.})_{\text{elastic}}\left\{1 - \frac{4t_0}{5\tau_1}\left[1 + \frac{1}{9}\left(\frac{4t_0}{\tau_1} - 1\right) + \frac{1}{9.13}\left(\frac{4t_0}{\tau_1} - 1\right)^2 + \frac{1}{9.13.17}\left(\frac{4t_0}{\tau_1} - 1\right)^3 - \ldots\right]\right\} \tag{15b}$$

The relative surface stress intensity $\sigma_s(1 - \nu) \div 2GT_0\alpha(1 + \nu)$ according to Eq. (15) has been evaluated

as a function of (t/ϑ) for the ratios $(\vartheta/\tau_1) = 25$, 10 and 0 (elastic case) and the surface heat transfer parameter $\beta = 5$, and presented in Fig. 1. The diagrams show that for a sudden increase T_0 of the ambient temperature the visco-elastic response of the plate causes a reduction of the maximum elastic stress intensity followed by a stress reversal prior to the complete stress relaxation. The sharp drop from the maximum stress intensity of the visco-elastic curves also suggests that even for delay times t_0 that are short in relation to the relaxation time of the material, so that almost the full elastic stresses can be built up, these stresses are only of short duration, decrease at a much faster rate than the temperature difference $(T_a - T_S)$ itself, and therefore disappear before the temperature gradients disappear. Since the maximum stress is of short duration, the critical design strength values of the material are the very short-time strength values, representing the stresses that can be safely sustained during a few minutes or even fractions of minutes; these stresses are significantly higher than the values which are usually considered to represent short-time strength.

When the response of the material is pronouncedly nonlinear as, for instance, in the case of an elastic plastic plate, a plastic region will spread from the surface as soon as $\sigma_s \geqq \sigma_0$ and extend as far inward as the elastic stress $\sigma > \sigma_0$. Subsequent reduction of the difference $(T_a - T_s)$ will produce elastic stresses of opposite sign proportional to this reduction, and thus residual stresses $\sigma_{RES} = \sigma_0 - \sigma_{elastic}$. In the course of a rapid change of ambient temperature of such magnitude that the elastic stresses at the peak difference $(T_a - T_s)$ exceed the yield point over a finite depth from the surface, the subsequent reduction of $(T_a - T_s)$ due to heat flow [Eq. (12)] may produce severe elastic stresses of opposite sign and therefore substantial residual stresses, even without reversal of the ambient temperature. If the residual stresses are not relaxed, they will increase the elastic stresses resulting from such reversal before and at the peak difference $[-(T_a - T_s)]$.

Whenever the yield stress is attained in a visco-elastic-plastic plate the stress will remain there only for a short time. During this time the visco-elastic stress distribution is changed and residual stresses are built up as soon as the stresses decrease below the yield point; these residual stresses are, however, eliminated by relaxation.

(*b*) *Aerodynamic Heating*

Conditions of aerodynamic heating are much less severe than those of thermal shock. It has been shown[9] that under certain simplifying assumptions the mean temperature increase of the skin is governed by the relation

$$T_W(t) = T_{W0}[1 - e^{-\gamma t}] \qquad (16)$$

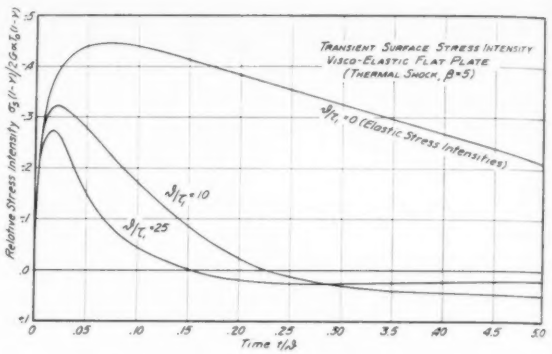

FIG. 1. Surface stress intensity in linear viscoelastic plate due to sudden increase of ambient temperature at time $t = 0$.

if the initial temperature of the structure is taken as zero, where T_{W0} is the adiabatic wall temperature rise and $\gamma = h/C\rho d$ is an inverse time parameter; in this relation the effect of heat radiation is neglected.

Assuming, as a rough approximation, that the transient temperature difference between surface and center of an idealized element of a flight structure produced by a temperature increase dT_W of the skin can be described by Eq. (12), the total temperature difference is obtained by integration

$$(T_a - T_S)/T_{W0} = -A\gamma \int (t/\vartheta)^{1/4} e^{-(a+\gamma\vartheta)(t/\vartheta)}\, dt \qquad (17)$$

Introducing this expression into Eq. (14), the differential equation for the visco elastic stress at the surface is obtained

$$\left(\frac{\partial}{\partial t} + \frac{1}{\tau_1}\right)\sigma_S = -2G\alpha T_{W0}\frac{1+\nu}{1-\nu}\gamma A (t/\vartheta)^{1/4} e^{-(a+\gamma\vartheta)(t/\vartheta)} \qquad (18)$$

the solution of which is

$$\sigma_S = -2G\alpha T_{W0}\frac{1+\nu}{1-\nu} A\gamma t (t/\vartheta)^{1/4} e^{-(a+\gamma\vartheta)(t/\vartheta)}\left[1 + \frac{4}{9}c(t/\vartheta) + \frac{4^2}{9.13}c^2(t/\vartheta)^2 + \frac{4^3}{9.13.17}c^3(t/\vartheta)^3 + \ldots\right] \qquad (19)$$

where $c = (a + \gamma\vartheta - \vartheta/\tau_1)$. The maximum surface stress is obtained by solving the equation $(d\sigma_S/dt) = 0$; neglecting terms in (t/ϑ) of higher than first order, the time t_0 at which this stress is reached is, in first approximation, $(t_0/\vartheta) = 9/4(a + \gamma\vartheta + \vartheta/\tau_1)$. Hence $ct_0/\vartheta = 9(1 - \kappa)/4(1 + \kappa)$ where $\kappa = \vartheta/\tau_1(a + \gamma\vartheta)$. For elastic response $\tau_1 \to \infty$ and therefore $\kappa \to 0$; the visco-elastic stress reduction depends on the value of $0 < \kappa < 1$, in which the effects of thermal coefficients of the material, surface heat transfer resistance, rate of heating and relaxation time are combined. For $\kappa = 0.5$ the maximum visco-elastic surface stress is about 0.42 of the elastic stress.

(V) Surface Stresses in Plates Subject to Linear Temperature Gradient

If the two surfaces of a flat plate or of a plate the curvature of which is small in relation to its thickness d are kept at temperatures T_e and T_i a steady state of heat flow is established after a certain time, which is associated with a linear temperature gradient. The difference between the change of length of the external fibers and the middle surface produces a spherical curvature of the unrestrained plate

$$1/\rho = \alpha(T_e - T_i)/d = \alpha T/d \tag{20}$$

If the edges of the flat plate are perfectly restrained against rotation, or if the plate is part of a circular cylinder or of a sphere of large radius, a constant bending moment $M_x = M_y = M$ is induced which restores the initial curvature.

Since for the elastic plate the relation between deflection w and bending moment

$$w_{xx} = w_{yy} = -M/D(1 + \nu) = -1/\rho$$

$$\text{where } D = \frac{Ed^3}{12(1 - \nu^2)} \tag{21}$$

the temperature moment

$$M = \alpha TD(1 + \nu)/d \tag{22}$$

and the maximum elastic fiber stresses

$$\sigma = \pm\alpha ET/2(1 - \nu) \tag{23}$$

For the linear visco-elastic plate according to Eq. (4a)

$$\dot{w}_{xx} = \dot{w}_{yy} = -\left(\frac{1 - \nu}{1 + \nu}\frac{\partial}{\partial t} + \frac{1}{3\tau}\right)6M/Gd^3 = -\frac{d}{dt}(1/\rho) \tag{24}$$

since at the surface $\epsilon_{xx} = \epsilon_{yy} = \mp dw_{xx}/2 = \mp dw_{yy}/2$ and $\sigma = 6M/d^2$. Hence the temperature moment is obtained from the differential equation

$$\left(\frac{1 - \nu}{1 + \nu}\frac{\partial}{\partial t} + \frac{1}{3\tau}\right)M = -\alpha\dot{T}D_v/d$$

$$\text{where } D_v = Gd^3/6 \tag{25}$$

For constant T and $\dot{T} = 0$ the solution of this equation describes the relaxation of an initially induced temperature-moment M_0, which proceeds exponentially with the relaxation time $\tau_1 = 3\tau(1 - \nu)/(1 + \nu)$. If the temperature difference T increases slowly so that the temperature gradient can be considered to remain invariably linear, the temperature moment is obtained as a solution of Eq. (25) for a given time function $T(t)$. For $T(t)$ according to Eq. (16)

$$M(t) = \alpha T_0 D_v \tau_1 \gamma(e^{-\gamma t} - e^{-t/\tau_1})/d\,(1 - \gamma\tau_1) \tag{26}$$

The moment thus increases from $M = 0$ at $t = 0$ to a maximum, which is attained at $t = \tau_1 \ln \tau_1\gamma/(\tau_1\gamma - 1)$. This maximum is considerably smaller than the elastic moment if τ_1 and $1/\gamma$ are of the same order of magnitude; for $1/\gamma = 0.5\tau_1$ the visco-elastic temperature moment does not attain one-half of the elastic moment.

For a linear increase of the temperature difference $T = T_0 t/t_0$

$$M(t) = \alpha T_0 D_v \tau_1(1 - e^{-t/\tau_1})/t_0 \tag{27}$$

If, from a time $t = t_1$ this difference remains constant, the moment $M(t_1)$ relaxes exponentially with relaxation time τ_1. Therefore, a decrease of the temperature difference, after a time which is sufficiently long to permit a substantial relaxation of the temperature moment caused by the preceding increase of the temperature difference, will produce thermal moments of opposite direction, as this increase is equivalent to an increase of negative sign with respect to the new stress-relaxed condition. Hence, in visco-elastic plates sufficiently long cycles of temperature difference between zero and a maximum will be accompanied by almost complete moment- and stress-reversals, leading to fatigue failures.

Consideration of the temperature dependence of τ_1 would require the introduction of a variable viscosity over the thickness of the plate according to Eq. (1a). The resulting stress distribution is nonlinear, since the viscous strain rate $\dot{\epsilon} = d/dt.\ (z/\rho) = -z\dot{w}_{xx} = \sigma/\lambda(T)$ and therefore $\sigma = -\dot{w}_{xx}z \cdot f(z)$ where $f(z)$ is obtained by introducing a linear temperature distribution into Eq. (1b). With increasing temperature differences the nonlinearity becomes more pronounced; the neutral axis moves toward the colder surface in which the fiber stress tends to increase faster than in the hotter surface.

For an incompressible nonlinear viscous material according to Eq. (5a) the differential equation for the thermal moment is obtained by expressing ϵ and σ in Eq. (5a) in terms of ρ and M and introducing ρ according to Eq. (20). Hence

$$M^n = -K_v^n \frac{d}{dt}\left(\frac{1}{\rho}\right) = -\alpha\dot{T}K_v^n/d \tag{28}$$

where

$$K_v = nd^{2n+1} \cdot \lambda_r/2(2n + 1) \tag{29}$$

Therefore for the nonlinear visco-elastic plate according to Eq. (5b) the differential equation of the temperature moment M

$$\frac{1 - \nu}{1 + \nu}\frac{\partial}{\partial t}(M/D_v) + (M/K_v)^n = -\alpha\dot{T}/d \tag{30}$$

or, with $c_n = [(1 + \nu)/(1 - \nu)]D_v/K_v^n$

$$\dot{M} + c_n M^n = -\frac{1 + \nu}{1 - \nu}\alpha\dot{T}D_v \tag{30a}$$

For a stationary temperature difference $T = \text{const.}$ and $\dot{T} = 0$ the relaxation of an initially induced temperature moment M_0 thus proceeds more slowly

than in the linear material, according to the equation

$$(M/M_0)^{n-1} = \frac{1}{1 + (n-1)M_0^{n-1}c_n t} \qquad (n > 1) \quad (31)$$

For a linear increase of the temperature difference $T = T_0 t/t_0$ the equation

$$\dot{M} + c_n M^n = -\frac{1+\nu}{1-\nu}\alpha T_0 D_r/t_0 = \text{const.} \quad (32)$$

is directly integrable; for less simple temperature histories numerical integration using finite differences is required.

In an elastic-plastic plate the yield limit is reached in the surface fibers when σ, according to Eq. (23), reaches σ_0; the critical temperature difference T_{0c} therefore

$$T_{0c} = 2\sigma_0(1-\nu)/\alpha E \quad (33)$$

If the temperature dependence of the yield limit according to Eq. (2) is considered, the critical temperature T_c in terms of the critical temperature T_{0c} is obtained from the equation

$$T_c = T_{0c}[1 - 4(T_c/T_m)^2] < T_{0c} \quad (33a)$$

For aluminum with $\sigma_0/E = 2 \times 10^{-3}$, $\alpha \doteq 2 \times 10^{-5}$ per °C. and $\nu = 0.35$, the critical temperature difference $T_{0c} = 130$°C.; with $T_m = 660$°C. the critical temperature difference corrected for temperature-dependent yield limit $T_c \doteq 113$°C.

For $T > T_c$ the plate under a constant moment is in the elastic state over a depth $z = \pm\xi(d/2)$ from the middle plane, and in the plastic state between $z = \pm\xi(d/2)$ and $z = \pm d/2$. Since the curvature of the plate is constant and determined by the maximum strain ϵ_0 in the elastic core

$$1/\rho = -w_{xx} = -w_{yy} = 2\epsilon_0/\xi d = 2\sigma_0(1-\nu)/E\xi d = \alpha T_c/\xi d \quad (34)$$

and since the relation between the bending moment M and the depth of the elastic core in an elastic-plastic plate[10]

$$M = M_{FL}\,[1 - (1/3)\xi^2] \quad (35)$$

where the "flow-moment" $M_{FL} = \sigma_0 d^2/4$ denotes the theoretical ultimate plastic carrying capacity of the plate, the relation between ξ and T obtained from Eqs. (20) and (34)

$$\xi = T_c/T \quad (36)$$

determines the relation between temperature difference and temperature moment in the elastic-plastic plate:

$$M/M_{FL} = 1 - \frac{1}{3}(T_c/T)^2 \qquad \left(\frac{2}{3}M_{FL} \leqslant M \leqslant M_{FL}\right) \quad (37)$$

A reduction of the temperature difference is accompanied by a reversed elastic moment according to Eq. (22), with a temperature difference $(-T)$. Hence for $T > T_{0c}$ a residual bending moment M_{RES} will remain in the plate after complete removal of the temperature difference

$$M_{RES} = M_{FL}\left[1 - \frac{1}{3}(T_c/T)^2 - \frac{2}{3}(T/T_c)\right] \quad (38)$$

The residual fiber stress

$$\sigma_{RES} = \sigma_0(1 - T/T_c) \quad (39)$$

For $T > 2T_{0c}$, $M_{RES} > (5/12)M_{FL}$, and $\sigma_{RES} > \sigma_0$: hence the removal of the temperature difference is accompanied by plastic deformation in the opposite direction. Repetition of temperature cycles in excess of $2T_c$ will therefore gradually lead to failure by "alternating plasticity" or "thermal fatigue."

When loads and temperature differences act jointly on an elastic-plastic plate the moments due to loads and to temperature-differences are not independent. Even in the simplest case of a constant load moment M_P and a constant temperature difference T producing a constant temperature moment M_t acting in the direction of the load-moment, the dependence of M_t on M_P cannot be easily evaluated. It is obvious that if, in this simple case, $M_P > {}^2/_3 M_{FL}$, the temperature moment for the same difference T will decrease for increasing load moment if the load moment is applied first. For less simple cases, particularly those of variable load moments with different signs over different portions of the plate a highly complex interaction must be expected in the elastic-plastic as well as in the nonlinear visco-elastic plate. Only in the elastic and linear visco-elastic plate with temperature-independent parameters is simple superposition of load and temperature effects permissible.

References

[1] Hoff, N. J., *Structural Problems of Future Aircraft*, Proc. Third Anglo-American Aeronautical Conference, London, 1951, pp. 89–95.

[2] Manson, S. S., *Behavior of Materials under Conditions of Thermal Stress*, NACA TN 2933, Washington, 1953. Coffin, L. F., *Study of the Effects of Cyclic Thermal Stresses on Ductile Metal*, Am. Soc. Mech. Eng., Paper No. 53-A-76, 1953.

[3] Freudenthal, A. M., *Inelastic Thermal Stresses*, von Mises Memorial Volume, Acad. Press, New York, 1954, to be published; *Effect of Rheological Behavior on Thermal Stresses*, J. Appl. Physics, Vol. 25, p. 1110, 1954.

[4] Freudenthal, A. M., *The Inelastic Behavior of Materials and Structures;* J. Wiley & Sons, New York, 1950, pp. 506 ff.

[5] Freudenthal, A. M., Ibid., p. 137.

[6] Heimerl, G. H., and Hughes, Ph. J., *Structural Efficiency of Various Aluminum, Titanium and Steel Alloys at Elevated Temperature*, NACA TN 2975, Washington, 1953.

[7] Freudenthal, A. M., loc. cit., 4, p. 257.

[8] Manson, S. S., loc. cit., p. 53. Heisler, M. P., *Transient Thermal Stresses in Slabs and Circular Pressure Vessels*, Am. Soc. Mech. Eng., Paper No. 53-APM-8, 1953.

[9] Davies, F. V., and Monaghan, R. J., *The Determination of Skin Temperature Attained in High-Speed Flight*, Aero. Res. Council, Tech. Report 123, London, 1953.

[10] Freudenthal, A. M., loc. cit.,[4] p. 422.

Readers' Forum

BRIEF REPORTS of investigations in the aeronautical sciences and discussions of papers published in the JOURNAL are presented in this special department. Publication is completed as soon as possible after receipt of the material. The Editorial Committee does not hold itself responsible for the opinions expressed by the correspondents.

Forced Convection from Surfaces at Nonuniform Temperatures*

Morton Finston
Department of Aeronautical Engineering, Massachusetts Institute of Technology, Cambridge, Mass.
June 4, 1954

THE TITLE PROBLEM has received considerable attention recently and is of considerable practical and theoretical interest. Principal available results are well summarized by Tribus and Klein[1] and the significance of variable surface temperatures is set forth by Schlichting.[2] Among their new results Tribus and Klein have generalized earlier work by Leveque which is restricted to the case of almost constant τ, the shear distribution. It is shown herein that this restriction is not essential since a simple coordinate transformation reduces the problem for arbitrary τ to that treated by Leveque.

As noted by Tribus and Klein the energy equation (we assume constant fluid properties, incompressible flow throughout)

$$\rho\, C_p(u\, T_x + v\, T_y) = k\, T_{yy} + \mu(U_y)^2 \tag{1}$$

is linear so that, given any particular solution, the problem is to solve

$$\rho\, C_p(u\, T_x + v\, T_y) = k\, T_{yy} \tag{2}$$

subject to appropriate boundary conditions. A typical set is

$$\left.\begin{aligned} T(x, 0) &= G(x), \text{ (given)} \\ T(x, \infty) &= 0 \\ T(0, y) &= 0 \end{aligned}\right\} \tag{3}$$

When it is possible to approximate u by

$$u = \frac{\tau(x)}{\mu}\, y \tag{4}$$

the continuity equation yields

$$v = -\frac{1}{2}\,\frac{\tau'(x)}{\mu}\, y^2 \tag{5}$$

If τ can be taken as constant, i.e., τ' is negligible, Eq. (2) becomes

$$\frac{\rho\, C_p \tau}{\mu}\, y\, T_x = k\, T_{yy} \tag{6}$$

This problem has been solved by Leveque for a step function in temperature and Tribus and Klein have considered arbitrary surface distributions of temperature and heat flux. The restriction on τ is often too severe and Eq. (5) must be considered.

Retaining τ, Eq. (2) becomes

$$\frac{\rho\, C_p}{\mu}\left[\tau\, y T_x - \frac{1}{2}\,\tau'\, y^2\, T_y\right] = k\, T_{yy} \tag{7}$$

Equations of this type occur in other heat transfer problems[3, 4] where a reduction to the form of Eq. (6) is made.

Let

$$\eta = y\sqrt{\tau(x)}, \qquad \xi = \mu\int_0^x \sqrt{\tau(\alpha)}\, d\alpha$$

Then Eq. (7) becomes

$$\rho\, C_p \eta T_\xi = k\, T_{\eta\eta} \tag{8}$$

Since in Eq. (6) τ is considered constant, it is equivalent to Eq. (8). The form of the boundary conditions is not affected. As a result the solution obtained in reference 1 can be used with arbitrary τ (hence, pressure gradient) as well as temperature or heat flux at the wall.

Similar results have been derived in a different way by Lighthill[5] who notes that the approximation implied by Eq. (4) corresponds to flow of high Prandtl Number fluids.

* This work was done as part of a program on heat transfer in the Naval Supersonic Laboratory under Contract AF33(616)-2042 with WADC.

REFERENCES

[1] Tribus, M., and Klein, J., *Forced Convection from Nonisothermal Surfaces*, in *Heat Transfer Symposium*, University of Michigan Press, 1953.

[2] Schlichting, H., *Der Wärmeübergang an einer langsangeströmten ebenen Platte mit veränderlicher Wand temperatur*, Forsch. a.d. geb. des Ing., Vol. 17, pp. 1–8, 1951.

[3] Finston, M., *Thermal Effects in Calendering Viscous Fluids*, J. Appl. Mech., Vol. 18, p. 12, 1951.

[4] Carrier, G. F., and Lewis, J. A., *On Heat Transfer Problems in Viscous Flow*, Q. Appl. Math., Vol. VII, p. 450, 1950.

[5] Lighthill, M. J., *Contributions to the Theory of Heat Transfer Through a Laminar Boundary Layer*, Proc. Roy. Soc. London, A, Vol. 202, pp. 359–77, 1950.

Applicability of Piston Theory to the Flow Around Wings in Unsteady Motion

Erik Mollo-Christensen and Holt Ashley
Massachusetts Institute of Technology, Cambridge, Mass.
June 6, 1954

HEASLET AND LOMAX[1] have pointed out that the pressures on a body which suddenly starts moving in a compressible fluid depend, at the first instant, only upon the local normal velocities of the surface.

Other situations in which the gas suddenly is made aware of the existence of an obstruction, as for certain problems in hypersonic flow, have also been solved by considering locally planar waves emanating from the body.[2, 3, 4] The observation made in reference 1 can also be applied to rapidly oscillating bodies, considering the frequency of oscillation as the primary variable rather than the time-constant of the motion.

In this note, it is shown that such a simplification of the problem of finding the pressures on oscillating wings can be deduced directly from small disturbance considerations, and criteria for the applicability of the simplified theory can be obtained in the process. The general expression for the pressures on an oscil-

TABLE 1

Exact and Approximate Force and Moment

Functions for the Oscillating Supersonic Airfoil (M = 2.5)

$1/k$	L_1	L_{1_p}	L_2	L_{2_p}	L_3'	L_{3_p}'	L_4'	L_{4_p}'
	0	0	0	0	0	0	0	0
0.119	0.0003	0	0.0473	0.0476	0.0057	0.0057	0.0476	0.0476
0.238	0.0008	0	0.0950	0.0952	0.0227	0.0226	0.0952	0.0952
0.476	-0.0100	0	0.1903	0.1904	0.0908	0.0906	0.1886	0.1904
0.496	-0.0108	0	0.1967	0.1984	0.0985	0.0984	0.1963	0.1984
0.992	0.0241	0	0.3755	0.3968	0.4019	0.3936	0.3742	0.3968
1.253	0.0411	0	0.4908	0.5012	0.6526	0.6280	0.4638	0.5012
1.701	0.0580	0	0.6938	0.6804	1.2250	1.1574	0.6178	0.6804
1.984	-0.0641	0	0.8224	0.7936	1.6793	1.5747	0.7160	0.7936
2.480	0.0706	0	1.0458	0.9920	2.6441	2.4601	0.8886	0.9920
$1/k$	M_1'	M_{1_p}'	M_2'	M_{2_p}'	M_3'	M_{3_p}'	M_4'	M_{4_p}'
	0	0	0	0	0	0	0	0
0.119	0.0006	0	0.0478	0.0476	0.0057	0.0057	0.0635	0.0635
0.238	0.0016	0	0.0953	0.0952	0.0227	0.0226	0.1273	0.1269
0.476	-0.0200	0	0.1978	0.1904	0.0898	0.0906	0.2537	0.2539
0.496	-0.0225	0	0.2025	0.1984	0.0972	0.0984	0.2643	0.2645
0.992	0.0188	0	0.3530	0.3968	0.3904	0.3936	0.5043	0.5291
1.253	0.0447	0	0.4663	0.5012	0.6379	0.6280	0.6235	0.6683
1.701	0.710	0	0.6712	0.6804	1.2074	1.1574	0.8281	0.9072
1.984	0.0806	0	0.8016	0.7936	1.6607	1.5745	0.9585	1.058
2.480	0.0908	0	1.0281	0.9920	2.6244	2.4601	1.1880	1.3227

lating wing is developed, and the results of sample calculations are compared to results of more exact theory. Lin, Reissner, and Tsien[5] have laid the systematic foundations for treatment of unsteady flow over slender bodies. Extending their considerations to flow over wings of finite aspect ratio, one finds that when the following conditions are satisfied:[7]

$$k = \frac{\omega b}{U} >> 1;\ k\delta M_1 << 1;\ 1/k = 0(M_1) \tag{1}$$

the equation for the perturbation velocity potential reduces to:

$$M_1^2 \frac{\partial^2 \varphi}{\partial t^2} = \nabla^2 \varphi \tag{2}$$

where:

M_1 = Mach Number at infinity ahead of the wing
ω = wing oscillation frequency
b = half-chord of wing
U = velocity infinitely far ahead of the wing (in positive x-direction)
k = reduced frequency
δ = ratio of thickness or amplitude of wing to maximum chord
$\nabla\varphi = (\vec{q} - \vec{U})/U$; $\vec{q}$ = gas velocity
t, x, y, z = appropriately nondimensionalized time and space coordinates.

The boundary condition to be satisfied on the wing plan form is:

$$\left(\frac{\partial \varphi}{\partial z}\right)_{z=0} = ikh(x, y)e^{ikt} \tag{3}$$

$h(x, y)$ being the dimensionless amplitude of wing oscillation. The pressure coefficient takes on the form:

$$C_p = -2(\partial\varphi/\partial t) \tag{4}$$

It can be shown that the order of magnitude of the terms in Eq. (2) are as follows:

$$\left.\begin{aligned} &\frac{\partial^2 \varphi}{\partial t^2} : 1 \\ &\frac{1}{M_1^2}\frac{\partial^2 \varphi}{\partial x^2} : 1/M_1^2k^2 \\ &\frac{1}{M_1^2}\frac{\partial^2 \varphi}{\partial y^2} : 1/M_1^2 \mathcal{R}^2 k^2 \\ &\frac{\partial^2 \varphi}{\partial z^2} : 1 \end{aligned}\right\} \tag{5}$$

The derivatives with respect to x and y can therefore be neglected when the additional conditions:

$$M_1^2 k^2 >> 1 \quad \text{and} \quad M_1^2 k^2 \mathcal{R}^2 >> 1 \tag{6}$$

are satisfied. These requirements simply state that the wave length of the acoustic waves emanating from the wing must be small compared to all dimensions of the wing plan form. The equation then takes on the form:

$$M_1^2 \frac{\partial^2 \varphi}{\partial t^2} = \frac{\partial^2 \varphi}{\partial z^2} \tag{7}$$

with the boundary condition and the pressure coefficient given by Eq. (3) and Eq. (4), respectively.

An integral of Eq. (7) satisfying the boundary conditions can be written down immediately for $z \geq 0$:

$$\varphi(x, y, z, t) = -\frac{h(x, y)}{M_1} e^{ik(t - M_1 z)} \tag{8}$$

The pressure coefficient is found to be:

$$C_p = \frac{2ikh(x, y)e^{ik(t - M_1 z)}}{M_1} \tag{9}$$

The corresponding expressions for arbitrary unsteady motion of the wing at points on the surface are

$$\varphi(x, y, 0, t) = -h(x, y)e^{ikt}/M_1 \tag{10}$$

$$C_p = 2ikh(x, y)e^{ikt}/M_1 \tag{11}$$

The pressure difference between tip and bottom of the wing is twice this amount for the lifting case. Eq. (9) can be integrated to yield lift and moments.

Calculations have been carried out and checked against the two-dimensional theory of reference 6. Table 1 shows the results at a typical supersonic Mach Number. The nomenclature is that of Garrick and Rubinow,[6] and subscript p refers to values obtained from the present simplified "piston theory." As might be expected, "piston theory" proves more accurate the higher the Mach Number, but the order of accuracy shown in the table persists down to $M_1 = 10/7$ for $k > 2$. In view of the remarkable simplicity of these calculations compared with more exact theory (especially for oscillating finite wings in supersonic flow), the possibility of using them for applications like flutter analysis deserves careful consideration. Occasionally flutter speeds are very sensitive to small charges in the phase angle of an aerodynamic quantity, like $(M_1' + iM_2')$, so that care must be exercised in interpreting such applications.

References

[1] Heaslet, M. A., and Lomax, H., *Two-Dimensional Unsteady Lift Problems in Supersonic Flight*, NACA Report No. 945, 1949.

[2] Goldsworthy, F. A., *Two-Dimensional Rotational Flow at High Mach Number Past Thin Airfoils*, Quarterly Journ. Mech. and Applied Math., Vol. 5, pp. 54–63, 1952.

[3] Lighthill, M. J., *Oscillating Airfoils at High Mach Number*, Journal of the Aeronautical Sciences, Vol. 20, No. 6, pp. 402–407, 1953.

[4] Hayes, W. D., *On Hypersonic Similitude*, Quarterly Appl. Math., Vol. 5, pp. 105–106, 1947.

[6] Lin, C. C., Reissner, E., Tsien, H. S., *On Two-Dimensional Nonsteady Motion of a Slender Body in a Compressible Fluid*, Journ. Math. and Phys., Vol. XXVII, No. 3, pp. 220–231, October, 1948.

[8] Garrick, I. E., and Rubinow, S. I., *Flutter and Oscillating Air-Force Calculations For an Airfoil in Two-Dimensional Supersonic Flow*, NACA TN No. 1158, 1946.

[†] In correspondence, Prof. J. W. Miles points out he has obtained results similar to Eqs. (1)–(4).

On the Nonsteady Climb of Turbojet Aircraft

Angelo Miele
Research Assistant Professor of Aeronautical Engineering, Polytechnic Institute of Brooklyn, Brooklyn, N.Y.
June 10, 1954

Symbols

a = speed of sound (fps)
C_{D0} = drag coefficient at zero lift
$C_{L*} = \sqrt{\pi\lambda e C_{D0}}$ = lift coefficient for maximum lift/drag ratio
D = drag (lb)
e = airplane efficiency factor
$E_{max.} = \sqrt{\frac{\pi\lambda e}{4C_{D0}}}$ = maximum lift/drag ratio
g = acceleration of gravity = 32.174 ft/sec²
h = height (ft)
h_* = altitude of the tropopause = 35,332 ft
$h_e = h + V^2/2g$ = energy height (ft)
M_c = Mach Number for best climb
M_{cs} = Mach Number for best climb determined from the equations of a steady flight
$M_e = \frac{1}{a}\sqrt{\frac{2W}{C_{L*}\rho S}}$ = Mach Number for level flight with maximum lift/drag ratio
R = air constant ≅ 1717 ft²/sec² °R
S = wing surface (ft²)
T = thrust (lb)
T_0 = thrust at sea level (lb)
T_* = thrust at the tropopause (lb)
V = velocity (fps)
V_c = velocity for best climb (fps)
V_{cs} = velocity for best climb determined from the equations of a steady flight (fps)
V_e = velocity corresponding to level flight with maximum lift/drag ratio (fps)
W = weight of the aircraft (lb)
$x = \frac{W}{TE_{max.}}$ = ratio of minimum drag of level flight to thrust
Γ = ratio of speed for best climb determined from the equations of a nonsteady flight (V_c) to the speed for best climb determined from the equations of a steady flight (V_{cs})
α = derivative of the temperature of the air with respect to the altitude (−0.003566°R/ft for troposphere; 0°R/ft for stratosphere)
γ = ratio of specific heat at constant pressure to specific heat at constant volume = 1.4 for air
λ = aspect ratio
σ = relative density of the air
σ_* = relative density of the air at the tropopause
ρ = absolute density of the air (lb sec² ft⁻⁴)

Discussion

Considerable attention has been devoted in recent years to the study of the problems associated with the nonstationary climb of high-speed aircraft. Some of the minimal problems investigated are the following:

(1) The determination of the speed-height relationship $V = V(h)$ which minimizes the time necessary to fly an aircraft from a given combination of speed and altitude (V_1, h_1) to another combination of speed and altitude (V_2, h_2).

(2) The determination of the speed-energy height relationship $V = V(h_e)$ which minimizes the time necessary to fly an aircraft from a given energy height level (h_{e1}) to another energy height level (h_{e2}), with free choice of the terminal velocities, V_1, V_2.

According to the terminology of the Calculus of Variations the first problem is a fixed end-points problem, while the second one, of lesser practical importance, is a free boundary value problem. Mathematically analogous problems may be formulated for the climbing flight with minimum fuel consumption and for the steepest climb.

The writer[1] analyzed the fixed end-points problem by using a transformation based on Green's theorem. This approach essentially avoided the difficulties inherent to the use of direct or indirect variational methods. Both problems of absolute optima and conditioned optima were handled in this way. In England K. J. Lush,[2] following a previous study by Kaiser,[3] treated the same fixed end-points problem with a graphic-analytic method based on the concept of energy height (h_e). He also analyzed the free boundary value problem. Later the writer[4, 5] generalized his previous solution to the climbing flight of minimum fuel consumption, to the steepest climb and to some special type of nonsteady gliding flight. Additional contributions to the same category of problems were developed by Kelly[6] and more recently by Rutowski[7] and Garbell.[8]

The following hypotheses are used: the small angle between the vectors thrust and velocity is neglected; the weight of the aircraft is assumed constant; the curvatures and the squares of the path inclination are considered negligible with regard to their effect on that part of the drag depending on the lift; the thrust is assumed a function $T = T(V, h)$ of the velocity and altitude only; the aerodynamic lag is disregarded; only flight paths contained in a vertical plane are considered.

The distribution of velocities $V = V(h)$ which, under the aforementioned assumptions, minimizes the time integral in the fixed end-points problem is composed of three branches.[1, 2, 4] Two of them, the initial and the final branches, depend on the boundary conditions of the problem.[1] The third one, the central branch, is independent of the b.c., being defined[1] by:

$$\left[\frac{\partial}{\partial V}\left(\frac{TV - DV}{W}\right)\right]_h = \frac{V}{g}\left[\frac{\partial}{\partial h}\left(\frac{TV - DV}{W}\right)\right]_V \qquad (1)$$

With a transformation of coordinates from the (V, h) plane to the (V, h_e) plane, Eq. (1) may be shown equivalent[2] to

$$\left[\frac{\partial}{\partial V}\left(\frac{TV - DV}{W}\right)\right]_{he} = 0 \qquad (2)$$

For the free boundary value problem the distribution of velocities $V = V(h_e)$ minimizing the time integral is composed by a unique branch defined by Eqs. (1) or (2).

Due to the lack of simple analytical expressions for the thrust and for the drag, a general solution of Eqs. (1) or (2) has not yet been found. Graphical methods[7, 8] are to be employed for each particular aircraft, above all when compressibility effects are of importance, as is the case for turbo-jet aircraft at the altitudes in the neighborhood of the ceiling.

On the contrary a rather simple solution, of use for preliminary design calculations, may be obtained if the following engineering assumptions are accepted for the thrust and the drag:

(1) The thrust is assumed to depend only on the altitude according to the following relationship:

$$T = K\sigma^r \qquad (3)$$

where

$K = T_0$, $r = 0.75$ for tropospheric flight
$K = \frac{T_*}{\sigma_*}$, $r = 1$ for stratospheric flight

(2) The polar of the aircraft is supposed parabolic with constant coefficients C_{D0}, e. This assumption leads to the following expression for the aerodynamic drag:

$$D = \frac{1}{2}C_{D0}\rho SV^2 + \frac{2W^2}{\pi\lambda e\rho SV^2} \qquad (4)$$

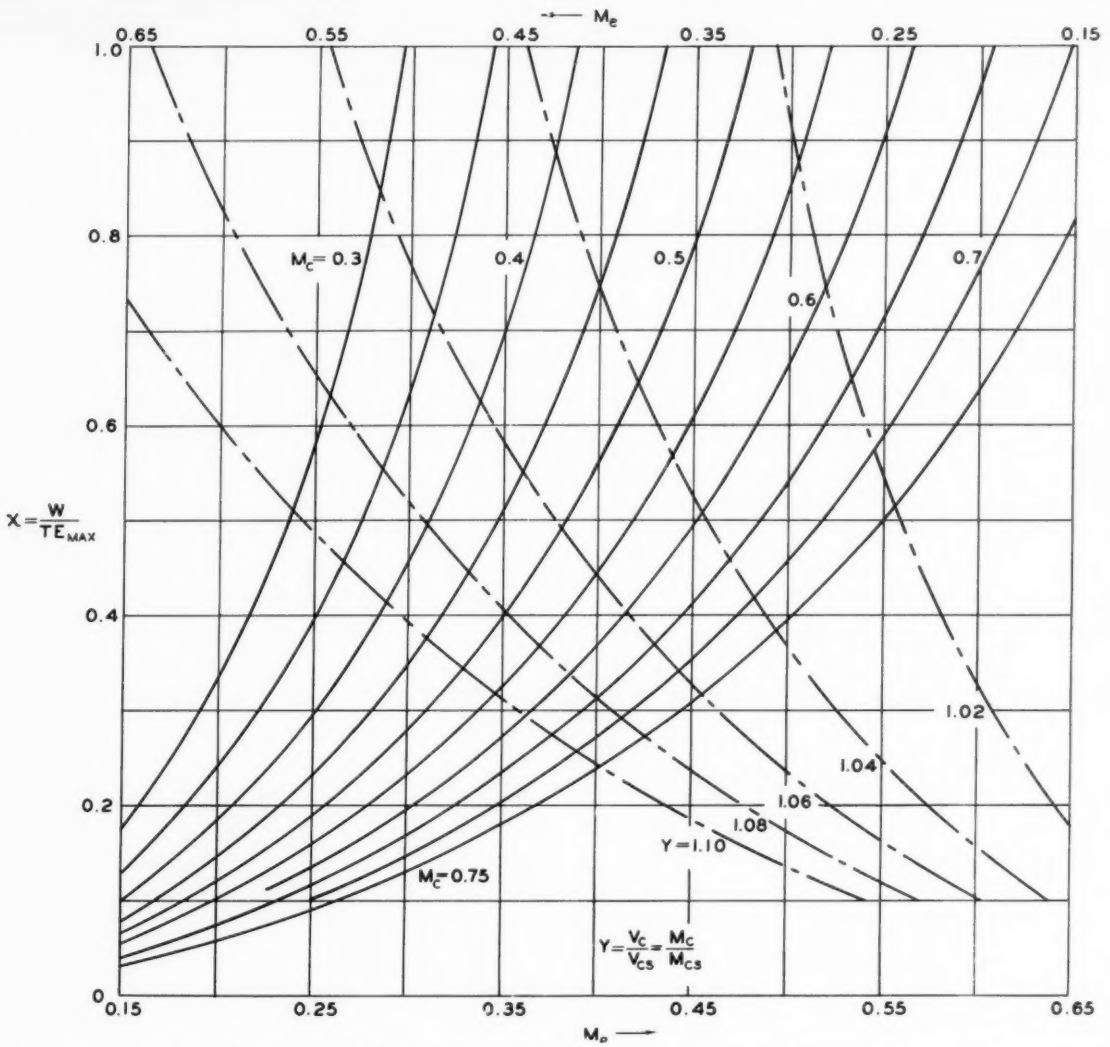

FIG. 1. Mach Number (M_c) for best climb (troposphere). Use the lower M_e scale to determine $M_c = f(x, M_e)$. Use the upper M_e scale to determine $Y = f(x, M_e)$.

From Eqs. (1), (3), (4) and from the Equations of the standard atmosphere, the speed for best climb (V_c) can now be calculated. Results may be expressed in the following simple nondimensional form by introducing the Mach Number (M_c) in place of the velocity as a variable and by using the parameters x, M_e already defined in the list of symbols:

$$M_c^6 + A M_c^4 + B M_c^2 + C = 0 \qquad (5)$$

where:

$$\left.\begin{aligned} A &= \frac{3}{\gamma m} - 2r\frac{M_e^2}{x} \\ B &= -\frac{2}{\gamma m}\frac{M_e^2}{x} - M_e^4 \\ C &= -\frac{M_e^4}{\gamma m} \\ m &= 1 + \frac{\alpha R}{g} \end{aligned}\right\} \qquad (6)$$

Eq. (5) is a cubic equation in M_c^2, which may be analytically solved with Cardano's formula or with equivalent trigonometric expressions. The coefficients B and C are always negative. For Δ(discriminant) ≤ 0 Eq. (5) has two real negative roots and one real positive root. For $\Delta > 0$ Eq. (5) has two complex conjugate roots and one real positive root. The only positive real root of Eq. (5) has been calculated and plotted in graphs 1 and 2 which enable one to carry out a rapid calculation of the optimum climbing program.

The Mach Number for best climb (M_c) depends on two parameters only: the ratio of minimum drag to thrust (x) and the Mach Number for level flight with maximum lift/drag ratio (M_e). These two parameters are fundamental in the study of the mechanics of flight of jet-propelled aircraft, since they embody the effects associated with the shape of the aircraft (C_{DO}, λ, e), the wing loading (W/S), the specific thrust (T/W), and the properties of the atmosphere in which the aircraft is flying (a, ρ).

It is of interest to compare the actual results with those previously derived from the old quasi-uniform analysis of the climbing flight. In the quasi-steady approach the speed (V_{cs}) for best climb is defined by:

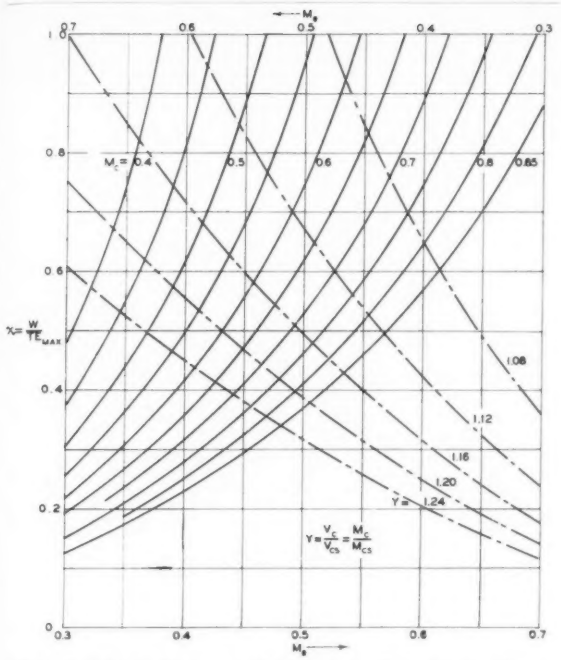

FIG. 2. Mach Number (M_c) for best climb (stratosphere.) Use the lower M_e scale to determine $M_c = f(x, M_e)$. Use the upper M_e scale to determine $Y = f(x, M_e)$.

$$\left[\frac{\partial}{\partial V}\left(\frac{TV - DV}{W}\right)\right]_h = 0 \tag{7}$$

For a parabolic polar and for $(\partial T/\partial V)_h = 0$ the velocity (V_{cs}) or the Mach Number (M_{cs}) solving Eq. (7) is given by

$$\frac{V_{cs}}{V_e} = \frac{M_{cs}}{M_e} = \sqrt{\frac{1 + \sqrt{1 + 3x^2}}{3x}} \tag{8}$$

M_{cs} being a function of x, M_e and M_c being a function of x, M_e it follows that the ratio $Y = (M_c/M_{cs}) = (V_c/V_{cs})$ is also a function of x, M_e. The function $Y = f(x, M_e)$ has been plotted in the graphs 1 and 2, which show that the speed for best climb determined with the actual nonsteady analysis is higher than the one determined with the old quasi-steady treatment. The relative difference $(V_c - V_{cs})/V_{cs}$ increases with the altitude up to about 8–10% for tropospheric flight (Fig. 1) and 16–20% for stratospheric flight (Fig. 2).

For a practical use of the present results the following remarks are of interest:

(1) At $h = h_*$ (tropopause) there are two velocities solving Eq. (1). One ($V_{c\ trop}$) is the terminal velocity of the tropospheric flight, the other one ($V_{c\ strat}$) is the initial velocity of the stratospheric flight. In Ref. 4 it was shown that following the tropospheric climb and preceding the stratospheric climb, the aircraft is to be accelerated at $h = h_*$ from $V_{c\ trop}$ to $V_{c\ strat}$ in order to achieve the optimum climb performance.

(2) The solution of Eq. (1) is much more sensitive to the *local* value of the thrust (T) than to its derivative (dT/dh) with respect to the altitude. Therefore, even if for a given turbo-jet engine the exponent r of Eq. (3) is different from the assumed value $r = 0.75$, graphs (1) and (2) may still be used with good approximation, provided the parameter $x = (W/TE_{max.})$ be determined on the basis of the effective thrust T at altitude from the graphs supplied by the turbo-jet maker.

(3) Results are to be handled with caution at high subsonic speeds, because the hypotheses $\partial C_{D0}/\partial M = 0$, $\partial e/\partial M = 0$ are no longer satisfied. When compressibility effects are of engineering importance graphical methods of solution of Eqs. (1) or (2) are to be preferred to the present one.

(4) For small values of $(\partial T/\partial V)_h$ the variability of the thrust with the velocity may be approximately accounted for by determining the parameter $x = W/TE_{max.}$ and the optimum velocity V_c (Eq. 5 or graphs 1 and 2) with trial and error method. When, on the contrary, the thrust is a rapidly varying function of the velocity, graphical methods of solution of Eqs. (1) or (2) are to be preferred to the present approach which neglects the terms containing $(\partial T/\partial V)_h$ in the equation defining the optimum speed.

REFERENCES

[1] Miele, A., *Problemi di Minimo Tempo nel Volo Non-Stazionario degli Aeroplani*, Atti della Accademia delle Scienze di Torino, Classe di Scienze Fisiche, Matematiche e Naturali, Vol. 85, pp. 41–52, 1950–1951.

[2] Lush, K. J., *A Review of the Problem of Choosing a Climb Technique, with Proposals for a New Climb Technique for High Performance Aircraft*, Aeronautical Research Council, R.M. 2557, 1951.

[3] Kaiser, *The Climb of Jet-Propelled Aircraft. Part I—Speed Along the Path in Optimum Climb*, Ministry of Supply, RTP/TIB Translation GDC/15/148T (April, 1944).

[4] Miele, A., *Soluzioni Generali di Problemi di Ottimo in Volo Non-Stazionario*, L'Aerotecnica, Vol. 32, No. 3, pp. 135–142, 1952.

[5] Miele, A., *Traiettorie Ottime di Volo degli Aeroplani Azionati da Turboreattori*, L'Aerotecnica, Vol. 32, No. 4, pp. 206–219, 1952.

[6] Kelly, L., *Optimum Climb Technique for a Jet-Propelled Aircraft*, The College of Aeronautics, Cranfield, Report No. 57, April, 1952.

[7] Rutowski, E. S., *Energy Approach to the General Aircraft Performance Problem*, Journal of the Aeronautical Sciences, Vol. 21, No. 3, pp. 187–195, March, 1954.

[8] Garbell, M. A., *Optimum Climbing Techniques for High-Performance Aircraft*, Garbell Aeronautical Series, No. 8, 1953.

Lift Distribution on Supersonic Wings with Subsonic Leading Edges and Arbitrary Angle of Attack Distribution*

Bernard Etkin and Frank A. Woodward

Associate Professor of Aeronautical Engineering, University of Toronto, and Aerodynamicist, A. V. Roe (Canada) Ltd., Respectively

June 14, 1954

THE INTEGRAL EQUATION for the perturbation velocity potential φ which satisfies the condition of tangential flow at a point Q on the surface of a wing is given by Evvard.[1]

* A complete discussion of this method will be published soon in the "Proceedings of the Second Canadian Symposium on Aerodynamics," published by the Institute of Aerophysics, University of Toronto.

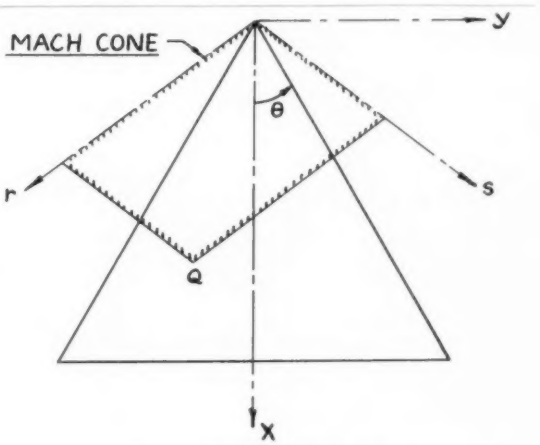

FIG. 1. Field of integration.

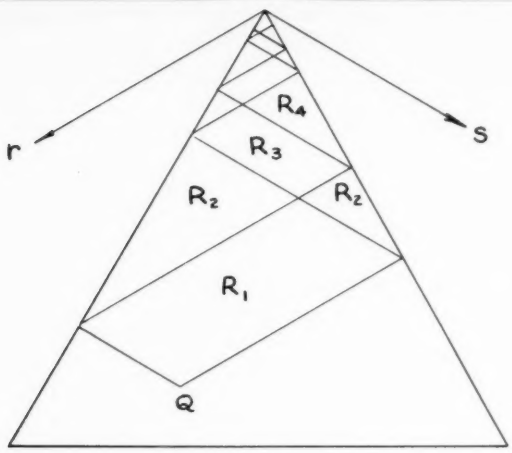

FIG. 2.

$$\varphi_Q = -\frac{1}{M_0\pi}\int\int_{S_w}\frac{w\,dr\,ds}{\sqrt{(r_Q - r)(s_Q - s)}} \qquad (1)$$

The region of integration is indicated in Fig. 1. If the forward running Mach lines from Q are reflected off the wing leading edges, as shown in Fig. 2, the wing surface is divided into a series of oblique rectangular regions, which are denoted by R_1, R_2, R_3, etc. The contribution to the potential at Q due to three of these regions is calculated by means of Eq. (1) and a knowledge

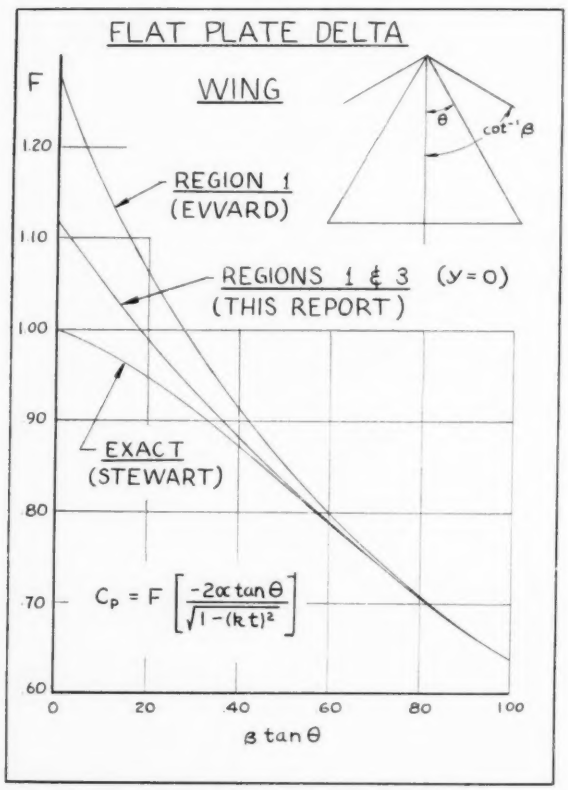

FIG. 3. Comparison of approximate and exact solutions for a flat delta wing.

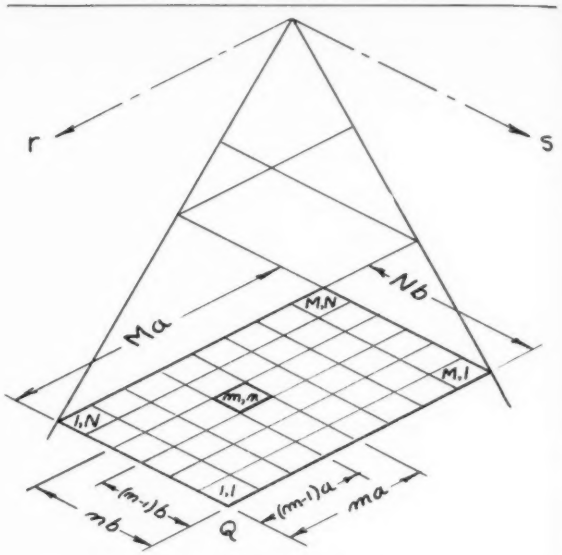

FIG. 4. Subdivision of region 1.

of the strength of the upwash field between the Mach cone and the leading edge of the wing (see Eqs. 38 and 39 of reference 1) to obtain

$$d\varphi_1 = \frac{U\alpha(r, s)\,dr\,ds}{M_0\pi\sqrt{(r_Q - r)(s_Q - s)}} \qquad (2)$$

$$d\varphi_2 = 0 \qquad (3)$$

$$d\varphi_3 = -d\varphi_1 \qquad (4)$$

Thus, the integral equation for φ at Q may be written

$$\varphi_Q = \int_{R_1} d\varphi_1 + \int_{R_2} d\varphi_2 + \int_{R_3} d\varphi_3 + \ldots \qquad (5)$$

The magnitude of the terms in this series decreases rapidly due to the presence of the radical in the denominators, and to the decreasing size of the more remote regions.

The approximation made by Evvard[2] in connection with yawed wings was to retain only the first term of the series. This gives

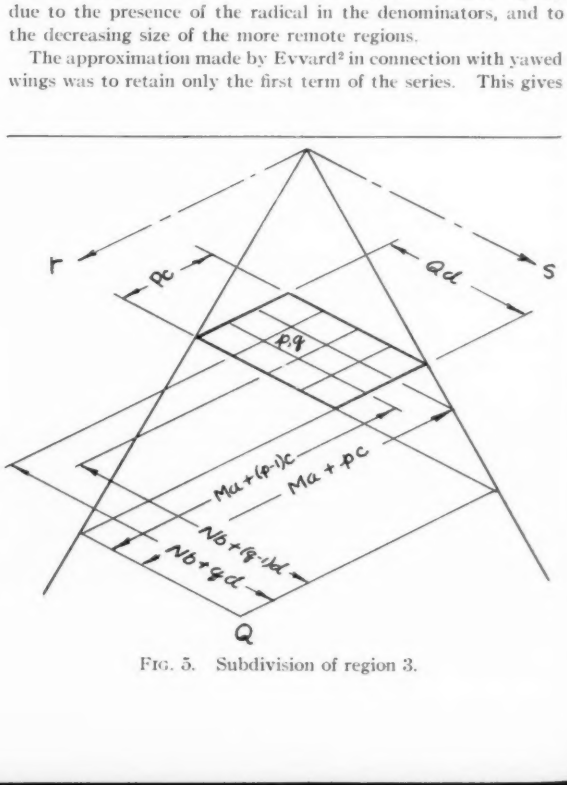

FIG. 5. Subdivision of region 3.

good results over a useful range of the parameters, but is considerably in error for highly swept wings, or for wings at low supersonic speeds. The second approximation, in which the integration is carried out over both Regions 1 and 3 is shown to give a significant improvement to the results for flat delta wings at small values of the parameter $\beta \tan \theta$, as is illustrated in Fig. 3.

The method may be extended to wings with nonplanar surfaces by further subdividing the regions as indicated in Figs. 4 and 5. For example, Region 1 is subdivided into MN equal parallelograms of sides a, b; the size being such that the local angle of attack $\alpha_{m,n}$ may be considered constant in each. Integrating Eq. (2) over one of these small parallelograms

$$\Delta\varphi_Q = \frac{4U\alpha_{m,n}}{\pi M_0}\sqrt{ab}\,(\sqrt{m}-\sqrt{m-1})\,(\sqrt{n}-\sqrt{n-1}) \tag{6}$$

Noting that, for wings with straight subsonic leading edges,

$$a = \frac{M_0}{\beta M(1+k)}(x-\beta k y)$$

$$b = \frac{M_0}{\beta M(1+k)}(x+\beta k y)$$

where

$$k = \frac{1}{\beta\tan\theta},\ \beta = \sqrt{M_0^2-1}$$

and (x, y) are the coordinates of Q,

$$\Delta\phi_Q = \frac{4U\alpha_{m,n}}{\beta\pi(1+k)}\frac{\sqrt{m}-\sqrt{m-1}}{\sqrt{M}}\frac{\sqrt{n}-\sqrt{n-1}}{\sqrt{N}}\times\frac{1}{\sqrt{x^2-(\beta k)^2y^2}} \tag{7}$$

Summing over the entire Region 1,

$$\varphi_Q = \frac{4U}{\beta\pi(1+k)}\frac{1}{\sqrt{x^2-(\beta k)^2y^2}}S_{m,n} \tag{8}$$

where

$$S_{m,n} = \sum_{m=1}^{M}\sum_{n=1}^{N}\frac{(\sqrt{m}-\sqrt{m-1})\,(\sqrt{n}-\sqrt{n-1})}{\sqrt{NM}}\alpha_{m,n} \tag{9}$$

The pressure coefficient at Q due to Region 1 may now be calculated

$$C_{p_Q} = -\frac{2}{U}\frac{\partial\varphi}{\partial x} = -\frac{8}{\beta\pi(1+k)}\times\left[\frac{S_{m,n}}{\sqrt{1-(kt)^2}}+\sqrt{1-(kt)^2}\cdot x\cdot\frac{\partial S_{m,n}}{\partial x}\right] \tag{10}$$

where $t = (\beta y)/x$.

Similarly, the pressure coefficient at Q due to Region 3 is given by

$$C_{p_Q} = \frac{2(k-1)^2}{\beta\pi(1+k)^3}\times\left[\frac{S_{p+q}}{\sqrt{1-(kt)^2}}+\sqrt{1-(kt)^2}\cdot x\cdot\frac{\partial S_{p+q}}{\partial x}\right] \tag{11}$$

where

$$S_{p+q} = \frac{1}{PQ}\sum_{p=1}^{P}\sum_{q=1}^{Q}\times\frac{\alpha_{p+q}}{\sqrt{\left(1+\frac{1+kt}{1-kt}\frac{Kp}{P}\right)\left(1+\frac{1-kt}{1+kt}\frac{Kq}{Q}\right)}}$$

The method may equally well be applied to nonplanar wings with curved subsonic leading edges by laying out the regions on a planform drawing of the wing and measuring off the required quantities directly. The pressure coefficient is obtained by a final numerical differentiation of the potential so calculated.

In a practical computation of the pressure distribution over a cambered wing, a drawing of the wing planform is divided into Regions 1 and 3, and these regions further subdivided to give the required net. If the local angle of attack contours are plotted on the wing drawing, the angle of attack matrices $\alpha_{m,n}$, $\alpha_{p,q}$ may be read off directly. The summations $S_{m,n}$ and $S_{p,q}$ are then computed, differentiated numerically, and placed in formulas (8) and (11), respectively, to give the desired pressure coefficients. It has been found that for most problems very little error is introduced by using a coarse net, although M or N should not be less than 3.

References

[1] Evvard, J. C., *Use of Source Distributions for Evaluating Theoretical Aerodynamics of Thin Finite Wings at Supersonic Speeds*, NACA TR 951, 1950.

[2] Evvard, J. C., *The Effects of Yawing Thin Pointed Wings at Supersonic Speeds*, NACA TN 1429, 1947.

[3] Stewart, H. J., *The Lift of the Delta Wing at Supersonic Speeds*, Quarterly of Appl. Math., Vol. IV, No. 3, pp. 246-254, October, 1946.

Probe Interference in Measurements in Supersonic Laminar Boundary Layers*

M. V. Morkovin and W. S. Bradfield

Department of Aeronautics, The Johns Hopkins University, and Rosemount Research Center, The University of Minnesota, Respectively

June 15, 1954

RECENTLY, EFFECTS OF THE SIZE of the total-pressure probe used for measuring velocity and other profiles of supersonic laminar boundary layers received considerable attention—e.g., in references 1, 2, and 3. Inference of the existence and partial evaluation of these effects were based (a) on comparison of results from different size probes in references 1 and 2 and (b) on comparison of results with boundary-layer theory (which cannot account for the complicating leading-edge effects) in references 1, 2, and 3. The purpose of this note is to present direct visual evidence of strong interference near the wall and discuss its implications.

Briefly, local, three-dimensional separation under various probes (hot-wire and total pressure) was observed in the Johns Hopkins University tunnel over a flat plate at $M = 1.72$ by the light-oil lamp-black technique. These observations were repeated and carefully documented for even the smallest practical total pressure probes[5] at the University of Minnesota at $M =$

* Work partially supported by the Office of Naval Research, USN, and by the Office of Scientific Research, USAF.

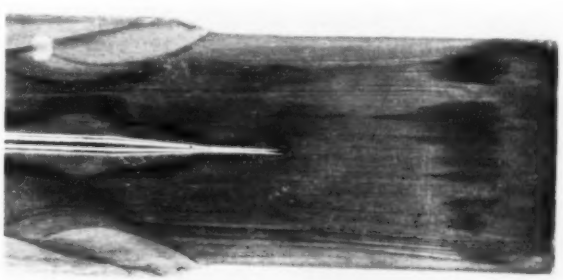

FIG. 1. Pattern for probe tip 4 mils above flat plate.

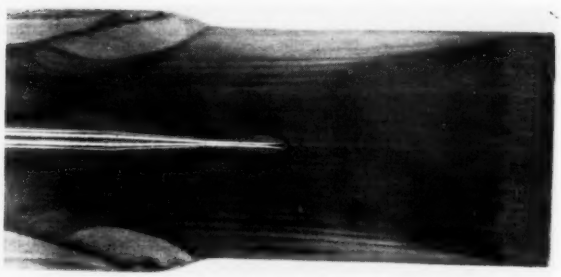

FIG. 2. Pattern for probe tip 7 mils above flat plate.

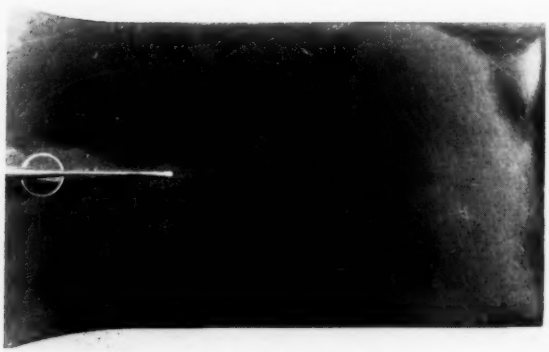

FIG. 3. Probe without background pattern.

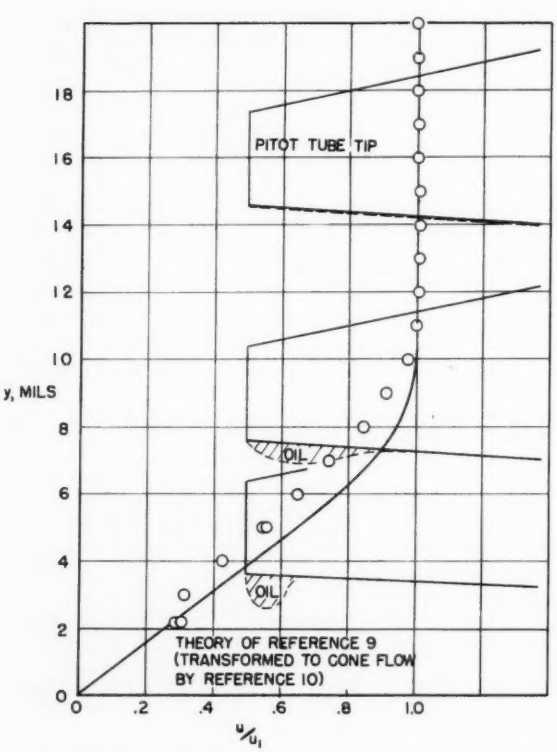

FIG. 4. Velocity profile inferred from pitot readings and oil film behavior at positions 5, 9, and 16 mils above cone surface.

3.05 with the aid of a short focus schlieren system and the china-film technique.[6] Fig. 1 gives the top view of the probe and the pattern when the center of the probe, 0.003 in. high and 0.020 in. wide (see photomicrograph in reference 3), was 0.004 in. above the plate as determined by a 20× microscope during running. In Fig. 2, the distance from wall is 0.007 in. and Fig. 3 shows the probe without the background pattern. Visual observations during running, accompanied by vertical and horizontal motion of the probes identify the "island" pattern as one of local three-dimensional separation with back flow immediately under the probe, extending upstream of the probe tip. The boundary-layer thickness in these cases was 0.025 in. and the Reynolds Number based on distance from the leading edge was 0.97×10^6. Fig. 4 displays the velocity profile of a thinner boundary layer measured with the same probe on a cone at $M = 3.05$ and diagrams illustrating the behavior of a thin oil film on the underside of the pitot tube. As the probe approached the surface the oil film initially distributed as shown in the top sketch began to collect, toward the leading edge of the under surface of the tube as shown, indicating reverse flow at the probe as well.

In case of larger probes upstream separation tends to persist even for positions of the probe nearer the edge of the boundary layer. From similar experiences with hot-wire probes one can surmise that the velocity profiles from the thinner layers near a leading edge reported in reference 3 as "*transitional*" (p. 8) and in reference 4 were actually obtained in a *laminar* layer with the extent of separation varying as the vertical position of the probe was changed. Even such more extensive separation is difficult to observe with schlieren systems because its lateral extent is small in comparison with the width of the plate. This is probably the reason why this effect has not been reported heretofore.

It has thus been demonstrated that when a probe of given height h is located at a distance from the wall of the order of h, a strong interference including local separation and back flow occurs. This finding supports the disregard of pitot tube data near the wall as practiced in references 1 and 2. Pitot tube data may still be subject to error when such separation does not occur or occurs downstream of the probe tip. Lighthill's discussion of viscous two-dimensional upstream influence without separation[7] can perhaps be used as a guide keeping in mind, (a) that three-dimensional effects should be milder, (b) that the pressure disturbances in front of the probes correspond to large x and y gradients to which boundary layer theory is not strictly applicable. Lighthill's upstream influence dies down exponentially, extending a distance comparable to ten boundary-layer thicknesses, depending upon Reynolds Number and Mach Number. Even if the effect were considerably decreased by the three-dimensional relieving action, some thickening of the layer with consequent oblique pressure waves in the supersonic part of the boundary layer should result. Thus, apart from the corresponding distortion of the layer the assumption of constant static pressure throughout, used in transforming the pitot data into velocity and mass flux information, is affected.

Fig. 4 of reference 2 and Fig. 22 of reference 1 show an apparent "overshoot" of momentum flux and velocity above the free stream values for the relatively larger (0.008 in.) probes even when *completely outside of the boundary layer* ($\delta \approx 0.04$ in.). (A similar observation was made in reference 4.) Since (a) this effect is not noticeable for the smallest probes in the same boundary layer and since (b) it vanishes as the larger probe moves still further away from the wall, the effect must be ascribed to upstream influence through the boundary layer. The pressure waves previously mentioned and the consequent small decrease in local free stream Mach Number would account for the higher pitot reading and the fictitious velocity overshoot. Using the Rayleigh formula, one can show that the error in indicated Mach Number, ΔM_1, is related to the rise in static pressure, Δp_1, in front of the pitot mouth by the formula:

$$\Delta M_1 = \frac{\Delta p_1}{p_1} \frac{(M_1^2 - 1)^2}{\gamma M_1 (2M_1^2 - 1)}$$

a similar formula in terms of the pitot tube reading shows that the overshoots indicated in Fig. 4 of reference 2 could be explained by a 1–5 per cent rise in static pressure p_1, in front of the pitot mouth. The preceding conjecture as well as the general upstream effect can be checked by taking *simultaneous* readings of pitot pressure at each y position and of static pressure from wall orifices under and slightly upstream of the pitot tip.

If there is a demonstrable effect of upstream influence when a relatively large probe is outside of the layer, it would follow that similar or even larger effects could occur throughout the boundary layer and that some effect should be present for smaller probes. The presence of this effect and that due to the leading edge makes the near agreement with theory (which takes account of neither) in references 1, 2, and 3 the more remarkable.

The question remains as to the non-dimensional parameters properly characterizing the above interference, with or without separation. Clearly, the probe height h has to be non-dimensionalized with respect to some characteristic layer thickness in order to account for the observed effect of "relative size." Just how this should be accomplished is not clear since it involves questions of pressure disturbance strength as function of y and the upstream viscous influence. The width of the probe must be significant since its increase means closer approach to the observed two-dimensional critical pressure disturbance for separation,

$$\Delta p_{cr} = 4\ \rho_\infty\ V_\infty{}^2\ R_x{}^{-0.4}$$

(or equivalent), which is readily transgressed. Cases have been observed where tendency to local separation near the probe was reinforced by pressure disturbances from the bulkier supports of the probe as much as 30 boundary layers downstream from the tip. Such spurious effects would, of course, spoil correlation of data based on tip size alone.

The framework of Lighthill's work indicates dependence on Reynolds Number R_x, Mach Number M, and wall-to-free-stream temperature ratio T_w/T_1; for instance, the upstream distance, s, through which a given (linearized) pressure disturbance at wall diminishes by a factor e^{-1}, measured with boundary layer thickness as a unit, depends on the parameters approximately as follows:

$$s = \frac{1.3}{\sqrt{M_1^2 - 1}} \frac{T_w}{T_1} R_x{}^{1/6} s^{-1/3} - \frac{M_1^2 + 2}{2\sqrt{M_1^2 - 1}} \left(\frac{T_w}{T_1}\right)^{0.7}$$

There does not appear to be data over a sufficient range of Mach and Reynolds Numbers to validate the simpler correlations attempted so far.

In the case of turbulent boundary layers the relative size of probes to boundary layer thickness is usually small Furthermore, the upstream influence, in units of boundary layer thickness, is also known to be very much smaller. Still, the effect of the sharp pressure gradients generated by probes in supersonic layers is likely to alter the simple field postulated in evaluation of the readings. Velocity profiles obtained from probes of different sizes in reference 8 indicate that there is a significant effect of size for probe-diameter to layer-thickness ratio larger than 1/20 at $M = 2$. If data for velocity ratios (u/V_∞) less than 0.6 were available, the range of discrepancies might be found more severe.

References

[1] Blue, R. E., and Low, G. M., *Factors Affecting Laminar Boundary Layer Measurements in a Supersonic Stream*, NACA Tech. Note No. 2891, February, 1953.

[2] Bradfield, W. S., DeCoursin, D. C., and Blumer, C. B., *The Effect of Leading Edge Bluntness on a Laminar Supersonic Boundary Layer*, Journal of the Aeronautical Sciences, Vol. 21, No. 6, p. 373, June, 1954.

[3] O'Donnell, R. M., *Experimental Investigation at a Mach Number of 2.41 of Average Skin-Friction Coefficient and Velocity Profiles for Laminar and Turbulent Boundary Layers and an Assessment of Probe Effects*, NACA Tech. Note No. 3122, January, 1954.

[4] Brinich, P. F., and Diaconis, N. S., *Boundary-Layer Development and Skin-Friction at Mach Number 3.05*, NACA Tech. Note No. 2742, July, 1952.

[5] Bradfield, W. S., and Yale, G. E., *Small Pitot Tubes with Fast Pressure Response Time*, Journal of the Aeronautical Sciences, Vol. 18, No. 10, p. 697, October, 1951.

[6] Murphy, J. S., and Phinney, R. E., *Visualization of Boundary Layer Flow*, Journal of the Aeronautical Sciences, Vol. 18, No. 11, p. 771, November, 1951.

[7] Lighthill, M. J., *On Boundary Layers and Upstream Influence II. Supersonic Flows Without Separation*, Proc. Roy. Soc. A, Vol. 217, p. 478, 1953.

[8] Wilson, R. E., and Young, E. C., *Aerodynamic Interference of Pitot Tubes in a Turbulent Boundary Layer at Supersonic Speeds*, Univ. of Texas, Defense Res. Lab., Rept. No. 228, December, 1949.

[9] Chapman, D. R., and Rubesin, M. W., *Temperature and Velocity Profiles in the Compressible Laminar Boundary Layer with Arbitrary Distribution of Surface Temperature*, Journal of the Aeronautical Sciences, Vol. 16, No. 9, p. 547, September, 1949.

[10] Hantzsche, W., and Wendt, H., *The Laminar Boundary Layer on a Cone in a Supersonic Air Stream at Zero Angle of Attack*, Jahrbuch 1941 der Deutschen Luftfahrtförschung. Also available as Translation No. RAT-6, Project RAND, November, 1947.

Electrical Resistance Networks for Beam and Column Problems

R. H. Scanlan

Centre National de la Recherche Scientifique, Châtillon-sous-Bagneux, Seine, France

June 21, 1954

Malavard and Boscher, in a series of condensed notes,[1–3] have exhibited the essential characteristics of a useful all-resistance electrical network which represents various two-dimensional fields. The fields may represent the potentials for stress or fluid flow or, for example, the deflection pattern of a plate or membrane. Their basic idea will first be briefly described here.

Consider two two-dimensional all-resistance networks I and II superposed and tied together at their nodes by other resistances (Fig. 1). Let us permit the entrance of outside currents from a source at potential U through still other resistances ($\Re$ and $\bar{R}$) above and below the two networks. One node of the system is shown in the figure.

If $\Re$, R, $\bar{R}$ are very much larger than r and ρ, it is possible (and this is currently being exploited in several directions) to solve, using the form of finite differences, two simultaneous systems governed by the equations

$$\frac{\partial}{\partial x}\left(m \frac{\partial \bar{V}}{\partial x}\right) + \frac{\partial}{\partial y}\left(n \frac{\partial \bar{V}}{\partial y}\right) = A\bar{V} + F$$

$$\frac{\partial}{\partial x}\left(p \frac{\partial V}{\partial x}\right) + \frac{\partial}{\partial y}\left(q \frac{\partial V}{\partial y}\right) = -C\bar{V} + BV + G$$

where m, n, p, q, A, B, C, F, G are known functions of x and y and V, $\bar{V}$ are the node voltages of the lower and upper networks, respectively, which correspond to the values of the functions sought. From a general point of view, and one which aids physically in visualizing the nature of these networks, it can be said that network II is the "higher voltage network" which regulates the nature of the voltage distribution in the "lower voltage network" I, it being assumed that the lower network has practically no effect on the upper. Typical values of the voltages and resistances used make this clear: r = 1,000 ohms, R = 1 megohm, ρ = 100 ohms, $\Re$ = 100,000 ohms, $\bar{R} \geq 1$ megohm. Voltages used may be U = 100, $\bar{V}$ about 3, V about 0.01 on the scale of maximum voltage taken as 100.

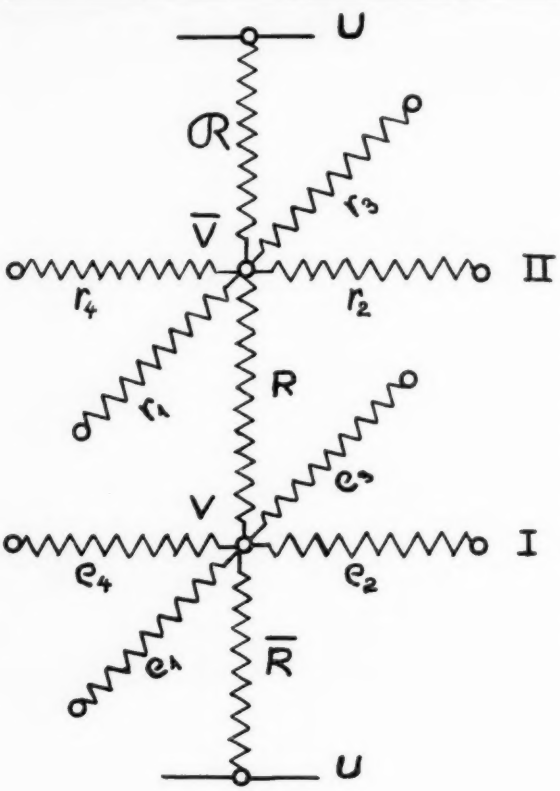

FIG. 1.

Here we note in particular the use of a *single line of nodes* cut out of one of these two-dimensional networks. This system (see Fig. 2) solves the classical beam equations (where h is deflection, M moment, p load, etc.)

$$\frac{d^2M}{dx^2} = p(x)$$

$$EI\frac{d^2h}{dx^2} = M(x)$$

Fig. 2 shows a setup used to obtain the influence coefficients of an aircraft wing spar. The accuracy obtained is of the order of 1 per cent. If the voltage U is called 100 (actually, as used, in the neighborhood of 30 volts), the voltage representing the beam deflection h can be read to within 0.001. Low frequency (120 cycle) a.c. electrical feed permitting the use of a cathode-ray oscillograph as a zero instrument is very convenient for this type of network, the low frequency reducing the possibility of a.c. effects in an essentially d.c. network.

It is easy, with a sufficiently large number of network nodes, to obtain the vibration modes of a beam by an iteration scheme which resembles very closely the classical matrix iteration. Through proper choice of the resistances $\bar{R}$ it is also possible to bring in easily the effects of rotary beam inertia. Naturally, variable section rigidity EI causes no more difficulty than constant rigidity, since R is chosen proportional to EI at each node. The typical beam boundary conditions are regulated simply by potentiometers. Higher modes are amenable to "sweeping matrix" type of operations.

Another resistance network of a simple nature is useful in representing the torsion equations of a bar. This is shown in Fig. 3 for a cantilever bar having four discrete sections of different stiffnesses GJ.

The voltage V corresponds to the angle of torsion θ of the bar, the currents which enter ($\approx U/R_1$) correspond to the applied torque T, and r corresponds to l/GJ. Here also we take $R \gg r$. This network is good for torsional vibration problems, worked out by iteration as before.

If the idea of an elastic or torsion axis can be tolerated in a given case, simultaneous iteration with the two networks like those of Fig. 2 and Fig. 3 and the standard equations of coupled vibration

$$d^2/dx^2\left[EI\left(\frac{d^2h}{dx^2}\right)\right] = \omega^2(\mu h + S\theta)$$

$$\frac{d}{dx}GJ(d\theta/dx) = -\omega^2(Sh + I\theta)$$

will yield rapidly the coupled mode of the system. (μ, S, and I are, respectively, the mass, static moment, and moment of inertia per unit length.)

Other characteristic value problems of structures can be attacked with the beam flexural network.[6] Among these, also solved by rapid iteration, are: critical loads of columns with any rigidities, end conditions, and distribution of longitudinal loading (the bar may also be assumed vibrating or resting upon elastic lateral supports of any stiffness); the buckling of arches in their planes; the lateral buckling of thin beams. Cases of beam-column deflection can be accurately solved by iterative approximation.

In view of the somewhat complicated form occasionally taken by electrical networks it is of interest to note that certain results of fairly wide application can be obtained, as here, by lesser means.

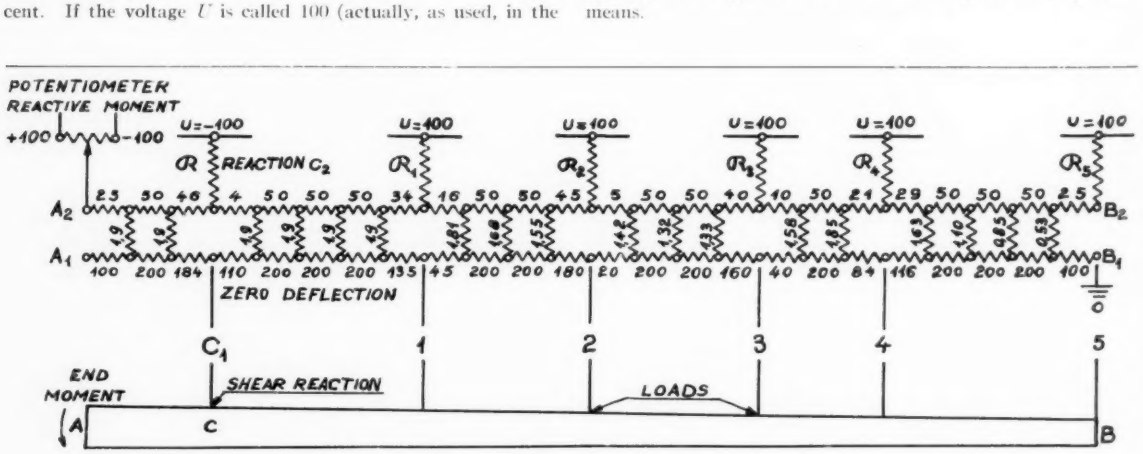

FIG. 2. R in Megohms; r and ρ in ohms; and $\mathcal{R}$ = 10,000 ohms.

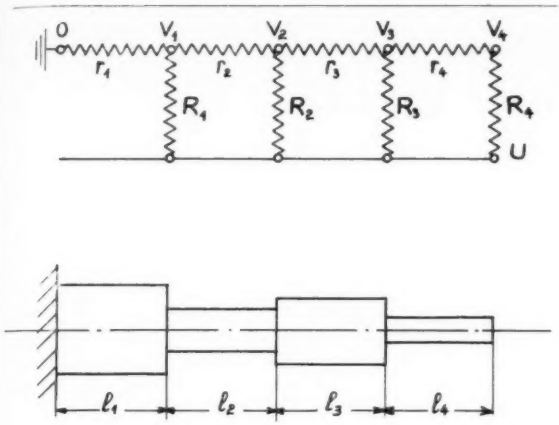

FIG. 3.

REFERENCES

[1] Boschet, J., *Sur la détermination numérique de fonctions biharmoniques par un procédé analogique de réseaux superposés*, Comptes Rendus Acad. Sci., t. 236, p. 44, December 10, 1952.

[2] Malavard, L., and Boscher, J., *Modèle analogique électrique pour l'étude de la flexion des poutres*, Comptes Rendus Acad. Sci., t. 236, p. 1130, March 9, 1953.

[3] Boscher, J., and Malavard, L., *Détermination analogique des fonctions biharmoniques*, Bulletin de la Société Française des Mécaniciens, 2nd Trimester, p. 43, 1953.

[4] Malavard, L., and Boscher, J., *Applications de la méthode des réseaux superposés à l'étude de divers problèmes d'élasticité*, Comptes Rendus Acad. Sci., t. 238, p. 1093, March 8, 1954.

[5] Boscher, J., *Sur l'application de la méthode des réseaux électriques au calcul de la déformation des plaques élastiques*, Comptes Rendus Acad. Sci., t. 238, p. 1189, March 15, 1954.

[6] Scanlan, R., *Sur l'emploi des réseaux résistifs superposés pour la solution de problèmes à valeur propre de poutres et colonnes*, Comptes Rendus Acad. Sci. t. 238, p. 1470, March 29, 1954.

Errata—"Differentiation of Experimental Data by Means of Higher Order Finite-Difference Formulas"

Chi-Teh Wang and Daniel F. De Santo
Daniel Guggenheim School of Aeronautics, New York University, New York
June 23, 1954

IN THEIR READERS' FORUM NOTE,[1] Wang and De Santo presented a method for differentiating experimental data by using the method of higher order finite-difference approximations. In that note they employed as an example the function

$$x = 6 \sin t + 0.5 \sin 3t \qquad (0 \leq t \leq 3) \qquad (1)$$

It was subsequently pointed out by Schurmann and Smith[2] that the values of dx/dt and d^2x/dt^2 calculated by the method of reference 1 at the first, second, next to the last, and last points on the respective curves might not be correct. The present authors have since recomputed the derivatives at these points and found that numerical errors had indeed been made in calculating these values. The correct values are presented in Fig. 1. It may be seen that the accuracy is now good over the entire range, including the points in the vicinity of the ends, and that the results compare favorably with those given by the method of reference 2.

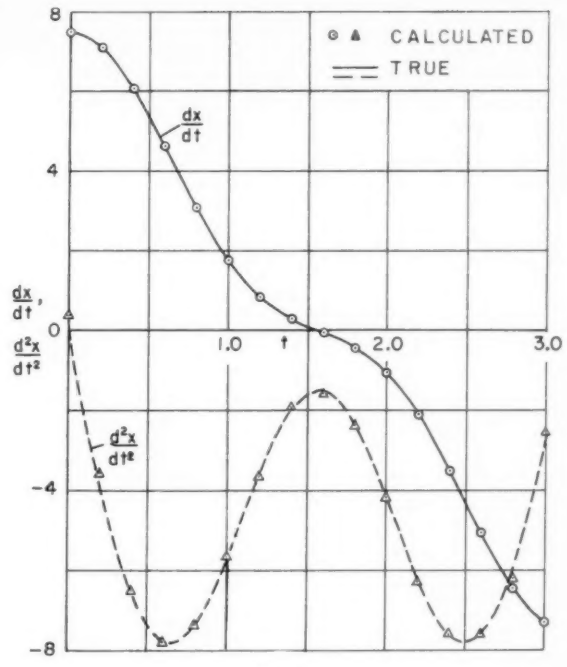

FIG. 1.

REFERENCES

[1] Wang, C. T., and De Santo, D. F., *Differentiation of Experimental Data by Means of Higher Order Finite-Difference Formulas*, Journal of the Aeronautical Sciences, Vol. 20, No. 11, pp. 792–793, November, 1953.

[2] Schurmann, E. E. H., and Smith, T. L., *Methods for Determining the First and Second Derivatives of Experimental Data*, Journal of the Aeronautical Sciences, Vol. 21, No. 6, pp. 420–421, June, 1954.

A Note on Rolling Pull-Out Calculations

George S. Campbell
California Institute of Technology, Pasadena, Calif.
June 26, 1954

IN A PAPER ENTITLED "Estimation of the Maximum Angle of Sideslip for Determination of Vertical-Tail Loads in Rolling Maneuvers,"[1] it was shown that the three linearized lateral equations of motion, including product of inertia terms, may not provide a sufficiently close estimate of the sideslip angles expected in rolling pull-outs. The results presented in the present note indicate that the nonlinear, four-degree of freedom system of equations used as a standard of comparison in reference 1 may provide results that are possibly just as questionable as those obtained from the linearized equations.

The exact equations of motion representing the six-degrees of freedom of a rigid aircraft are conveniently given in a recent text by W. J. Duncan.[2] The yawing-moment equation, for example, has the following form under the assumption of body axes which are principal axes of inertia:

$$N = I_z\dot{r} - (I_x - I_y)pq \qquad (1)$$

When the complete expressions for the angular velocities p, q, and r, as given in reference 2, are introduced into Eq. (1), the yawing-moment equation becomes

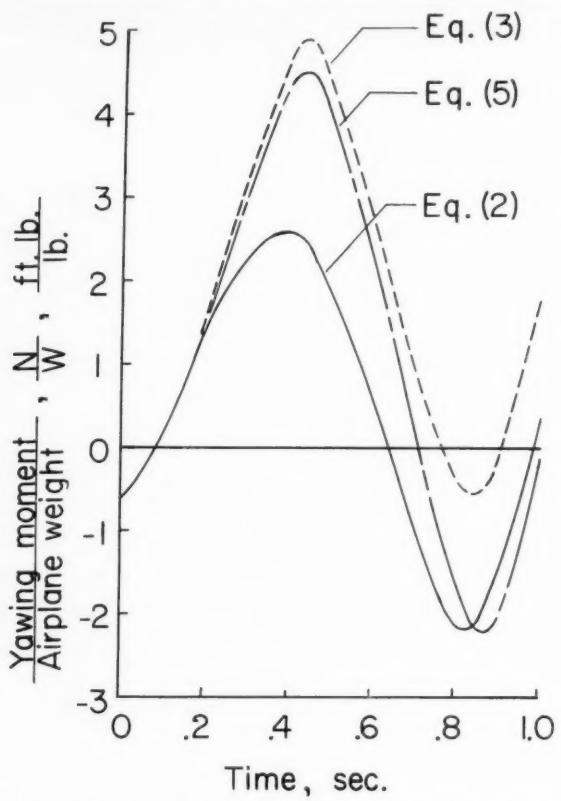

FIG. 1. Effect of nonlinear terms on the aerodynamic yawing moments during a rolling pull-out.

$$N = I_z(\ddot{\psi}\cos\phi\cos\theta - \ddot{\theta}\sin\phi - \dot{\psi}\dot{\phi}\sin\phi\cos\theta) + (I_x - I_y)\dot{\psi}\sin\phi\cos\theta(\dot{\psi}\sin\theta - \dot{\phi}) - (I_z + I_x - I_y)\dot{\phi}\dot{\theta}\cos\phi - (I_z - I_x + I_y)\dot{\psi}\dot{\theta}\cos\phi\sin\theta \quad (2)$$

For comparison, the yaw-equation used for the nonlinear calculations of reference 1 is

$$N = I_z\ddot{\psi} - (I_x - I_y)\dot{\phi}\dot{\theta} \quad (3)$$

This form is actually subject to some serious linearizing approximations, for it is obtained from Eq. (1) by assuming

$$\left.\begin{aligned} p &= \dot{\phi} \\ q &= \dot{\theta} \\ r &= \dot{\psi} \end{aligned}\right\} \quad (4)$$

Equations (4) are valid approximations only if ϕ, θ, and ψ are small quantities, and it is evident that ϕ, for example, may reach large values in rolling maneuvers.

Finally, the usual linearized equation of yawing motion may be written

$$N = I_z\ddot{\psi} \quad (5)$$

In order to determine whether the nonlinear equations used in reference 1 are sufficiently close approximations to the complete six-degree-of-freedom equations of motion, the results for the case of a rolling pull-out presented in Fig. 4 of reference 1 may be used. Curves presented in Fig. 1 of the present note represent the aerodynamic yawing moments required to produce the specified rolling pull-out maneuver. These yawing moments are calculated from the three expressions [Eqs. (2), (3), and (5)] for the inertial reaction during the maneuver. It is evident from these results that the terms which are neglected when Eq. (3) is used for time-history calculations are not necessarily negligible for the case of a rolling pull-out. For if these terms actually had no significant effect on the time histories, the values of the yawing moment as calculated from Eq. (2) would coincide with the curve obtained from Eq. (3).

It is further seen from Fig. 1 that the use of only one nonlinear term, as in reference 1, may produce results which could be in greater disagreement with results obtained from the complete nonlinear expression than would have been obtained from the much simpler linear equations.

From these results, it is suggested that if one is willing to accept the complications arising from the inclusion of *any* nonlinear terms in the equations of motion, then the use of *all* the nonlinear terms is probably necessary in order to obtain reliable results. The question of whether four degrees of freedom are adequate for the rolling pull-out is a separate consideration beyond the scope of this note.

REFERENCES

[1] Stone, Ralph W., Jr., *Estimation of the Maximum Angle of Sideslip for Determination of Vertical-Tail Loads in Rolling Maneuvers*, NACA Rep. 1136, 1953 (formerly NACA TN 2633).

[2] Duncan, W. J., *The Principles of the Control and Stability of Aircraft*, Cambridge, 1952.

Airplane Stopping Distance

B. Saelman
Engineering Consultant, North Hollywood, Calif.
June 29, 1954

THE DRAG FORCES acting on the airplane during the deceleration from touchdown to the stop are:

(a) Rolling resistance of the nose gear tire.

(b) Rolling and brake resistance of the main wheels (skidding force if brakes are locked).

(c) Aerodynamic drag on the airplane.

(d) Positive or negative propeller or jet thrust.

In reference 1 a formula for stopping distance is derived based on the assumption that the braking force is given by

$$F = \mu(W - L)$$

This will apply to airplanes with brakes on both the main and nose wheels. However, when the brakes are applied only to the main wheels, as is usually the case, this assumption is not realistic and, if used, can lead to considerable error. For this case, formulas are derived below, and have yielded answers which have closely checked measured stopping distances when an average coefficient of friction of 0.3 was used.

Taking moments about the nose wheel and solving for the main wheel reaction,

$$P_{V_M} = \frac{n\left[K_1 + K_2\left(\frac{dx}{dt}\right)^2\right]h_1 + \rho_0\frac{\sigma S C_D\left(\frac{dx}{dt}\right)^2}{2}h_2 + (W - L)\,b + \frac{W}{g}\frac{d^2x}{dt^2}e}{l} \quad (1)$$

Summing the drag forces and equating to zero,

$$\frac{W}{g}\frac{d^2x}{dt^2} + \frac{\rho_0\sigma\ C_DS}{2}\left(\frac{dx}{dt}\right)^2 + \left\{n\left[K_1 + K_2\left(\frac{dx}{dt}\right)^2\right]h_1 + \frac{\rho_0\sigma C_DS\left(\frac{dx}{dt}\right)^2 h_2}{2} + \left[W - \frac{\rho_0\sigma C_LS}{2}\left(\frac{dx}{dt}\right)^2\right]b + \frac{W}{g}\frac{d^2x}{dt^2}e\right\}\left(\frac{\mu}{l} + n\left[K_1 + K_2\left(\frac{dx}{dt}\right)^2\right] = 0 \quad (2)$$

In these equations the terms are as defined in reference 1 and in Fig. 1. Letting $y = dx/dt$, Eq. (2) can be simplified to:

$$(dy/dt) - \beta y^2 + N = 0 \quad (3)$$

where

$$\beta = \frac{\frac{\rho_0\sigma SC_L\mu b}{2l} - \left(1 + \frac{\mu h_2}{l}\right)\frac{c_D\rho_0\sigma S}{2} - nK_2\left(1 + h_1\frac{\mu}{l}\right)}{\frac{W}{g}\left(1 + \mu\frac{e}{l}\right)} \quad (4)$$

$$N = \frac{W\frac{\mu b}{l} + nK_1\left(\frac{\mu h_1}{l} + 1\right)}{\frac{W}{g}\left(1 + \frac{\mu e}{l}\right)} \quad (5)$$

Assuming β positive, integrating Eq. (3), and using the initial condition that $dx/dt = V_L$ when $t = 0$,

$$\frac{dx}{dt} = \frac{E - \tanh \phi t}{H - G \tanh \phi t} \quad (6)$$

Using the terminal condition that $dx/dt = 0$ when $t = T$, we have the time of the ground run

$$T = \frac{1}{\phi}\tanh^{-1} E \quad (7)$$

where

$$\phi = \sqrt{\beta N}, \qquad E = \sqrt{\frac{\beta}{N}}V_L, \qquad H = \sqrt{\frac{\beta}{N}}, \qquad G = \frac{\beta}{N}V_L \quad (8)$$

If $\beta < 0$

$$T = \frac{1}{\phi}\tan^{-1} E \quad (9)$$

where $\beta_1 = -\beta$ is substituted in Eq. (8).

Integrating Eq. (6) and using the terminal conditions the stopping distance is:

$$X_B = \frac{E - B}{(B^2 - 1)G\phi}\log_e\frac{B - E}{B\sqrt{1 - E^2}} \quad (10)$$

where

$$B = \frac{1}{\sqrt{\beta/N}\ V_L} \quad (11)$$

$$X_B = \frac{\frac{1}{2g}\left(1 + \frac{e}{l}\frac{\mu}{}\right)V_L^2}{\left(\frac{C_L\mu b}{l} - \frac{C_Dh_2\mu}{l} - C_D\right)\frac{1}{C_{L_L}} - \frac{nK_2h_1\mu V_L^2}{Wl} - \frac{nK_2V_L^2}{W}} \times \log_e\frac{\frac{nK_1}{W} + \frac{nK_1\mu\ h_1}{Wl} + \frac{b\mu}{l}}{\frac{nK_1}{W} + \frac{nK_1\mu h_1}{Wl} + \frac{b\mu}{l} - \left(\frac{C_L\mu b}{l} - \frac{C_Dh_2\mu}{l}\right)\frac{1}{C_{L_L}} + \frac{nK_2h_1\mu V_L^2}{lW} + \frac{nK_2\ V_L^2}{W} + \frac{C_D}{C_{L_L}}} \quad (12)$$

where

$$C_{L_L} = (391W)/(V_{L_{m.p.h.}}{}^2\ \sigma S) \quad (13)$$

when the jet or propeller thrust is zero, Eq. (12) becomes

$$X_B = \frac{13.05W\left(1 + \frac{e}{l}\frac{\mu}{}\right)}{\sigma S\left(\frac{C_L\mu b}{l} - \frac{C_Dh_2\mu}{l} - C_D\right)}\log_e\frac{\frac{b\mu}{l}}{\frac{b\mu}{l} - \left(\frac{C_L\mu b}{l} - \frac{C_Dh_2\mu}{l}\right)\frac{1}{C_{L_L}} + \frac{C_D}{C_{L_L}}} \quad (14)$$

In reference 1 and in this discussion it was assumed that μ was constant and independent of velocity, and that μ was consistent with the "torqueability" of the brakes. This latter phenomenon is quite significant and is often overlooked. It is well described in an unpublished work by K. S. Carter from which Fig. 2 is taken. Fig. 2 shows the variation of torque with speed in a typical dynamometer test wherein brake pressure is held at a constant value throughout the stop. The solid line shows the variation in torque (at constant brake pressure) which results from the combined effects of brake disc speed changes

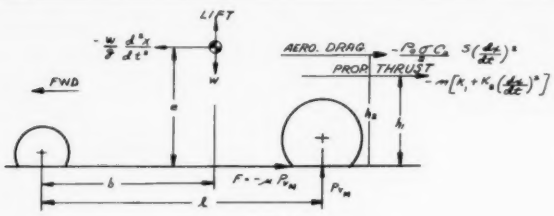

FIG. 1.

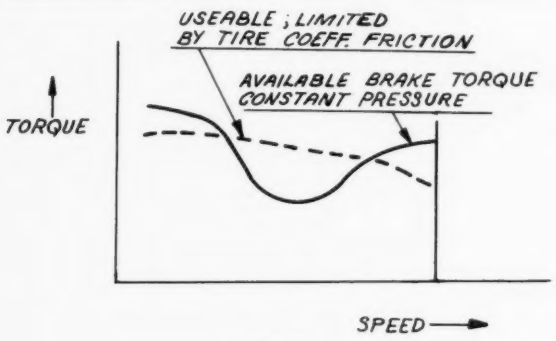

FIG. 2.

and temperature changes which occur during the stop. The dotted line shows the torque which is usable on the airplane, and is defined as the maximum torque which can be applied to the brakes, at each instant of the stopping period, without danger of skidding the tires. This torque is a function of airplane speed and wing lift at the instant, together with the coefficient of friction which can be developed by the tire against the runway surface.

REFERENCE

[1] Crockett, Harold B., and Bonney, Arthur E., *Reverse Pitch Propellers as Airplane Landing Brakes*, Journal of the Aeronautical Sciences, Vol. 12, No. 4, p. 441, October, 1945.

A Reply—Load Distributions on Delta Wings at Supersonic Speeds

Julian H. Kainer
Aerodynamics Engineer, Ryan Aeronautical Company, San Diego, Calif.

July 2, 1954

IN A RECENT PAPER[1] in the Readers' Forum, Mr. Zienkiewicz derived the load distributions on some twisted and cambered delta wings with supersonic leading and trailing edges. Upon comparing the results of Eq. (8) therein, Mr. Zienkiewicz erroneously concluded that his results differed from the load distributions we presented previously[2] by a factor of $1/\beta$. Both results[1, 2] were compared to the load distribution for the classical Ackeret region ($\Delta p/q = 4\alpha/\beta$) from which comparison it was shown that our results[2] reduced to $\Delta p/q = 4\alpha$.

A similar observation was first brought to my attention by Dr. Godfrey Lance who has completed some comprehensive studies which include the effects of both symmetric and antisymmetric downwash distributions for twisted and cambered wings having subsonic, transonic, and supersonic leading edges. Through correspondence with Dr. Lance, it was established that our results are correct.

It is the purpose now to emphasize the fact that we defined for convenience an "effective" loading function and abbreviated it with an asterisk as a superscript. The "effective" function (i.e., pressure distribution, velocity potential, horizontal perturbation velocity, section properties, and overall wing characteristics) is defined as the product of β and the desired function, i.e.—$\left(\frac{\Delta p}{q}\right)^* \equiv \beta\left(\frac{\Delta p}{q}\right)$—(See Symbols[2]). Thus the observation Mr. Zienkiewicz should have been made was that $(\Delta p/q)^* = 4\alpha$ which is the same as $\Delta p/q = 4\alpha/\beta$! To indicate this more concretely let us look at a few specific formulas from our results:[2] the lifting pressure distribution was given as

$$\frac{\Delta p}{q} = \frac{4}{V}\phi_x \tag{12a}$$

and the generalized horizontal perturbation velocity *parameter* was defined as

$$\left(\frac{\pi}{V}\right)(\beta/x')^i(\phi_x/a)_i^* \equiv B_i(t) \tag{13b}$$

For the classical limiting case mentioned above, the conical functions, $B_i(t)$ were indicated by the barred quantities, $\bar{B}_i(t)$. Thus, for $i = 0$, Eq (13b) becomes

$$\left(\frac{\pi}{V}\right)(\phi_x/a)_0^* = \pi$$

or

$$\phi_x = \frac{V\alpha}{\beta}$$

Substitution of which into Eq. (12a) gives the expected result, $\Delta p/q = 4\alpha/\beta$. This result was graphically demonstrated[2] in Fig. 2.

In the original version,[2] the relationship between the asterisked function and the corresponding function without asterisk was more explicitly defined than in the more current version.[2] In the Symbols of the former, the asterisked loading function was described as an effective loading function *defined* as the product of β and the loading function in question. It is hoped that the omission of this definition will not continue to be a source of confusion.

REFERENCES

[1] Zienkiewicz, H. K., *Load Distributions on Some Twisted and Cambered Delta Wings With Supersonic Leading and Trailing Edges*, Readers' Forum, Journal of the Aeronautical Sciences, Vol. 20, No. 6, pp. 421–423, June, 1954.

[2] Kainer, J. H., *Equations for the Loading on Triangular Wings Having Supersonic Leading and Trailing Edges Due to Various Basic Twist Distributions*, Journal of the Aeronautical Sciences, Vol. 20, No. 7, pp. 469–476, July, 1953.

[3] Kainer, J. H., *Equations for the Potential, Pressure and Span Load Distributions on Triangular Wings Having Supersonic Leading Edges Due to Various Basic Twist Distributions with Application to the Aeroelastic Problem*, Republic Aviation Corp., Report No. EAR-273, September, 1952.